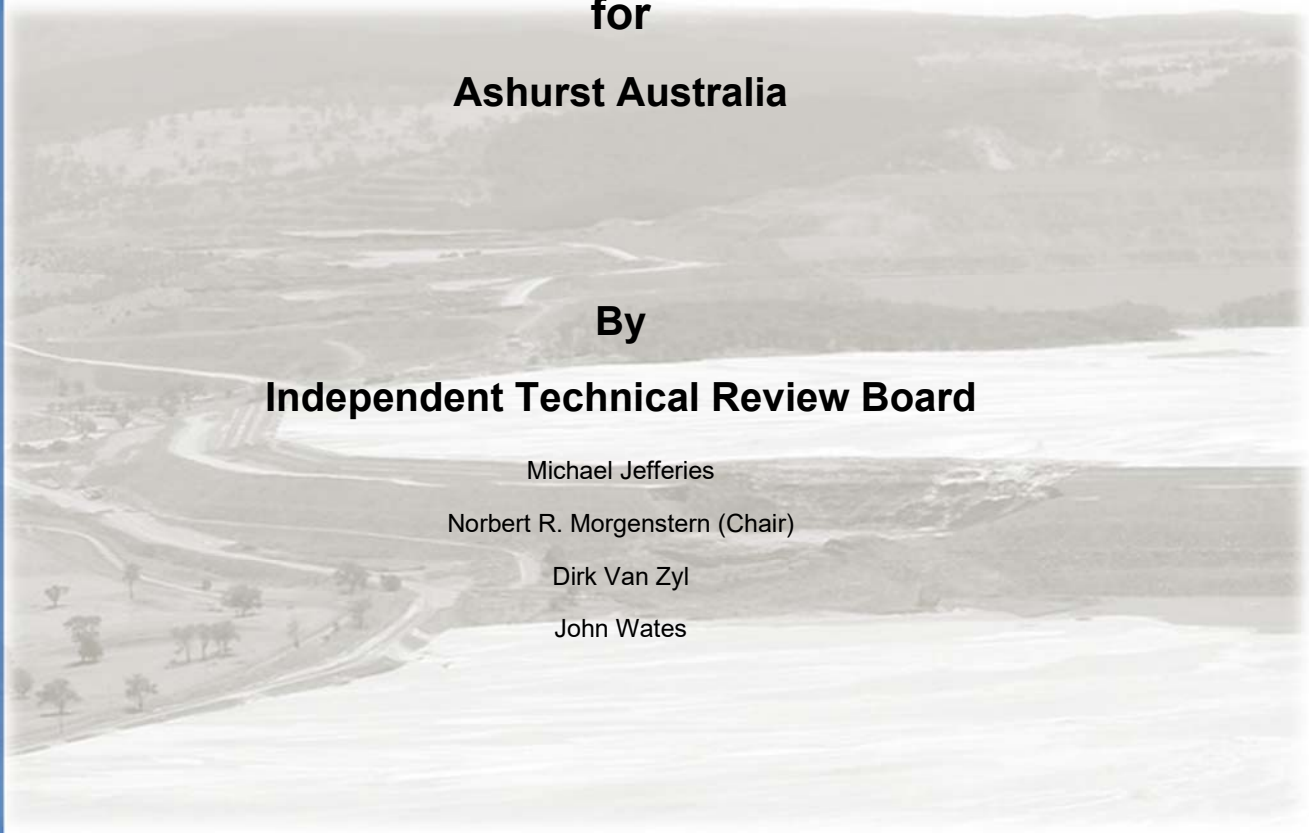
Report on NTSF Embankment Failure

Cadia Valley Operations

for

Ashurst Australia



By

Independent Technical Review Board

Michael Jefferies

Norbert R. Morgenstern (Chair)

Dirk Van Zyl

John Wates

Date: April 17, 2019

H356804-00000-22A-230-0001, Final

Table of Contents

Executive Summary ..... **vi**

1. Introduction **1**

1.1 Terms of Reference 3
1.2 Organisation of the Study 3
1.3 Operations 4
1.4 Report Organisation 4

2. The Event **5**

3. Design, Construction and Response **7**

3.1 Introduction 7
3.2 Overview of Design and Construction 7
3.2.1 Stage 1 7
3.2.2 Stage 2A and 2B 8
3.2.3 Stage 3 9
3.2.4 Stages 4 to 9 9
3.2.5 Stage 10 10
3.3 Overview of Performance 11
3.3.1 Introduction 11
3.3.2 Piezometers 12
3.3.3 Seepage 13
3.3.4 Displacements 13
3.3.5 Seismicity 16
3.3.6 Direct Observation 16

4. NTSF Field Characterisation **19**

4.1 Overview 19
4.2 Geology 19
4.2.1 Stratigraphy 19
4.2.2 Weemalla Formation 19
4.2.3 Forest Reef Volcanics 19
4.2.4 Waugoola Group 19
4.2.5 Tertiary Basalt 19
4.2.6 Paleosoils 19
4.2.7 Geologic Structure 20
4.3 Previous Investigations 20
4.3.1 Foundation Investigations 20
4.3.2 Tailings Investigations 21
4.3.3 Construction Materials Investigations 23
4.4 ITRB Field Investigations 23
4.4.1 Overview 23
4.5 GHD Investigations 24
4.6 Newcrest Investigations 24
4.7 Geological Model at Slump 25

5. Material Properties **31**

5.1 Introduction 31
5.2 Foundation Materials 31
5.2.1 Material Types 31
5.2.2 Insitu Void Ratio 32
5.2.3 Laboratory Testing 32
5.2.4 Compressibility 33
5.2.5 Consolidation 34

5.2.6 Stress-Strain Behaviour ... 34
5.2.7 Direct Shear Tests ... 35
5.2.8 Strength Trends ... 36
5.2.9 ITRB Assessment of Foundation Properties ... 38
5.3 Tailings ... 39
5.3.1 Introduction ... 39
5.3.2 Sampling ... 39
5.3.3 Laboratory Investigation ... 41
5.3.4 Critical State ... 42
5.3.5 Strength ... 42
5.3.6 Earthquake (cyclic loading) Response ... 43
5.3.7 Insitu State ... 44
5.3.8 ITRB Assessment of Tailings ... 46
5.4 Embankment Dam ... 48
5.4.1 Fill Zonation ... 48
5.4.2 Rockfill ... 48
5.4.3 Clay Core ... 48
5.4.4 Filter Materials ... 49
5.4.5 ITRB Assessment of Embankment Properties ... 49

6. Failure Hypotheses ... 51

6.1 Introduction ... 51
6.2 Causes of Instability ... 51
6.3 Failure Mechanisms ... 52

7. Stability Analyses ... 54

7.1 Introduction ... 54
7.2 LEA (2D) ... 54
7.3 LEA (3D) ... 56

8. Deformation Analyses ... 59

8.1 Overview ... 59
8.2 Observations Honoured ... 61
8.3 Representation of NTSF ... 62
8.3.1 Staged Construction ... 62
8.3.2 Material Zones Modelled ... 62
8.3.3 Piezometric Conditions ... 63
8.3.4 Material Properties Used ... 63
8.4 2D Analysis (Phase 1) ... 64
8.4.1 Models Simulated ... 64
8.4.2 State Parameter Evolution ... 64
8.4.3 Deformations ... 65
8.4.4 Progressive Failure of Foundation Under Static Load (Mechanism 1) ... 66
8.4.5 Rising Ground Water (Mechanism 2) ... 70
8.4.6 Seismic Triggering of Liquefaction (Mechanism 3) ... 71
8.5 3D Analysis (Phase 1) ... 73
8.5.1 Objectives ... 73
8.5.2 Description of 3D Model ... 74
8.5.3 Deformations ... 74
8.5.4 Inferred Foundation Properties ... 77
8.5.5 Inferred Tailings Behaviour ... 79
8.5.6 Tailings Instability ... 80
8.5.7 ITRB Commentary ... 81
8.6 Slump Development (Phase 2) ... 82
8.6.1 Transition from Drained to Undrained Behaviour ... 82
8.6.2 Available Undrained Strength in Tailings ... 82
8.6.3 Stability at Liquefaction ... 84

9. Conclusions 86

9.1 Commentary 86
9.2 Why Did the Event Occur? 87
9.3 Why Did the Event Occur Where it Happened? 88
9.4 Why Did the Event Occur When it Happened? 88
9.5 Why Won't a Similar Event Happen Anywhere Else? 89

10. Acknowledgements 92

11. References 93

12. Symbol List 95

13. List of Abbreviations 97

14. Glossary of Technical Terms 99

List of Tables

Table 3-1: Summary of Design and Construction 7
Table 4-1: Summary of previous foundation investigations 20
Table 4-2: Summary of drillhole information 21
Table 4-3: Summary of 2013 Tailings Investigation 22
Table 4-4: Summary of 2017 NTSF Tailings Investigation 23
Table 4-5: Geological section at NTSF slump 26
Table 5-1: Summary of advanced foundation testing program 33
Table 5-2: Summary of advanced tailings testing program 41
Table 5-3: Adopted critical state parameters for tailings 43
Table 7-1: Material parameters adopted for foundation parametric back analyses 56

List of Figures

Figure 1-1: Location Map Showing Cadia Valley Operations 1
Figure 1-2: Location Map showing the NTSF and STSF 2
Figure 1-3: Organisation for Study of NTSF Embankment Failure 4
Figure 2-1: NTSF Slump on March 10, 2018, 10:00 5
Figure 2-2: Annotated Section Through Slump on March 10, 2018 5
Figure 2-3: Post failure cross-section of Aznalcóllar Tailings Dam: (Alonso & Gens, 2006a) 6
Figure 3-1: Original ultimate design concept using modified centreline construction (1997-001) 8
Figure 3-2: Stage 1 Starter Embankment 8
Figure 3-3: Stage 2A and 2B Embankments 9
Figure 3-4: Stage 3 Embankment 9
Figure 3-5: Stage 4 to 9 Embankment Configuration 10
Figure 3-6: Stage 10 Embankment Configuration 10
Figure 3-7: Exposed foundation on January 18, 2018 11
Figure 3-8: Longitudinal profile of piezometric surface with time 12
Figure 3-9: Ch1800 drain flow and NTSF decant pond level 13
Figure 3-10: Survey prism movement in five years preceding the slump 14
Figure 3-11: InSAR surface movement measurements based on data from a single satellite 15
Figure 3-12: InSAR surface movement measurements at Ch 2000 15
Figure 3-13: Prism 6 - Comparison of survey and InSAR SMM data 16
Figure 3-14: Photograph of cracking on the Stage 5 crest beside Standpipe P9 taken at 07:48, March 9, 2018 17
Figure 3-15: Stage 8 crest cracking looking west, March 9, 2018 17
Figure 3-16: Cracking and heaving of haul road at Chainage 2060, March 9, 2018 18
Figure 4-1: Illustration of CPT rig (left) and probe details (right) 21
Figure 4-2: Excavated (a) and partially boxed undisturbed block sample (b) 24
Figure 4-3: Forest Reef Volcanics – void ratio & dry density vs depth 25
Figure 4-4: Geological units intersected at NTSF slump 27
Figure 4-5: Low density soils develop on FRV under a sub-tropical climate 29
Figure 4-6: Alluvium is deposited along paleo valleys 29

Figure 4-7: Basalt flows down valleys and covers paleo alluvium 30
Figure 4-8: Stream downcutting results in the formation of Rodds Creek 30
Figure 5-1: Plasticity of NTSF foundation materials 31
Figure 5-2: Liquidity Index vs depth 32
Figure 5-3: Confined compression (oedometer) data for FRV Unit A 33
Figure 5-4: Coefficient of consolidation in confined compression 34
Figure 5-5: Undrained stress-strain data in direct simple shear (FRV Unit A) 35
Figure 5-6: FRV Unit A - Drained Direct Shear Test 35
Figure 5-7: Peak undrained strength ratio in direct simple shear 36
Figure 5-8: Residual undrained strength ratio in direct simple shear 37
Figure 5-9: Brittle post-peak strength loss in direct simple shear 37
Figure 5-10: Confined compression modulus trends in FRV Unit A 38
Figure 5-11: Examples of undrained triaxial compression of FRV Unit A 39
Figure 5-12: CPT-N04 and samples adjacent to the NTSF slump 40
Figure 5-13: Particle size distributions of characteristic tailings tested 41
Figure 5-14: Comparison of CSL for NTSF tailings 42
Figure 5-15: Definition of the sate parameter (Jefferies & Been, 2016) 43
Figure 5-16: Measured cyclic response of NTSF tailings 44
Figure 5-17: Insitu state parameter at CPT-N04 45
Figure 5-18: CPT-N04 –Shuttle and Cunning tailings state plot 47
Figure 5-19: CPT-N04 – Robertson tailings state 47
Figure 5-20: Compacted core strength in triaxial compression 49
Figure 5-21: Leps (1970) data including fine grained igneous rocks 50
Figure 6-1: Schematic illustration of potential failure mechanisms 53
Figure 7-1: Stability section model geometry 55
Figure 7-2: Foundation back analysis, drained tailings φ' = 34° 56
Figure 7-3: Adopted failure surface geometry 57
Figure 7-4: Cross-section of slump through Stage 1 Buttress showing modelled failure surface 57
Figure 7-5: Variation in Factor of Safety with undrained strength ratio of foundation 58
Figure 8-1: Illustration of tailings strength evolution with strain (typical for NTSF) 59
Figure 8-2: Definition of Instability Locus 60
Figure 8-3: Idealisation of the NTSF embankment at CH1950 for numerical analysis 63
Figure 8-4: Distribution of state parameter in tailings on completion of Stage 10 raise 65
Figure 8-5: Comparison of displacements from 2D best-fit simulations with those measured 65
Figure 8-6: Development of strain weakening (shown as yellow zone) in Unit A 67
Figure 8-7: Distribution of controlling stress ratio in tailings after berm construction 67
Figure 8-8: Measured soil behaviour at 'Point 1' along computed stress path 69
Figure 8-9: Undrained instability following drained loading 70
Figure 8-10: Results of laboratory test for Point 1 under rising ground water pressure 71
Figure 8-11: Ground motion input to CDSS test simulating earthquake motion at Point 1 72
Figure 8-12: Response of Point 1 tailings to 8 Mar 2018 earthquake in cyclic simple shear 73
Figure 8-13: Oblique view of slump illustrating extent of 3D model 74
Figure 8-14: FLAC 3D computed and measured prism displacements perpendicular to the dam axis 75
Figure 8-15: FLAC 3D computed and InSAR SMM trends 75
Figure 8-16: Heave computed at end of Stage 10 raise 76
Figure 8-17: Heave computed after Stage 1 Buttress construction 76
Figure 8-18: Horizontal displacement contours at 8 March 2018 77
Figure 8-19: FRV Unit A strengths used in best-fit FLAC 3D simulation 78
Figure 8-20: Development of strain weakening in best-fit FLAC 3D simulation 78
Figure 8-21: State parameter profile at N04 location on completion of Stage 10 Raise 79
Figure 8-22: Influence of state parameter on extent of mobilised tailings strength 80
Figure 8-23: Instability locus for NTSF tailings 81
Figure 8-24: Undrained instability of loose soil during drained loading 82
Figure 8-25: Displacement vectors following change from drained to undrained loading 84
Figure 8-26: Contours of mobilised stress ratio η_{IL}/M_t after a small undrained perturbation 85
Figure 9-1: Longitudinal Cross section along the TSF showing ERI and drillholes 91

List of Appendices

Drawings

Appendix A **Operations of the ITRB**

Appendix B **History of NTSF**

Appendix C **Geology and Field Characterisation**

Appendix D **Foundation Laboratory Testing**

Appendix E **Tailings Properties**

Appendix F **Hydrogeology**

Appendix G **Limit Equilibrium Analysis**

Appendix H **Deformation Analysis**

Appendix I **Seismology**

Appendix J **NTSF Project Document Referencing**

Executive Summary

Cadia Holdings Pty. Ltd. (CHPL), a wholly owned subsidiary of Newcrest Mining Limited (NML), is the owner and operator of Cadia Valley Operations (CVO) that combines a suite of mining, mineral processing facilities and related infrastructure. At the time of the NTSF failure, there were two operational tailings storage facilities (TSF) at CVO, the Northern TSF (NTSF) and the Southern TSF (STSF).

On March 9, 2018, a slump (the Event) occurred in the southern wall of the NTSF, causing it to lose containment of tailings. The tailings were captured within the basin of the STSF, and there were no injuries or loss of life, primarily due to a perceptive and timely evacuation of the site prior to the Event in accordance with the CVO Dam Safety Emergency Plan.

In response, CHPL engaged Ashurst Australia to co-ordinate and manage an independent technical investigation into the Event. This would be undertaken by independent subject matter experts comprising an Independent Technical Review Board (ITRB). An additional investigation team was retained to co-ordinate, manage and support the ITRB during its investigation.

The specific terms of reference to the ITRB were to provide independent and unbiased professional judgement and expertise in determining the immediate technical cause(s) of the Event. In so doing, it was requested to focus on the following questions:

- Why did the Event occur?
- Why did the Event occur where it happened?
- Why did the Event occur when it happened?
- Why won't a similar Event happen anywhere else?

The ITRB was not asked to provide an opinion on the roles and responsibilities of individuals or corporations; nor did it do so.

In support of its inquiries, the ITRB undertook a comprehensive compilation of the history of the NTSF up to and including the Event. It commissioned the following;

- Extensive geological investigations, including drilling and sampling activities to characterise the site,
- Laboratory tests, both routine and advanced, were performed to determine the range of properties exhibited by these materials, and
- Advanced numerical simulations of both deformation behaviour and ultimate failure states were computed to validate the hypotheses of the cause(s) of the Event under consideration.

In addition, other subject matter experts were retained to support the ITRB by;

- Integrating all of the hydrogeological information available and development and calibration of a hydrogeological model for the NTSF,
- Assisting with numerical simulation of deformation with advanced models, and
- Providing a synthesis of site seismicity as well as recommending ground motions to be used in seismic response analysis.

All of these focused activities are summarised in appendices to the Report and form an integral part of it. These appendices together with the Report indicate the complexity and breadth of the investigation that was necessary to lead to the conclusions contained herein. Both extensive field and laboratory programs were challenging and time consuming but necessary to support analyses and evaluation.

The ITRB found it convenient to evaluate the evolution of the Event as characterised by two phases. Phase 1 incorporates all of the precursors of movement up to and including the time at which the worksite was evacuated. Movements in Phase 1 were slow, as the failing mass adjusted to changing states of equilibrium. While not directly observed, Phase 2 must have incorporated relatively sudden losses of resistance and/or increases in loading to create conditions to accelerate movements to the distances ultimately achieved. While the major consequences of the Event resulted from Phase 2, the cause resides in Phase 1. As demonstrated in the Report, the mechanics of Phase 1 are a necessary condition for the occurrence of Phase 2. However, had Phase 1 terminated without triggering Phase 2, the consequences of the failure of the NTSF would have been much reduced.

Major findings from the synthesis of the historical information for Phase 1, were that movements were occurring in the wall of the NTSF for many months prior to the Event. Movements monitored in 2017 by terrestrial based techniques were small. The movements accelerated in early 2018 as indicated by satellite based techniques, obtained after the Event. These movements were able to be correlated with the Stage 1 Buttress construction prior to Phase 2. Terrestrial based techniques were not used during this period due to operational constraints associated with construction. Detailed visual observations of ground deformations prior to the evacuation of the worksite and potential impact zone, were symptomatic of movements deep into the foundations of the embankment which provided some guidance for the targets of the field characterisation investigation.

The geology of the site is complex due to its stratigraphic and structural history, with added complexity, from a geotechnical perspective, of differential weathering profiles. However, the field characterisation program was ultimately successful in discovering a low-density foundation layer in the vicinity of the slump; Forest Reef Volcanics (FRV) Unit A. This material, which had not been previously identified, is relatively weak, highly compressible, and strain-weakening (brittle) when subjected to load. The presence of the FRV Unit A constitutes the most significant controlling factor that led to the Event.

The material properties of the FRV Unit A have now been established by a variety of laboratory tests. The ITRB is content that it has been adequately characterised and its propensity for strain-weakening (loss of resistance), under increasing load and for contractive behaviour that will generate pore pressures has been demonstrated.

The geotechnical behaviour of the tailings relies on data from in-situ testing carried out prior to the design of the last raise, augmented by some additional sampling and testing undertaken by the ITRB. Prior to failure, the tailings were generally saturated as a result of the design, very loose, and highly contractive when sheared. This makes the tailings disposed to liquefaction if the right combination of triggering conditions should prevail.

The various analyses conducted support the view that the foundation yielded during the Stage 1 Buttress construction, particularly during Phase 1, when additional buttresses were being added. The tailings liquefied as a result of a rapid increase in foundation deformations, and the substantial driving force created by the liquefied tailings was greater than the remnant foundation resistance, and hence the embankment was propelled forward.

The analyses of Phase 1 behaviour, leading to the triggering of liquefaction of the tailings are made more challenging by the occurrence of two small earthquakes that occurred the day before the Event. It should be noted that deformations due to foundation yielding were well advanced by this time. An important question is whether the earthquakes were the predominant cause of the event, or whether they were not consequential.

Detailed seismic response analyses carried out by the ITRB were not able to demonstrate that these small earthquakes contributed to the triggering of liquefaction. Extensive analyses supported the view that liquefaction was triggered by ongoing foundation deformations.

A brief response to the questions put to the ITRB follows;

- The Event occurred because of deformation in the foundations during the last months of Stage 10 construction, led to the removal of support for the tailings thus triggering liquefaction of the loose saturated tailings.
- The dominant factor controlling the location of the Event is the spatial distribution of the FRV Unit A layer. Other factors contributing are the local height of the dam, the prevailing phreatic conditions, and the additional excavation at the toe of the structure.
- The timing of the Event was controlled by the deformations accumulated through the construction history which were sufficient to trigger static liquefaction in the loose saturated tailings stored in the NTSF. The occurrence of the earthquakes prior to the Event had no role in Phase 1 and did not contribute to Phase 2.
- The ITRB understands that it is NML's intent to restore the operations of the NTSF and maintain both the NTSF and STSF as upstream constructed facilities. It must be recognised that this implies management of loose, saturated, and potentially liquefiable tailings for the full life cycle of the facilities. To avoid the type of failure that has been experienced in the Event, NML should:
    a. ensure that the foundation conditions are analysed along the length of the NTSF and STSF walls; and
    b. where weak material comparable to the FRV Unit A is identified, this foundation strength is taken into account in the ongoing design of the facility. In addition, NML should ensure ongoing integration of the observations made on the foundation geology during construction, to support this understanding, and appropriate instrumentation is installed to demonstrate that the foundation is behaving as intended.

1. Introduction

Cadia Valley Operations (CVO) is a gold/copper mining and processing complex 25 km south of the town of Orange, central west NSW (Figure 1-1). Cadia Holdings Pty. Ltd. (CHPL), a wholly owned subsidiary of Newcrest Mining Limited (NML), is the owner and operator of CVO.

The CVO complex comprises the Cadia Hill, Ridgeway and Cadia East mines, mineral processing facilities and associated infrastructure. Mining commenced in 1998, with current approvals taking the project through to 2031.

At the time of the NTSF embankment failure, there were two operational tailings storage facilities (TSF) at CVO; the Northern TSF (NTSF) and the Southern TSF (STSF). Both TSF embankments were constructed across the former Rodds Creek, the NTSF being at the upstream location and the STSF at the downstream location. The location of the NTSF and the STSF are shown on Figure 1-2.

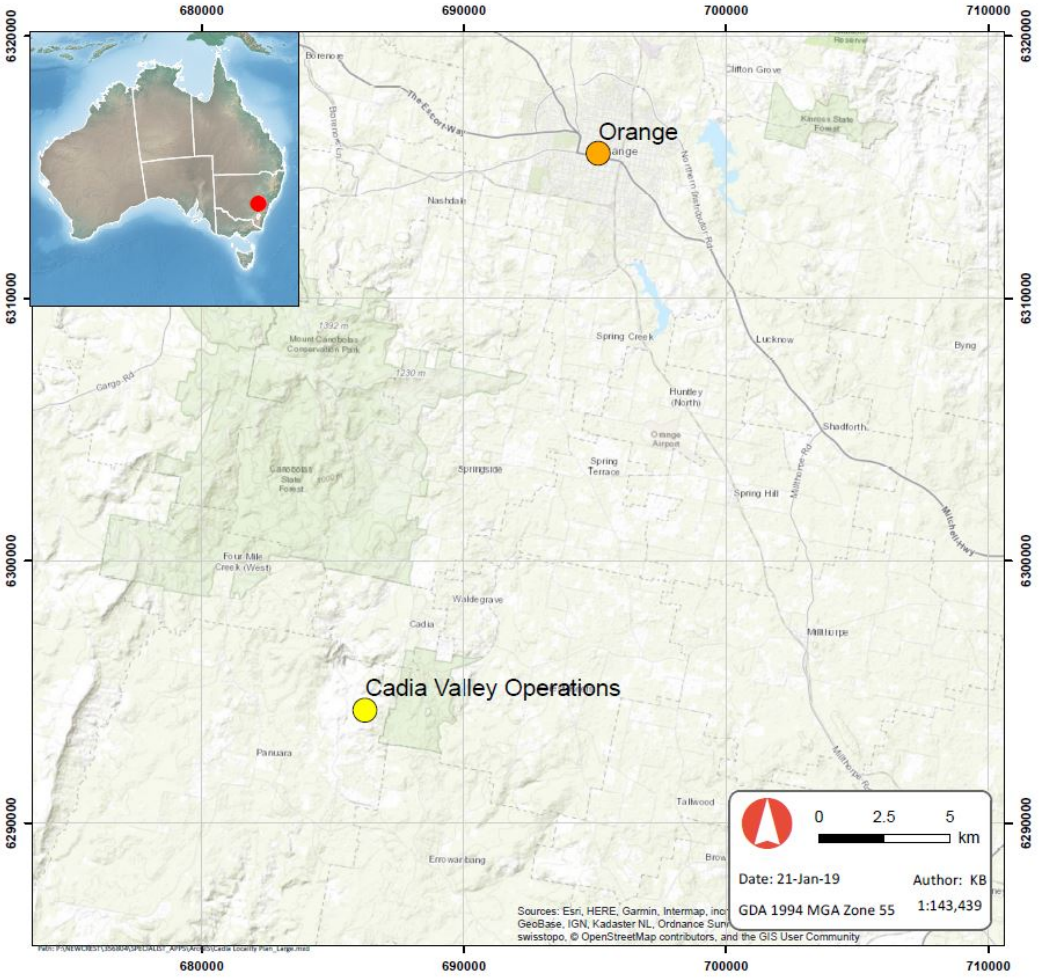


Figure 1-1: Location Map Showing Cadia Valley Operations

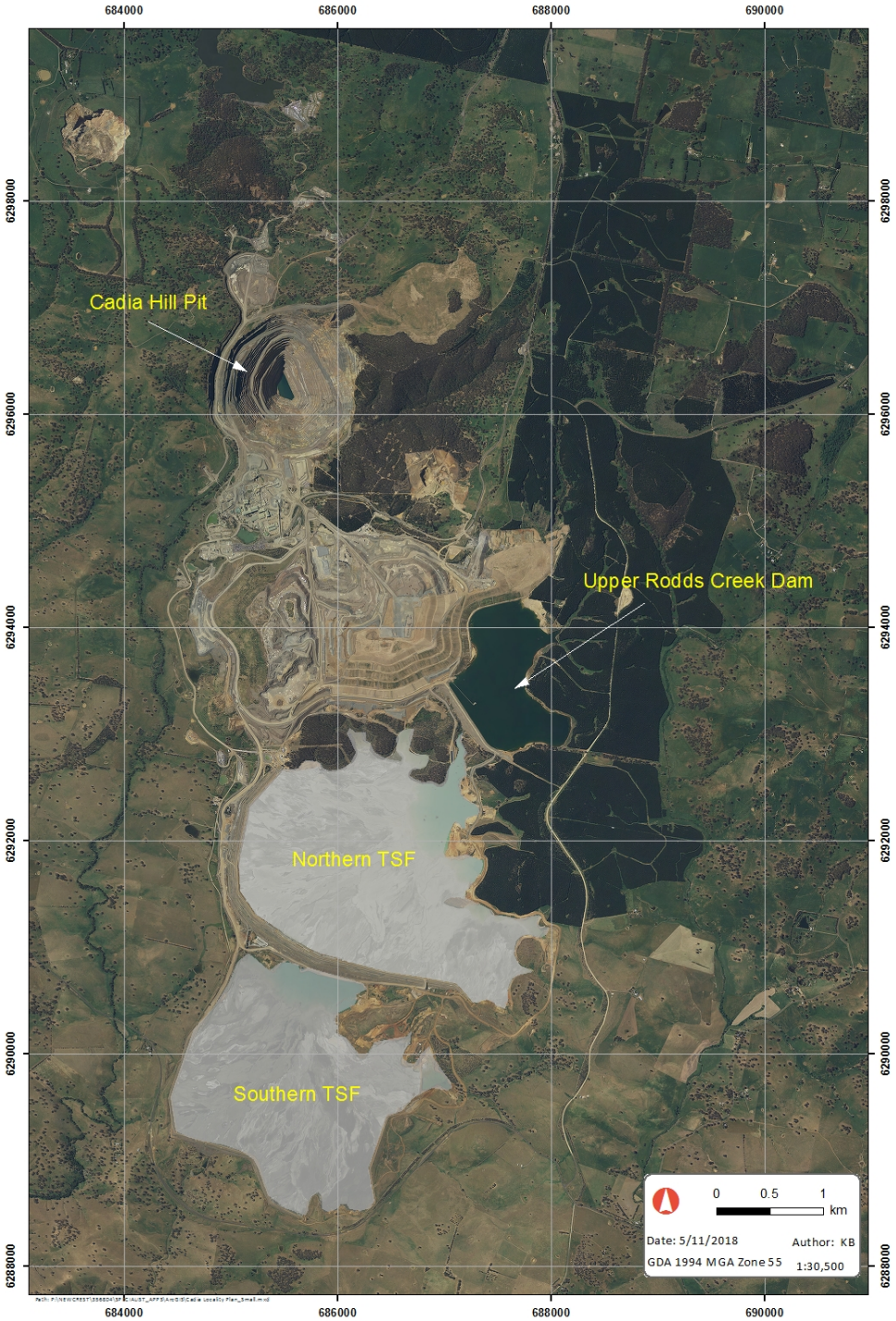


Figure 1-2: Location Map showing the NTSF and STSF

1.1 Terms of Reference

On March 9, 2018, a slump (the Event) occurred in the wall of the NTSF. NML and CHPL engaged Ashurst Australia (Ashurst) to provide legal advice in connection with the Event and to act in any legal proceedings which may arise in relation to the Event.

In order for Ashurst to provide NML and CHPL with legal assistance in connection with the Event, it was necessary for an independent technical investigation to be established into the Event. On behalf of both NML and CHPL, Ashurst engaged:

- Hatch Pty Ltd (Hatch) personnel Ian Gordon and Leigh Cowan, to co-ordinate and manage an independent technical investigation into the Event; and
- An Independent Technical Review Board (ITRB) to undertake the independent technical investigation, with Hatch to co-ordinate, manage and support the ITRB during its investigation. The ITRB members are independent subject matter experts (SMEs) in disciplines of relevance to the investigation of the Event.

The specific terms of reference to the ITRB was to provide independent and unbiased professional judgement and expertise in determining the immediate technical cause(s) of the Event. In so doing, it was requested to focus on the following questions:

- Why did the Event occur?
- Why did the Event occur where it happened?
- Why did the Event occur when it happened?
- Why won't a similar Event happen anywhere else?

The ITRB was not asked to provide an opinion on the roles and responsibilities of individuals or corporations; nor did it do so.

The Terms of Reference for the Operation of the ITRB are included in Appendix A.

1.2 Organisation of the Study

The ITRB members are:

- Mr Michael Jefferies
- Dr Norbert Morgenstern (Chair)
- Dr Dirk van Zyl
- Mr John Wates

Short biographies of each ITRB member appears in Appendix A.

Mr Ian Gordon, acting as Principal Investigator, managed the Hatch team and coordinated their deliverables.

At the recommendation of the ITRB, additional SMEs were retained by Ashurst for specific tasks; Seismology (Dr Gail Atkinson), Hydrogeology (Dr Chris Dickinson) and Deformation Modelling (Dr Joseph Quinn). Short biographies of each of the above are also presented in Appendix A.

Figure 1-3 summarises the organisation and flow of information within the study group.

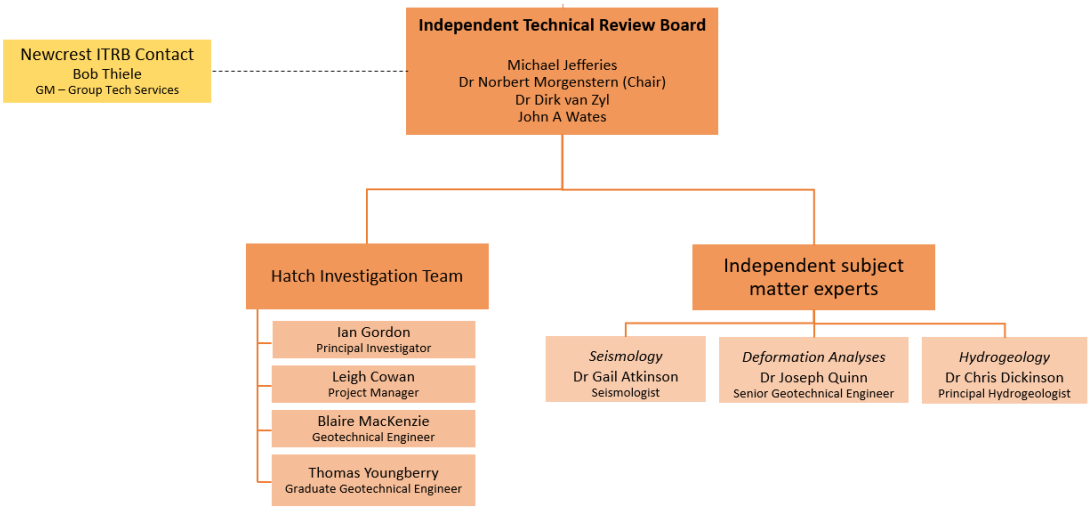


Figure 1-3: Organisation for Study of NTSF Embankment Failure

1.3 Operations

Much of the communication of the ITRB was conducted by teleconference or email. However, it did convene for in-person meetings as follows:

- April 16-20, 2018, at site (excluding Dr Morgenstern)
- July 1-4, 2018, in Vancouver
- October 12-15, 2018, in Vancouver
- January 19-25, 2019 in Brisbane, at site and in Melbourne (excluding Michael Jefferies).
- February 22-26, 2019, in Vancouver

Field, laboratory and analytical studies by Hatch were ongoing throughout the whole study period. Dr Atkinson was commissioned by Ashurst and reported on September 10, 2018. Both Dr Dickinson and Dr Quinn were retained by Ashurst in August 2018. Dr Dickinson reported on January 23, 2019 and Dr Quinn submitted his report on February 27, 2019.

1.4 Report Organisation

The Report that follows is intended to stand alone. However, it relies intimately on the Appendices that are included together with the Report, and they should be taken as a whole for purposes of detailed interpretation. The Appendices identify all of the documents referenced. They include all of the field and laboratory work undertaken, and all of the analytical studies that underpin the interpretation and conclusions made by the ITRB. Internal project document referencing appears in Appendix J in the format YYYY- 001 etc. All reference citations in the main body of the Report are recorded in the normal way: by author and title.

2. The Event

A detailed timeline around the failure is presented in Appendix B. In general terms, prominent cracks in the south face of the NTSF were first observed between 08:00 and 09:00 on the morning of March 9, 2018. Senior site personnel inspected the cracks and identified further cracks throughout the day as they developed. Processing plant operations ceased at 15:00. At 16:00, significant ground heave was detected at the toe of the NTSF adjacent to the cracks observed higher up. This prompted an evacuation of the worksite and a small number of downstream residents. Between 18:45 and 19:00, the failure was discovered by site personnel, who had travelled to the NTSF to make displacement observations. An approximately 300 m section of the NTSF wall had failed between chainage 1850 – 2150 with displacement extending southward by about 170 m as shown in plan on Figure 2-1 and in section on Figure 2-2.

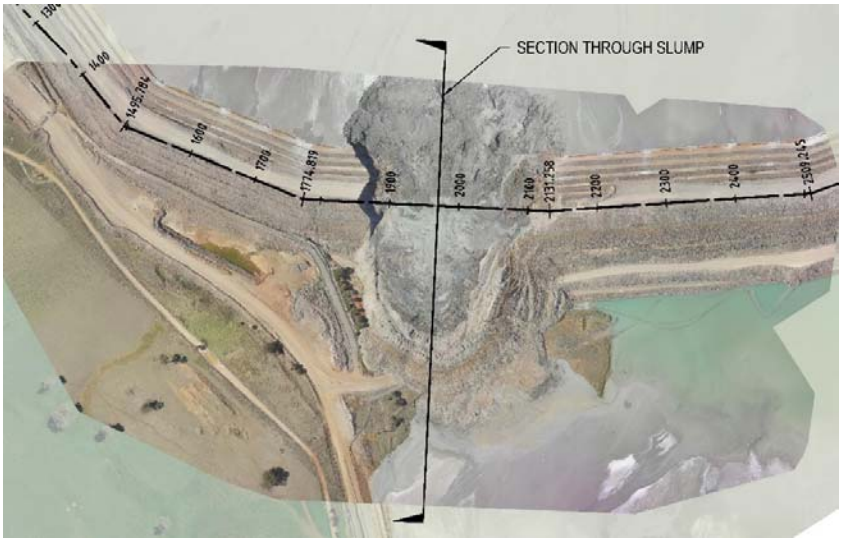


Figure 2-1: NTSF Slump on March 10, 2018, 10:00

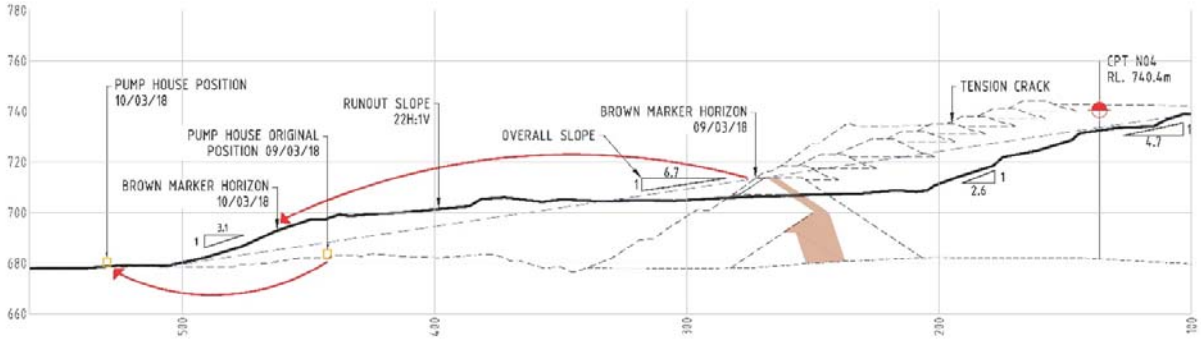


Figure 2-2: Annotated Section Through Slump on March 10, 2018

Morphologically, the movement may be classified as a SLUMP and, given the extent of its movement, prior to its cessation, it can be described as a MOBILE SLUMP. The kinematics of the slump are more translational than rotational, indicating that foundation conditions constituted a controlling factor in the mechanics of the failure. However, at an early stage of the investigation, it was important to screen all reasonable explanations for the failure.

An aerial photograph of the slump area was taken using a drone on March 9, 2018, immediately prior to the slump, (Drawing 1). Aerial photographs were also taken twice daily for a number of days thereafter. The annotated aerial photographs taken on March 9, 10 and 14, 2018 (Drawing 2, Drawing 3, and Drawing 4), show features of the NTSF embankment immediately prior to the slump, features of the slump approximately 15 hours after the Event, and features of

the slump after a secondary liquefaction event which occurred at 19:21 on March 11, 2018. The secondary liquefaction event raised the surface of the slump by approximately 3 m and overflowed the initial slump obscuring a number of the initial features. It extended the runout by a further 50 m. Features of the slump shown on these aerial photographs include: the distribution of materials; the location of sand boils; and the dislocation of recognisable features such as marker beds, pipes, a pump house etc. Annotated sections through the slump on these respective days are provided on Drawing 5. The cracks observed on March 9, 2018 are also shown on the annotated sections. The measured and calculated statistics of the slide are listed below.

- Width at Stage 1 Buttress (RL735) 280 m
- Lateral displacement of rockfill toe 170 m
- Volume of slump (defined by assumed potential failure surface) 720,000 m^3
- Volume of slump on March 10, 2018 1,170,000 m^3
- Volume of slump after March 14, 2018 1,330,000 m^3

The evolution of the Event on March 9, 2018 is characterised by two phases. Phase 1 incorporates all of the precursors of movement up to and including the time at which the worksite was evacuated. Movements in Phase 1 are slow, as the failing mass adjusts to changing states of equilibrium. While not directly observed, Phase 2 must have incorporated relatively sudden losses of resistance and/or increases in loading, to create conditions to accelerate the movements to the distances ultimately achieved. Detailed explanations of both Phases are presented later in this Report. However, it is important to note that had movements terminated in Phase 1, loss of containment would not likely have occurred and the NTSF would have been repairable with relative ease. This was not the actual situation, and the worksite was evacuated prior to the onset of Phase 2. The ITRB were advised that this evacuation followed the CVO Dam Safety Emergency Plan.

In the view of the ITRB, the failure of the Aznalcóllar Tailings Dam in Spain in 1998 has a number of similarities. The post-failure configuration is shown in Figure 2-3. With little to no precursors, the dam failed instantaneously, and the central portion of the dam travelled about 40-50 m. The Aznalcóllar Tailings Dam failed as a result of progressive foundation failure of high plasticity over-consolidated brittle clay. As the dam moved laterally, support of the loose saturated tailings loading the dam was reduced leading to static liquefaction, thereby increasing the load on the dam. The reduction in foundation resistance and the increase in pressure due to liquefaction resulted in accelerating the failing mass to its final position. The circumstances leading to progressive failure were first identified in the forensic investigation following the failure, commissioned by the owner (Servicios de Ingenieria S.A. Eptisa, 1998). The detailed analysis of the failure through its phases have been presented by (Alonso & Gens, 2006b).

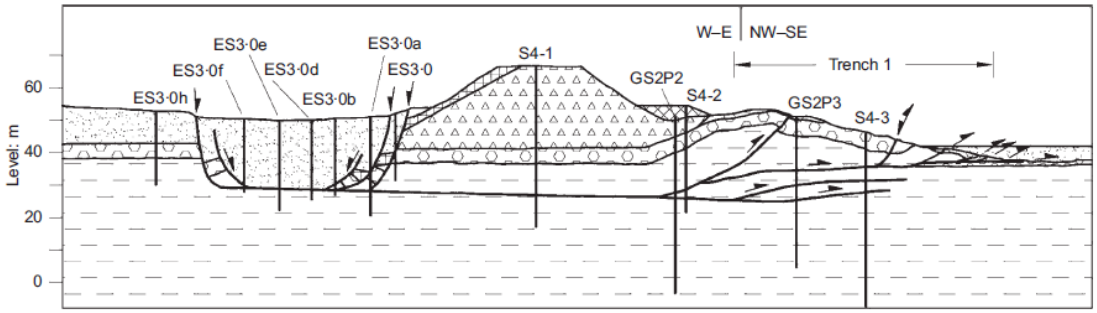


Figure 2-3: Post failure cross-section of Aznalcóllar Tailings Dam: (Alonso & Gens, 2006a)

3. Design, Construction and Response

3.1 Introduction

This section of the Report is intended to summarise many aspects of the design, construction and performance of the NTSF through to the commencement of Phase 2 of the Event. As such, it will contain all salient observations of behaviour that need to be considered in support of the explanation of the Event. Section 3 relies on Appendix B for details.

3.2 Overview of Design and Construction

Initial construction of the NTSF commenced in August 1997 to a height of 50 m. Since then, it has been raised eleven times, with the most recent raising being Stage 10 which commenced in 2017. A summary of the design and construction characteristics is provided in Table 3-1. Details for each stage are noted below.

Table 3-1: Summary of Design and Construction

Stage	Crest Level (mAHD)	Max Height (m)	Construction Type	Design By	Construction Completed
1	700.0	50.0	Conventional	KP	May 1998
2A	707.0	57.0	Downstream	WC	Aug 2000
2B/1	710.5	60.5	Downstream	URS	May 2002
2B/2	714.0	64.0	Downstream	URS	June 2003
3	718.5	68.5	Centreline	URS	Nov 2005
4	723.0	73.0	Upstream	URS	Oct 2008
5	729.0	79.0	Upstream	URS	Aug 2011
6	732.0	82.0	Upstream	URS	Dec 2012
7	735.0	85.0	Upstream	URS	Feb 2014
8	738.0	88.0	Upstream	AECOM	Oct 2015
9	741.0	91.0	Upstream	AECOM	Dec 2016
10	744.0	94.0	Upstream	ATCW	In Progress

Notes:

KP Knight Piesold,
WC Woodward Clyde,
ATCW ATC Williams.
Woodward Clyde was acquired by URS who were subsequently acquired by AECOM.

3.2.1 Stage 1

The Stage 1 starter embankment is an earth and rockfill dam with a maximum height of 50 m. At the time, the final design had the starter dam being raised a further six times using modified centerline construction to a final height of 91 m see Figure 3-1. The Stage 1 embankment was 1680 m long, with a sloping clay core supported by rockfill shoulders with upstream and downstream slopes of 1.5H:1V. A wide transition/filter zone was provided between the clay core and the downstream shoulder of the embankment. Special provisions were made in the layout of the facility to control runoff during construction and seepage. Figure 3-2 shows the typical section for the Stage 1 embankment. Foundation investigations for the Stage 1 embankment relied on drillholes and a large number of test pits. Details are provided in Appendix B.

Little information is available on foundation stripping and core trench excavation. In general, the shoulders of the embankment were designed to be founded on hard clay or extremely weathered rock. However, a large portion of the clay beneath the downstream shoulder of the dam was excavated for use in the clay core.

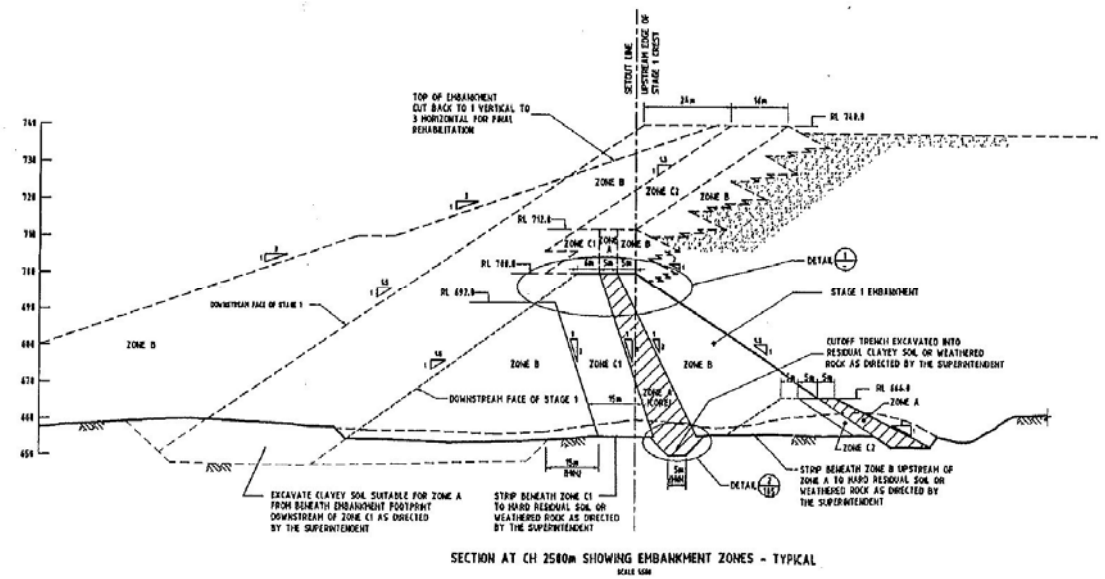


Figure 3-1: Original ultimate design concept using modified centreline construction (1997-001)

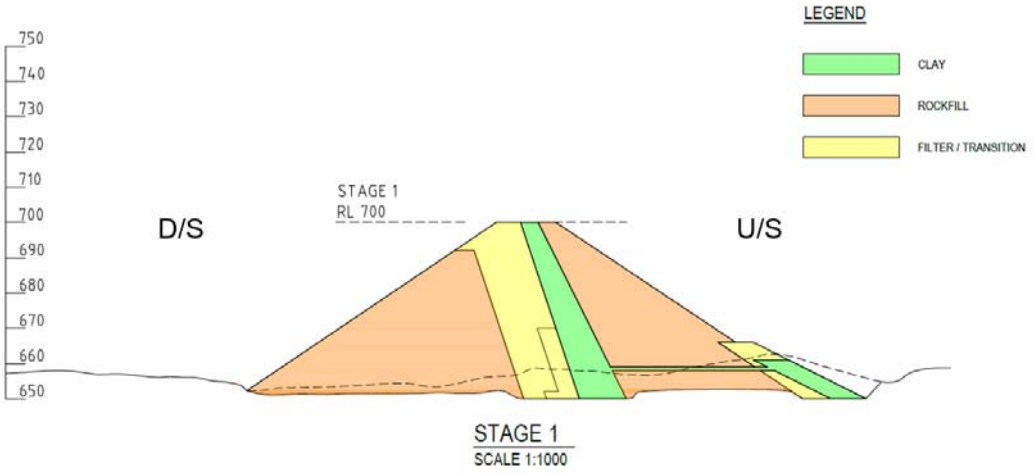


Figure 3-2: Stage 1 Starter Embankment

3.2.2 Stage 2A and 2B

The Stage 2A embankment was a 7 m downstream raise, comprised of a zoned earth and rockfill embankment keyed into the top of the Stage 1 core and where extended on the abutments, the Stage 1 key trench was lengthened. The Stage 2B embankment was also designed as a 7 m downstream raise with zoning identical to Stage 2A, however Stage 2B was constructed in two separate lifts, Stage 2B/1 and Stage 2B/2, each of 3.5 m height. The general arrangement of the Stage 2A and 2B raises is shown in Figure 3-3.

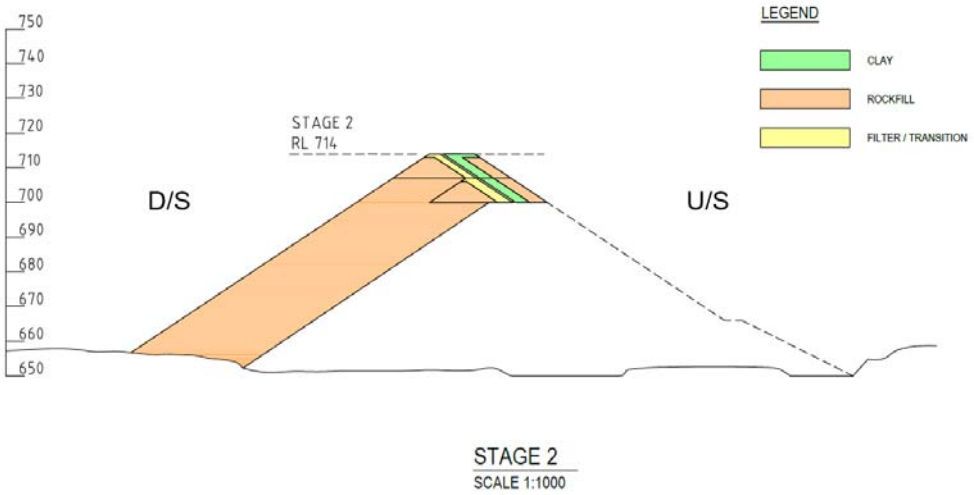


Figure 3-3: Stage 2A and 2B Embankments

3.2.3 Stage 3

Stage 3 began the transition to upstream construction. It has a 4.5 m high zoned earthfill embankment with a central core and rockfill shoulders. Where the embankment was constructed over tailings, a rockfill platform was provided while the core was keyed into the top of the Stage 2B core. The downstream slope in the rockfill remained at 1.5H:1V. The arrangement of the Stage 3 embankment is shown in Figure 3-4.

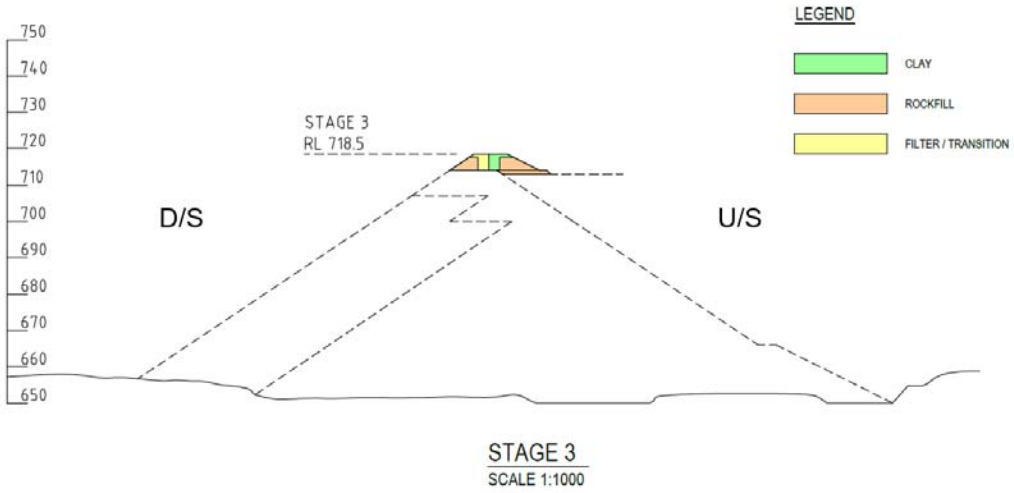


Figure 3-4: Stage 3 Embankment

In addition to the raise, an underdrain system consisting of a slotted collection pipe encapsulated within a filter blanket was provided over the full length of the upstream toe of the Stage 3 embankment. Outlet pipes were provided from the collection pipe to the downstream rockfill batter at 200 m intervals between Chainage 1800 and 3600. The outlet pipes were concrete encased through the clay core with a filter sand plug immediately downstream of the concrete encasement.

3.2.4 Stages 4 to 9

Stages 4 to 9 are upstream raises to the existing embankment with individual heights ranging between 3 and 6 m and with crest widths of 9 m. Except for Stage 5, the downstream slopes are 2H:1V. In the case of Stage 5, it was flattened to 2.5H:1V. Each stage required a working platform of mine waste to be placed over the tailings surface. The rockfill shoulder in these stages was encapsulated in clay which eliminated tailings migration as well as reducing local drainage. Figure 3-5 shows the section to the end of Stage 9.

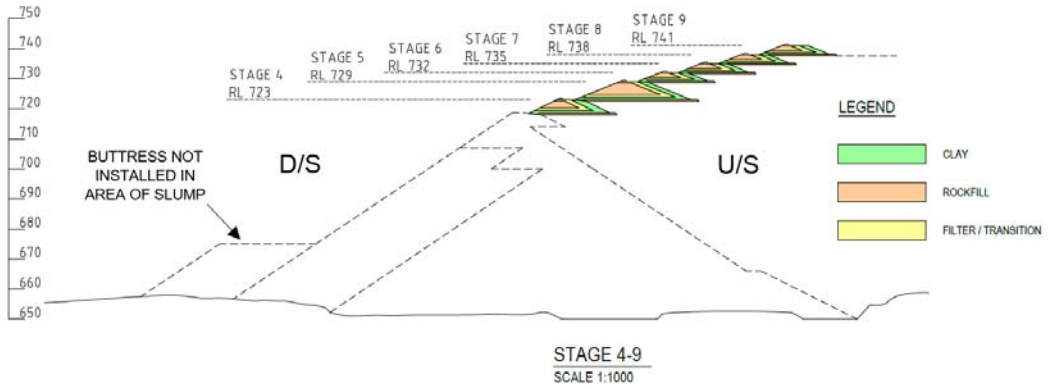


Figure 3-5: Stage 4 to 9 Embankment Configuration

In addition to raising the embankment, prior to the construction to the Stage 4 raise in mid-2007, a 35 m wide berm of igneous mine waste was placed through the STSF decant pond at the toe of the NTSF. Over the following years, the berm was progressively raised and lengthened to keep it above the STSF decant pond level. This berm did not extend to the location of the Event.

It is noteworthy that the design implemented from Stage 4 to Stage 9 differed significantly from that initially proposed at Stage 1, as shown in Figure 3-1.

3.2.5 Stage 10

The instability of the NTSF occurred during construction associated with the Stage 10 raise, and therefore, it is of some importance to understand the details. The Stage 10 embankment is a 3 m high zoned earthfill embankment similar to the previous raises. It commenced on February 27, 2017, and generally advanced from the northwest (Chainage 0) to the south and east. Weekly plans indicate that the Stage 10 embankment construction in the vicinity of the Event (Ch. 1800-2200) was essentially complete by the end of July 2017.

However, following a campaign of cone penetration tests in 2017, the designers concluded that the overall strength parameters, when used in stability analyses, resulted in Factors of Safety that were too low. As a consequence, they recommended the construction of two buttresses to achieve acceptable Factors of Safety under both static and dynamic loading. The two buttresses, referred to as Stage 1 Buttress and Stage 2 Buttress, are shown in Figure 3-6 together with Stage 10. The buttress that is shown to be supporting the Stage 2 Buttress did not exist in the slump area.

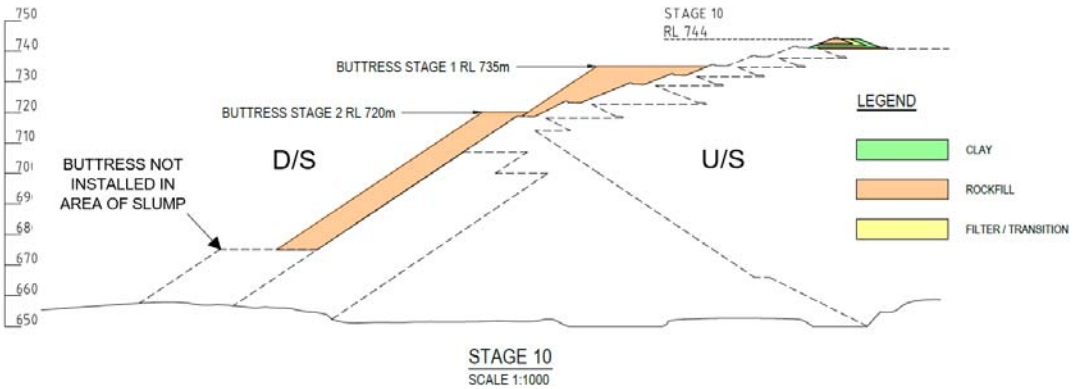


Figure 3-6: Stage 10 Embankment Configuration

An assessment of construction progress, primarily from satellite imagery, reveals that the Stage 1 Buttress construction through the NTSF slump began on December 15, 2017, and was completed by March 5, 2018.

At the time of the Event, the Stage 2 Buttress construction had not commenced in the slump area but had commenced in other sections of the NTSF. Based on information obtained from test pits, the designers, in 2017, had identified the need for stripping at the toe of the NTSF prior to Stage 2 Buttress placement. In one stripping area, where the slump eventually occurred, in excess of 4 m of tailings had accumulated in a depression which required at least partial removal. This excavation (approximately 5.5 m deep), was undertaken in January 2018, exposing weak weathered foundation material. This is illustrated in Figure 3-7. This exposure remained open until the time of the Event.



Figure 3-7: Exposed foundation on January 18, 2018

3.3 Overview of Performance

3.3.1 Introduction

Monitoring of the performance of TSF structures is routinely carried out to verify that the structures are behaving as intended. At the NTSF, monitoring was undertaken of pore water pressures generated in the impounded tailings, of seepage emissions, and of deformation of the structure. Details of these monitoring programs are given in Appendix B.

Another factor possibly affecting performance, visible or not, was the influence of two earthquakes with proximate epicentres that occurred prior to the failure. This is also addressed in this study.

Finally, as the NTSF approached the end of Phase 1, and about 8 hours before the Event, adverse effects in the form of cracks and bulges were observed and recorded. The explanation of failure in this Report has reconciled these observations to the degree practical.

3.3.2 *Piezometers*

Piezometers are used to measure the water pressures in the ground. The higher the water pressure at a location, the lower is the available strength, and hence, the stable design of a tailings dam generally has limitations on tolerable water pressures associated with it.

The longevity of such instrumentation is variable, and at the NTSF, the installation was continually upgraded as regarded appropriate. Water pressure data are also obtained as part of cone penetration testing. Annual surveillance reports from the NTSF did not raise any concerns with regard to the observations from the piezometers. Details are provided in Appendix B. The last surveillance report prior to the Event notes the following with regard to the piezometric data;

- the large variation in interpreted piezometric levels is due to their spatial location and depth of installation;
- levels have generally increased in accordance with the increasing decant pond level, but at a reduced rate;
- both vibrating wire piezometers and pneumatic piezometers show a similar trend in level, but not a consistent variation;
- no piezometric response to the sequential raises or to the construction of the Stage 1
- piezometers on the western side of the NTSF indicate piezometric levels generally higher than the eastern side (at elevation RL 735 m); the failure zone appears to correspond with the location of relatively high pore pressure (significantly higher than the drain situated at elevation RL 714 m. (see Figure 3-8); and
- deeper piezometers (and pore water pressure dissipation tests undertaken as part of the 2017 CPTu program) indicate a reduction in pore pressure trend which has been interpreted to be the result of downward drainage, with a pressure head that is less than hydrostatic.

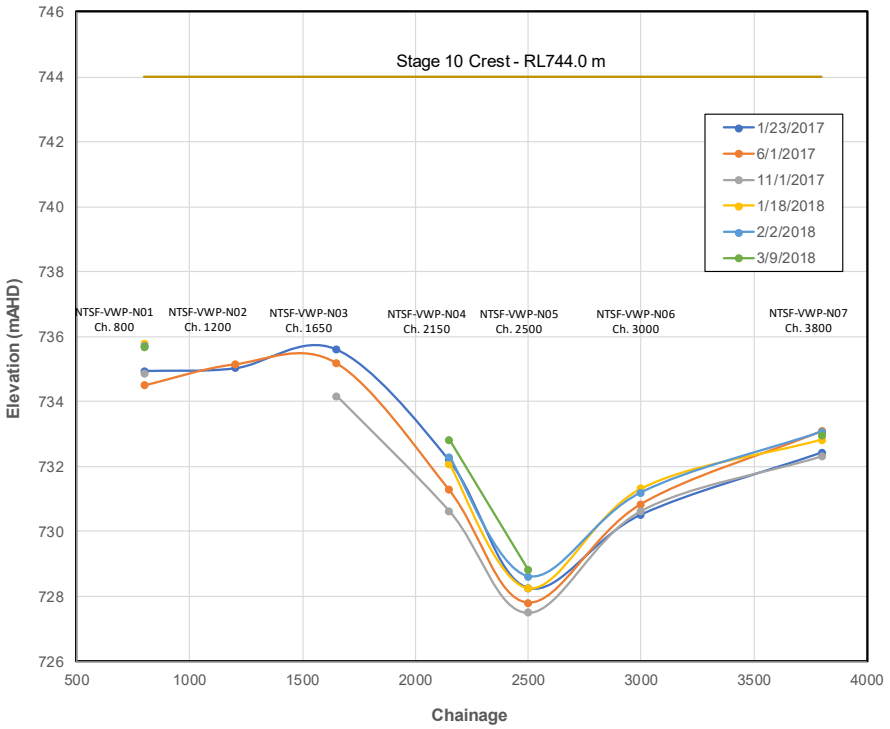


Figure 3-8: Longitudinal profile of piezometric surface with time

The piezometric data are discussed more fully in Appendix B and have been incorporated in a site-wide hydrogeological synthesis that is presented as Appendix F.

3.3.3 Seepage

In 2000, seepage was observed emerging from the right abutment rockfill toe at Chainage 2200 and downstream of the toe of the left abutment at Chainage 2850. Since 2006, when the decant pond and tailings from the STSF had begun to encroach on the toe of the NTSF, there had been limited opportunity to observe and monitor seepage from beneath the Southern Embankment of the NTSF.

A drainage system was installed at the upstream toe of the Stage 3 embankment with outlets to the downstream face at 200 m intervals between Chainage 1800 and 3600. Some underdrains were also installed at a few locations below the Stage 5 and Stage 8 western embankments of the NTSF. Details are provided in Appendix B.

The Stage 3 drains have generally remained dry, except for the drain at Chainage 1800 which intercepts seepage along the full length of the western embankment. Drain flow measurements between early 2015 and February 2018 range between 30 and 50 litres/minute as shown in Figure 3-9. Other observations of wet spots are summarised in Appendix B.

As with the piezometric information, seepage response has also been incorporated in the site-wide hydrogeological synthesis presented in Appendix F.

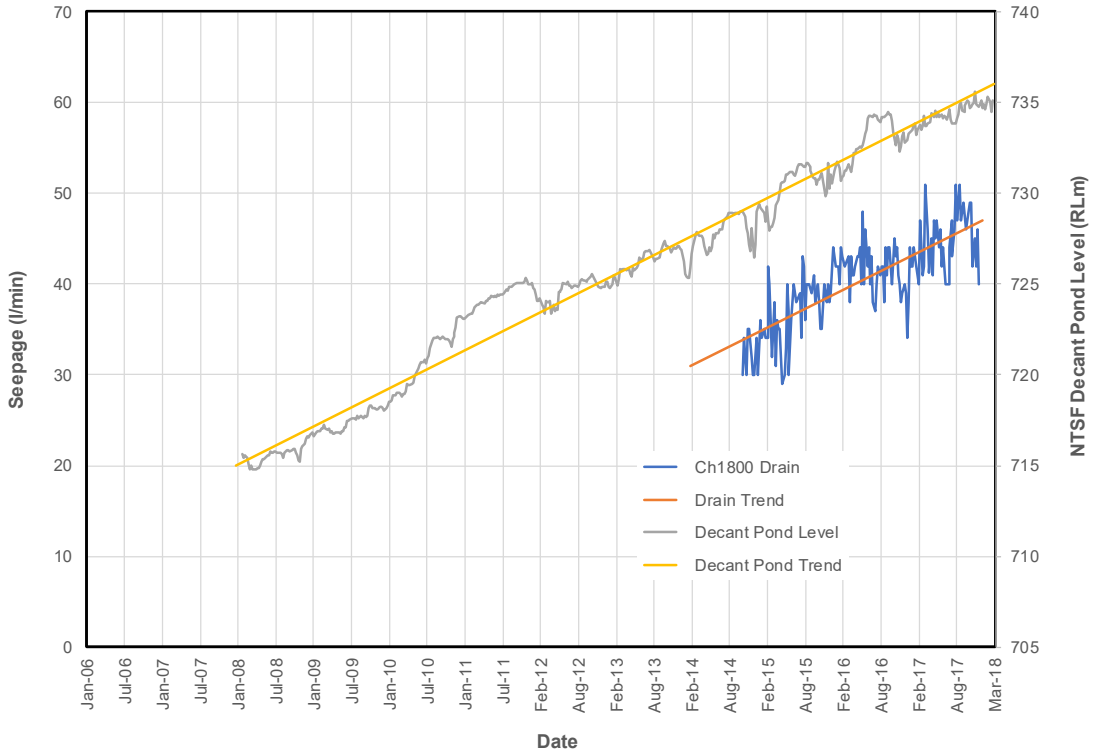


Figure 3-9: Ch1800 drain flow and NTSF decant pond level

3.3.4 Displacements

3.3.4.1 *Terrestrial Monitoring*

Initially, survey reference pins were concreted into the crest of each raise to monitor both horizontal and vertical movement. However, as the pins were surveyed using Global Positioning System (GPS), it was found that the data were unreliable, and an alternative method was implemented.

From October 2013, survey prisms grouted into large boulders on the dam crests were used for monitoring deformations. Prisms were located on the crests of Stages 4, 5 and 7. However, these were not placed in position until the subsequent embankment stage had been constructed. Both vertical and horizontal displacements were recorded. Displacements perpendicular and parallel to the dam axis, together with vertical displacements are shown in Figure 3-10.

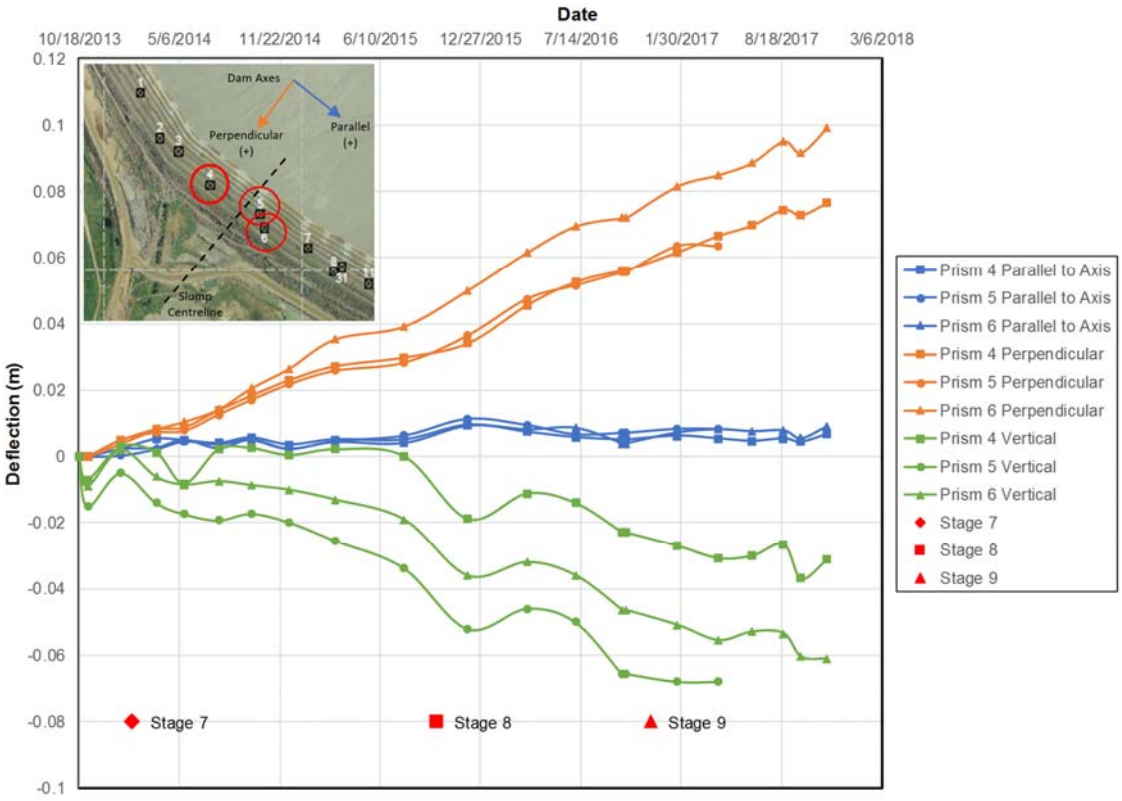


Figure 3-10: Survey prism movement in five years preceding the slump

From an assessment of the staged response recorded, the following conclusions can be made;

- Terrestrial survey of prisms located on Stages 4, 5 and 7 crests indicate a down valley movement that is consistent with an earth and rockfill embankment of the height of the NTSF, including its upstream raises;
- However, the down valley movement in the vicinity of the slump is larger than that observed at a similar embankment height on the eastern side of the valley and is similar to that observed at the maximum embankment section. This suggests the influence of a potential underlying weakness in the embankment or foundation.

3.3.4.2 Satellite Monitoring

Satellite monitoring was not being used by site prior to the Event. However, following the Event, Ashurst engaged Otus Intelligence Group Pty. Ltd. (Otus) to derive surface movement measurements in the vicinity of the NTSF using historical satellite Interferometry Synthetic Aperture Radar (InSAR) data. Whereas the movements from terrestrial survey can be resolved into three components (x,y,z), the surface movements measurements (SMM) associated with this InSAR data can only be resolved in a single direction in the satellite line-of-sight (LOS). This concept is shown on Figure 3-11 and is discussed in Appendix B, Annexure BG. As a result, the data cannot be directly compared with terrestrial survey, but can be in terms of trend.

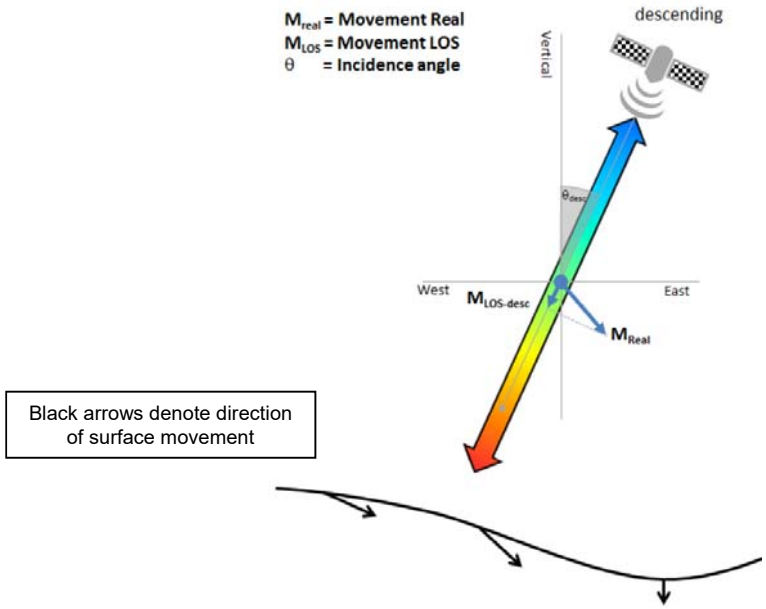


Figure 3-11: InSAR surface movement measurements based on data from a single satellite

The results of the satellite monitoring, together with a critical review of the reliability and accuracy of the data are presented in Appendix B. InSAR data processed by others was also available to the ITRB for comparison. Both produced similar results, showing either increased movement or increased rate of movement in the vicinity of the failure, prior to the Event. The Otus data for the crest, mid-height and toe in the vicinity of the slump (Ch. 2000) are presented in Figure 3-12.

Data at the crest show an increased rate of movement from January 8, 2018. A small rate of movement was observed at mid-height while none was apparent at the toe. Comparing this with terrestrial survey data reveals a similar rate of movement of the NTSF embankment increasing markedly at the beginning of January 2018, see Figure 3-13. It is of interest to note that this corresponds with the construction of the Stage 1 Buttress and excavation at the toe of the NTSF.

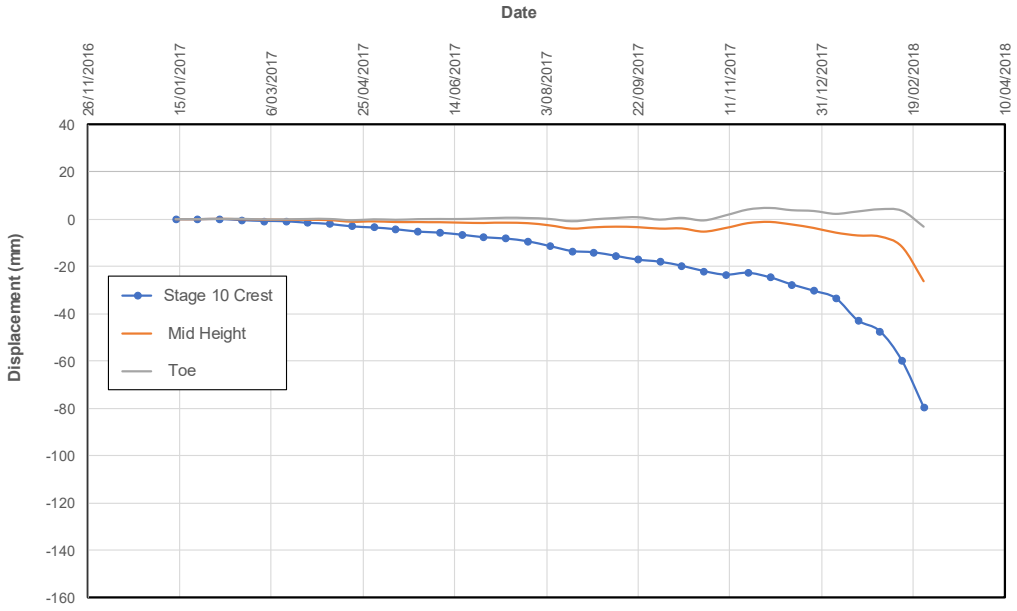


Figure 3-12: InSAR surface movement measurements at Ch 2000

As the SMM data cannot be resolved into the three components of movement and can only be compared with terrestrial measurements in terms of trend, vertical scales on Figure 3-13 are different.

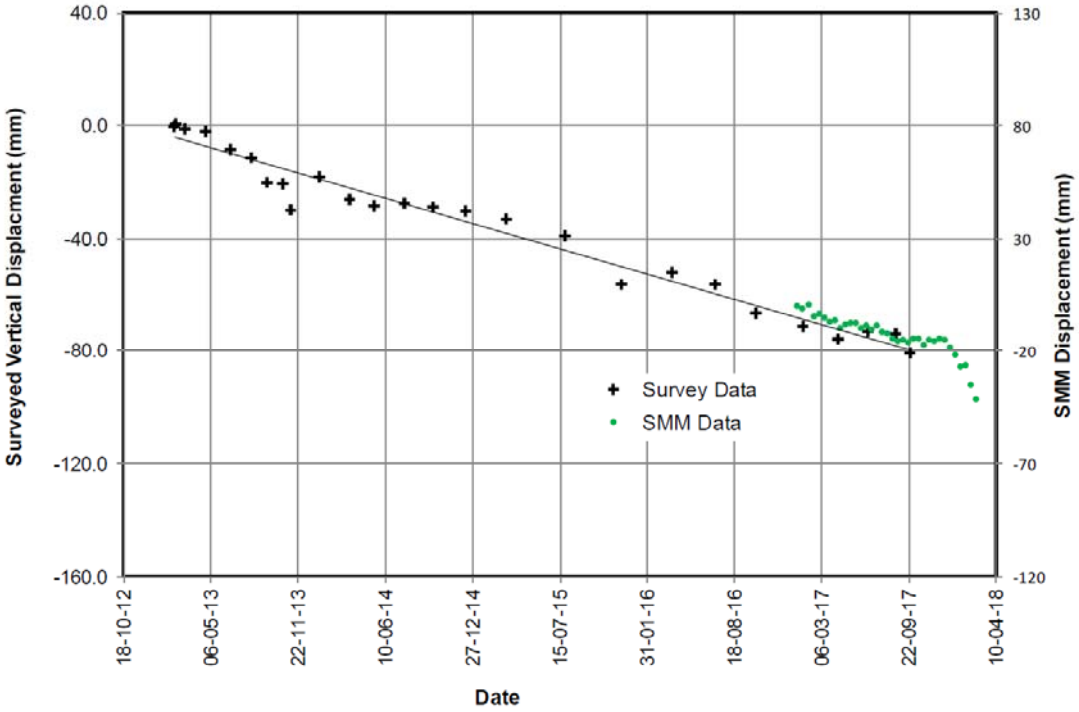


Figure 3-13: Prism 6 - Comparison of survey and InSAR SMM data

3.3.5 *Seismicity*

In addition to increasing loading on the foundation prior to the Event, the site also experienced two earthquakes (Magnitude ~ 3) on March 8, 2018. This was one day before the Event. While under normal conditions such small earthquakes would not be regarded as consequential to the stability of a large dam designed to conventional criteria, experience such as that at Samarco (Fundão Tailings Dam Review Panel, 2016) indicated that when a structure is in a fragile state, (such as in the process of yielding), and is loaded by even small earthquakes, the implications may be consequential. The seismic history of the site and recommended ground motions are presented in Appendix I and the influence of these design ground motions on the performance of the NTSF are evaluated in Section 8 and are provided in more detail in Appendix H.

3.3.6 *Direct Observation*

Direct observations of the behaviour of the NTSF, just prior to the Event, provide invaluable information regarding the kinematics of the emerging mechanism. A summary of all such observations is also included in Appendix B.

Figure 3-14 shows cracking on the Stage 5 crest at 07:48 on the morning of the Event. Figure 3-15 shows cracking in Stage 8 looking west, and Figure 3-16 taken between 15:50 and 16:30 shows cracking and heaving at the toe of the embankment, indicating that failure was imminent. In line with the CVO Dam Safety Emergency Plan, the decision was made to evacuate the work-site which, given the dynamics of Phase 2 of the Event, most likely prevented substantial injury to site staff. The observation that the vertical cracks on the various stages displayed no vertical offset, but did indicate a significant extension displacement, is also of diagnostic value.



Figure 3-14: Photograph of cracking on the Stage 5 crest beside Standpipe P9 taken at 07:48, March 9, 2018



Figure 3-15: Stage 8 crest cracking looking west, March 9, 2018



Figure 3-16: Cracking and heaving of haul road at Chainage 2060, March 9, 2018

4. NTSF Field Characterisation

4.1 Overview

NTSF field characterisation activities span over many years. Regional and site-specific geological studies combined with foundation investigations form the basis for development of an understanding of the foundation materials in the area of the TSFs. Insitu investigations of the tailings provide their characterisation.

Further details of the NTSF field characterisation activities are provided in Appendix C. This section reviews the highlights of these activities.

4.2 Geology

4.2.1 Stratigraphy

The regional geology of the Cadia district is complex and is discussed in detail in Appendix C. Formations outcropping in the immediate vicinity of the NTSF are shown in Drawing 6 and are described below.

4.2.2 Weemalla Formation

In the Cadia district the observed thickness of the Weemalla Formation is between 1300 m and 3500 m and comprises laminated siltstone and lesser siliceous siltstone, mudstone and feldspathic sandstone.

Although the regional contact between the Weemalla Formation and overlying Forest Reef Volcanics (see Section 4.2.3) is gradational, the contact in the vicinity of the NTSF is faulted, with the Weemalla Formation lying to the west of the NTSF.

4.2.3 Forest Reef Volcanics

The Forest Reef Volcanics (FRV) are the dominant rock type in the vicinity of both the NTSF and STSF. The FRV comprises a thick (2.5 km) sequence of mafic to intermediate volcanic derived sedimentary breccias and lesser sandstones intercalated with basaltic andesite and andesitic lavas. Deposition of the FRV spanned the Late Ordovician to Early Silurian.

Volcanic eruptions appear to have occurred from a low relief, submarine volcanic complex with multiple vents, producing thickly stacked lava sequences. Explosive volcanism occurred during the later stages of the FRV resulting in ash fall deposits in a shallow water environment.

Petrographic analyses of rocks undertaken as part of the ITRB investigations indicate that the FRV are comprised of altered andesite and pyroxene andesites that were potentially extruded into shallow water.

4.2.4 Waugoola Group

The Silurian Waugoola Group lies to the north and east of the NTSF, of which the gently dipping Cadia Coach Shale is the dominant Formation in the vicinity of the NTSF. The Cadia Coach Shale was intersected in the north western foundation area of the NTSF.

4.2.5 Tertiary Basalt

Tertiary basalt crops out along elevated ridgelines adjacent to both the NTSF and STSF. The basalts are typically olivine basalt and are part of the now dissected Canobolos Volcanic Complex. The basalts are of Middle Miocene age. They comprise at least six separate flows and are up to 80 m thick.

4.2.6 Paleosoils

Paleosoils are soils developed under a past geological environment preserved by overlying materials. At CVO, basalts overlie paleosoils comprising alluvium and residual soils developed over both the FRV and Weemalla Formation.

In the context of this report, paleo residual soils are included as part of the residual profile of their respective underlying formations while alluvial paleosoils are referred to as paleo alluvium.

The presence of basalt overlying weaker substrates such as paleo alluvium and weathered FRV deposits constitutes a significant complexity and challenge for site characterisation at CVO.

4.2.7 *Geologic Structure*

The most prominent fault in the vicinity of the TSFs is the roughly north-south striking Wyangala-Werribee Thrust Fault system also known as the Werribee – Cadiangullong Fault Zone. The faults are located to the west of Rodds Creek and traverse the western side of both the NTSF and STSF. The faults extend over 30 km and appear as a series of two or three parallel westward dipping thrust faults.

To the south of the STSF, the position of the Werribee – Cadiangullong Fault Zone has been confirmed by geological mapping, while in the vicinity of the NTSF where it is overlain by basalt, it has been largely inferred from early (1997) aeromagnetic surveys.

North of the NTSF, detailed mapping completed for the Cadia East and Cadia Hill areas in 2007, revised the location of the Werribee – Cadiangullong Fault Zone and placed it to the west of its original position. This latter position has been confirmed by drilling undertaken as part of the ITRB investigations.

4.3 Previous Investigations

4.3.1 *Foundation Investigations*

Foundation investigations completed in the vicinity of the NTSF and STSF are summarised in Table 4-1 and additional details are provided in Appendix C.

Table 4-1: Summary of previous foundation investigations

Year	Drillholes	Test Pits	Comments
1995	9	64	NTSF Foundations & Storage
1997	10	23	NTSF Foundations & Storage
1997	-	31	NTSF Stage 1 Core Trench
2000	7	41	STSF Foundations & Storage
2017	-	9	Buttress Foundations
2018	5	-	NTSF & STSF Clay Foundations

The locations of previous investigations in the vicinity of the NTSF are shown in Drawing 6. Table 4-2 provides a summary of the drillholes located in the vicinity of the NTSF embankment failure, while geotechnical logs of these drillholes (reproduced in gINT format) are included in Appendix C, Annexure CK.

Table 4-2: Summary of drillhole information

Hole ID	Embankment Chainage	Total Depth (m)	Soil (m)	Basalt (m)	Paleosol (m)	Forest Reef Volcanic	Sedimentary Strata
BH107	1470	20.0	5.2	0.9	1.8		12.0
BH106	1750	15.8	4.3	7.9	1.9	1.7	
BH020	1950	15.0	1.0	14.0 (1)			
BH101	2090	20.6	3.3			17.3	
BH102	2330	14.8	2.6			12.3	
BH017	2480	32.2	5.0			27.2	
BH103	2690	21.3	2.9			18.4	

Notes:

(1) Although basalt was recorded for the full depth of this hole it is considered that this hole was either incorrectly located or incorrectly logged, in which case it is most likely FRV.

4.3.2 Tailings Investigations

4.3.2.1 Methodology

Due to the excessive disturbance associated with sampling and handling procedures, it is not common to test tailings in the laboratory in an undisturbed condition. Therefore, practice relies on insitu tests with the cone penetration test (CPT) being the method of choice. The CPT is standardised and has been adopted in this study for tailings characterisation. The CPT involves hydraulically pushing a probe (most usually 35 mm diameter) into the ground at a steady rate (20 mm/sec) and measuring tip resistance (q_c), sleeve friction (f_s) and the pore water pressure (u_2). Figure 4-1 illustrates equipment used for pushing the probe and provides an illustration on the internal construction of the probe.



Figure 4-1: Illustration of CPT rig (left) and probe details (right)

An important application of the CPT is to determine the state of the tailings insitu. Granular material like tailings behave in different ways depending on their insitu density. If loose they contract when sheared and if dense they dilate (expand). With ongoing deformation, the material converges on a state with no changes of volume or void ratio. This is known as the critical state. The CPT provides a method for quantifying the void ratio of the tailings with respect to this critical state.

Identification of tailings that are loose of critical state (i.e. have a higher void ratio at a given stress level), is a critical element for evaluating the potential for liquefaction.

4.3.2.2 CPT 2004

Prior to the Stage 3 design, three CPT tests to a maximum depth of 16 m were completed. The tests were supplemented by hand vane shear tests. The aim of the tailings investigation was to provide a tailings strength profile for use in the stability analyses of Stage 3-6 upstream raises.

The locations of these tests are not known, and data are in hard copy format only (2004-001).

4.3.2.3 CPTu 2013

In 2013, additional CPT tests were conducted at three locations where fingers were constructed onto the tailings surface. The locations of the tests are shown on Drawing 7, while a summary of the type and number of tests is provided in Table 4-3.

Two CPTu (CPT with pore pressure measurements) tests were completed at each location, with the second mostly being used to conduct pore water pressure dissipation tests (PWPD) at specified depths. At the time, the CPTu data was used to assess the liquefaction potential of the tailings.

Table 4-3: Summary of 2013 Tailings Investigation

Investigation Type	Test Location					
	N1/1	N1/2	N2/1	N2/2	N3/1	N3/2
CPTu Depth (m)	31.5	27.9	39.5	39.5	39.5	39.5
CPTu Dissipation Tests	-	4	2	1	-	3

4.3.2.4 CPTu 2017

As part of the Stage 10 design eleven CPTu tests with dissipation testing were completed (2017-010). In addition, vane shear testing and seismic shear wave testing as well as disturbed and undisturbed sampling were undertaken. Piezometers were also installed in some CPTu locations as part of this work. This work provided sufficient and particularly valuable information to the ITRB.

Seven CPTu tests were carried out approximately 25 m upstream of the Stage 9 embankment, one CPTu test was carried out approximately 45 m upstream of the Stage 9 embankment and three tests were carried out through the Stage 5 embankment crest. At the latter locations, holes were pre-drilled through the Stage 4 and 5 embankments.

Investigation locations are shown on Drawing 7, whilst a summary of the type and number of field tests is provided in Table 4-4. Interpreted CPTu profiles are provided in Appendix E.

Vane shear testing was carried out adjacent to three of the CPTu tests and recorded both peak undrained strength and the residual undrained strength after large deformations. Tests were undertaken using either a 50 x 100 mm or 75 x 150 mm vane and a constant rotation of 12 degrees/min. These were used to provide a correlation between cone resistance and undrained shear strength.

An unusual and important aspect of this investigation was recovery of undisturbed tailings using a piston-pneumatic-injection (PPI) sampler, with subsequent careful sample handling and density measurement. Disturbed tailings samples were recovered using a Vertek Sampler.

Shear wave velocity measurements were made separately to the CPTu using a seismic dilatometer (SDMT) with a sensor spacing of 0.5 m.

Table 4-4: Summary of 2017 NTSF Tailings Investigation

Investigation Type	Test Location (Prefixed by N)										
	01	02	02A	03	04	05	06	07	08A	09	10
Stage 9 Fingers	✓	✓	✓	✓	✓	✓	✓	✓			
Stage 5 Crest									✓	✓	✓
CPTu Depth (m)	38.4	39.4	15.0	51.6	58.7	65.5	51.8	28.6	24.4	25.0	23.6
CPTu Dissipation Tests	2	2	1	3	4	4	3	2	2	-	1
Shear Wave Velocity Depth (m)	36	38		48	57	63	45	27			
Vane Shear Tests	5				4			6			
Undisturbed Samples (63 mm)	1			2	2	2		4			
Piezometer Depth (m)	10	10		10	16	16	16	16			

4.3.3 *Construction Materials Investigations*

A number of investigations were completed around the NTSF to identify suitable clay for low permeability sections of the embankments. These investigations identified materials ranging from high plasticity residual basaltic and andesitic clays to low plasticity Tertiary and Quaternary sandy clays, all of which were considered appropriate for use in the TSFs. Detailed results of these investigations and associated laboratory testing are summarised in Section 5.4.

4.4 ITRB Field Investigations

4.4.1 *Overview*

Following the initial ITRB site visit in April 2018, a Scope of Works (SOW) for Geotechnical Field Investigations in the vicinity of the NTSF embankment failure was prepared by Hatch and endorsed by the ITRB. The subsurface investigations endorsed by the ITRB had a number of objectives. These included:

- Obtaining representative samples of tailings from both upstream of the NTSF failure and within the slump for advanced laboratory testing;
- Confirming the geological model for the foundations, in particular the distribution of Tertiary basalt and presence of paleosoils beneath the basalt;
- Assessing the hydraulic gradient within the foundation bedrock, in particular the Tertiary basalt;
- Obtaining undisturbed samples of foundation soils for advanced laboratory testing to determine their strength and deformation parameters;
- Obtaining undisturbed samples of the embankment clay core for advanced laboratory testing to determine its strength and deformation parameters; and
- Identifying the depth of tailings and potential embankment remnants in the NTSF failure zone.

The investigations completed on behalf of the ITRB consisted of the following:

- Four test pits with undisturbed block sampling;
- One hand auger hole and one hand sample;
- Fourteen sonic drillholes with a total depth of 618 m;
- Vibrating Wire Piezometer (VWP) installation in ten drillholes; and
- Electrical Resistivity Imaging (ERI) traverse, total length 650 m.

With the exception of one test pit (TP405), the location of the ITRB investigations are shown on Drawing 8. Figure 4-2 displays the effort and quality associated with undisturbed block sampling. Detailed discussions of sampling procedures are also presented in Appendix C.

a) b)

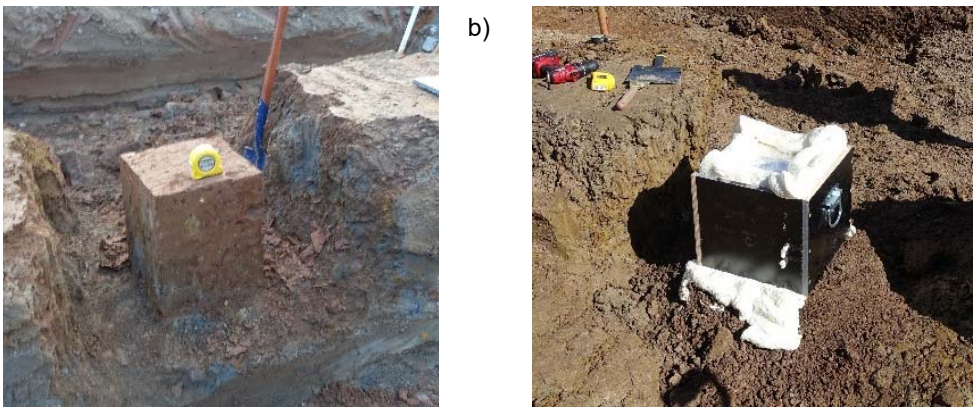


Figure 4-2: Excavated (a) and partially boxed undisturbed block sample (b)

4.5 GHD Investigations

Following the Event, GHD were retained by Ashurst to undertake geotechnical investigations to confirm the adequacy of the STSF to receive tailings discharge, as well as four drillholes in the immediate vicinity of the NTSF.

Investigations completed by GHD included:

- Nineteen drillholes numbered CE382 to CE393 and CE398 to CE404;
- Seismic refraction traverses (SRT) ~ 10 km; and
- ERI ~ 10 km

The location of drillholes CE398, CE399, CE400, CE401, CE403 and CE404 are shown on Drawing 8, while geotechnical logs of these holes are included in Appendix C Annexure CF.

4.6 Newcrest Investigations

Newcrest drilled four inclined holes and one vertical hole with a total length of 2094 m to assist in resolving the location of faulting in the vicinity of the NTSF embankment failure. Drillholes CE380, CE381, and CE396 were located approximately 600 m west of the slump and confirmed the location of the Wyangala-Werribee Fault. Drillholes CE409 and CE431 were a pair of ‘scissor holes’ angled beneath the slump and did not identify the presence of bedrock faulting.

The location of these holes is shown on Drawing 8. All of this information led the ITRB to the view that the presence of bedrock faulting was not consequential to the Event.

4.7 Geological Model at Slump

The results from the drilling and sampling investigation conducted by the ITRB has been summarised and integrated in Appendix C. This integration reveals that basalt present at the site has been partially removed by weathering, and paleosoils beneath the basalt appear to either lens out or be removed by erosion. In addition, the underlying FRV materials are variably weathered. A major finding of this investigation is the existence of low density materials within the FRV, see Figure 4-3. On the basis of this information, it is possible to distinguish between two units; FRV Unit A and FRV Unit B. FRV Unit A has a significantly higher void ratio and lower density when compared with FRV Unit B. More importantly, as will be discussed in detail in Section 5, FRV Unit A is relatively weak, highly compressible, and strain weakening when subjected to load. Due to its close proximity to the foundation level, FRV Unit A constitutes the most significant controlling feature that led to the Event.

It is the view of the ITRB that the geological section at the NTSF embankment failure is best described by drillhole CE416 located on its western edge. This hole, together with the hole at the centre of the slump (CE435) and the hole immediately east of the slump (CE432) are summarised in Table 4-5.

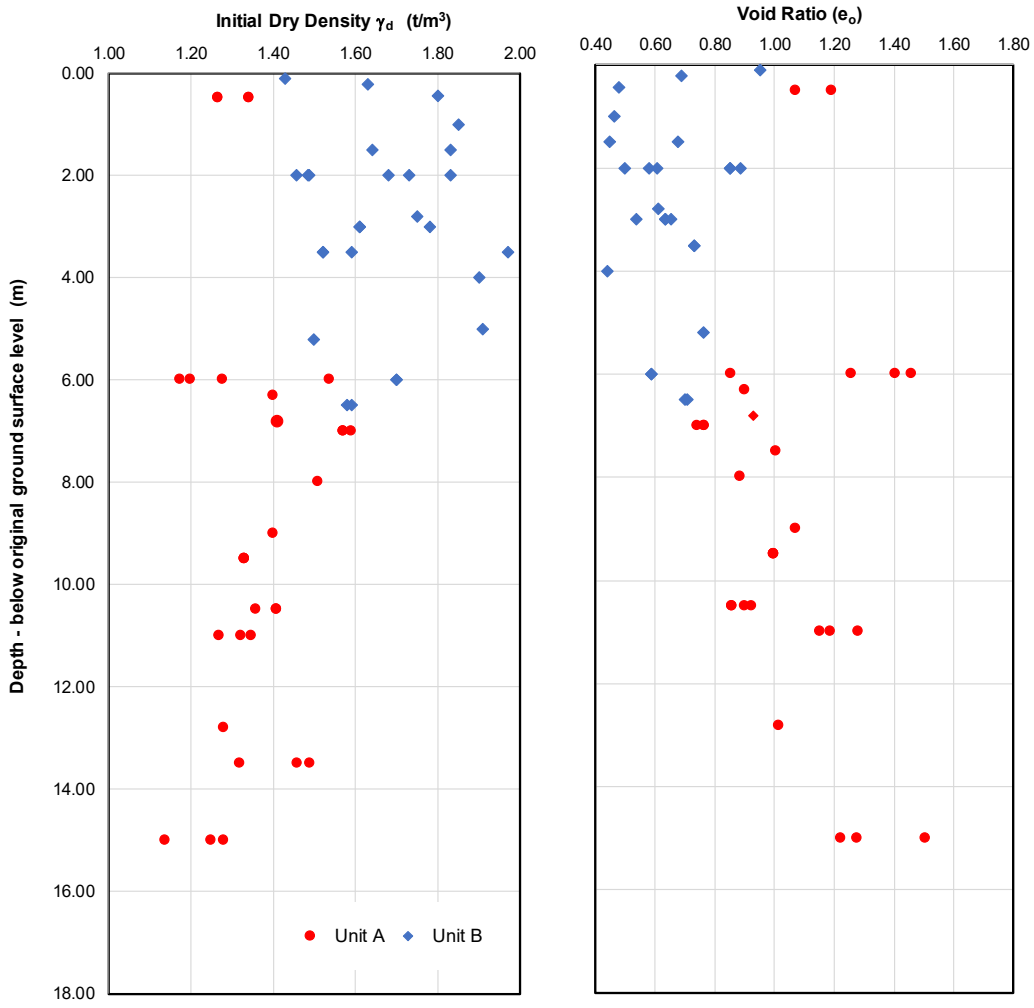


Figure 4-3: Forest Reef Volcanics – void ratio & dry density vs depth

Table 4-5: Geological section at NTSF slump

	CE416		CE435		CE432	
	RL	Th	RL	Th	RL	Th
Original Ground Surface	689.0		684.0		671.0	
Material Removed		2.2		5.30		2.0 (2)
Residual Basalt	686.8 685.7	1.10				
HW to MW Basalt	685.7 683.8	1.9				
Paleo Alluvium	683.8 682.6	1.2				
Unit A - FRV	682.6 676.0	6.6				
Unit B - FRV	676.0 671.5	4.5	678.7 (1) 674.3	4.2	669.0 660.5	8.5
MW - FRV	671.5 668.0	3.5	674.3 671.5	2.8	660.5 653.0	7.5
SW to Fresh - FRV	668.0 666.0	+2.0	671.5 669.8	+1.7	653.0 652.5	+0.5

Notes:

RL Reduced Level (m)

Th Layer Thickness (m)

(1) Base of slump recorded at RL677.15 in CE433

(2) Topsoil noted at base of rockfill; original ground surface level may be in error.

Key features of the geological model at the NTSF embankment failure are:

- The base of rockfill, in drillholes CE416 and CE432 is ~2 m below the original ground surface level (implying a 2 m depth of excavation). However, topsoil was logged in CE432 indicating a lesser depth of excavation;
- Approximately 1 m of high plasticity, residual basaltic clay remained on the western side of the NTSF embankment failure;
- Two metres of high to moderately weathered basalt was intersected in CE416, with the base of the basalt at RL683.8 m. Basalt was not recorded in TP113 (80 m SE of CE416), where the original ground surface level was RL683.9 m. At TP113, it would appear that the basalt has been removed by erosion;
- Paleo alluvium in CE417 (100 m W of CE416), was 6 m thick and contained organic black clay. At CE416 the paleo alluvium had thinned to 1.2 m and only comprised high plasticity, grey Silty CLAY. As the paleo alluvium was not observed in TP113, it would appear that it had either lensed out before TP113, or had been removed by erosion;
- Residual soil; extremely and highly weathered FRV, was intersected in both CE416 and CE432. However, the weathering profile beneath the Tertiary basalt is deeper than that where the basalt has been removed by erosion;

- FRV Unit A to the west of the NTSF embankment failure includes both residual soil and extremely weathered FRV;
- FRV Unit B to the east of the NTSF embankment failure includes both residual soil and highly weathered FRV, while to the west of the NTSF embankment failure it is only highly weathered FRV;
- Pink / purple colouring and white mottling characteristic of FRV Unit A and similar to that observed at the toe of the NTSF embankment (PL1 BS1), can be seen in photographs of TP113, excavated into residual soil and extremely weathered FRV;
- The depth of weathering in CE435 is less than that which could be reasonably inferred from adjacent drillholes; and
- Depending on the depth of stripping below the downstream shoulder of the NTSF, the NTSF slump has removed between 3 m and 5 m of residual volcaniclastic soil.

The geological model in the vicinity of the NTSF embankment failure is summarised in Figure 4-4.

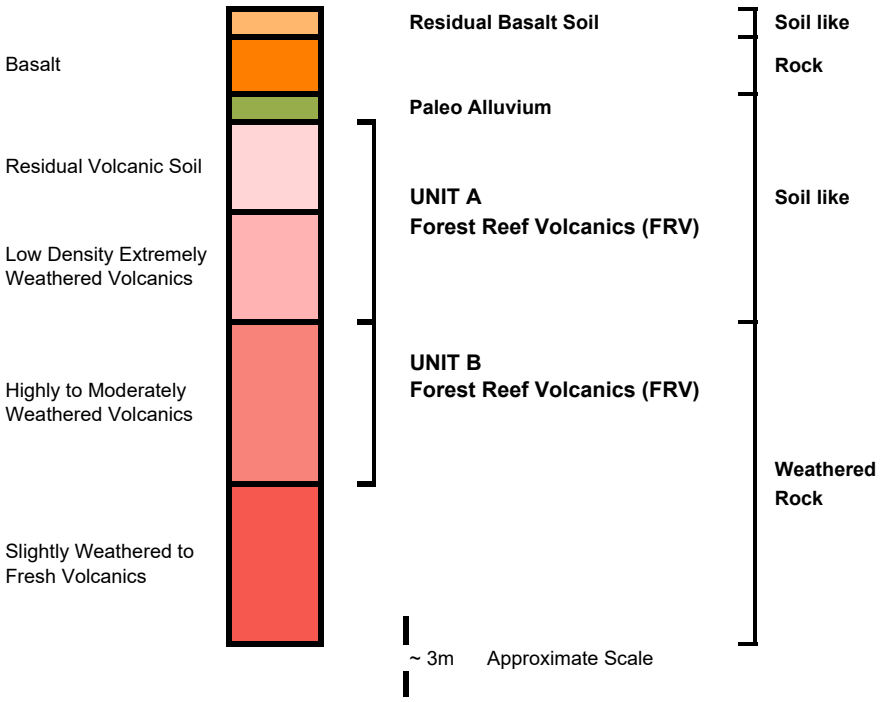


Figure 4-4: Geological units intersected at NTSF slump

Figure 4-5 to Figure 4-8 are sketches for illustrative purposes that show a possible paleo-geographic reconstruction of the NTSF area and have been prepared to explain the distribution of low density weathering products in the FRV.

Figure 4-5 shows the Silurian and Ordovician basement rocks at the NTSF that had been uplifted and exposed by erosion. Sedimentary strata, the Weemalla Formation in the west and Cadia Coach Shale in the east, have been faulted against the FRV. Deep weathering and low density soils developed over the FRV in a subtropical environment and drainage channels were broadly aligned along the eastern and western faults. Low density soils did not develop on the adjacent sedimentary strata.

Prior to the Miocene, and possibly in response to a cycle of increased erosion, alluvium was deposited along paleo-valleys as depicted in Figure 4-6. It is possible that a number of cycles of deposition and erosion may have occurred as the paleo alluvium ranges from low energy lacustrine (lake) deposits to high energy fluvial (stream) deposits. Erosion of ridges adjoining the paleo alluvium most probably reduced the thickness of low density FRV in these areas.

During the Middle Miocene a volcanic centre developed in the Mount Canobolas area and basalt flowed to the south filling valleys and burying the paleo alluvium and underlying low density soil developed in the FRV (Figure 4-7). The total thickness of the basalt was up to 80 m so it is likely that higher intervening ridges were not covered by the basalt.

A deeply weathered profile and an absence of basalt along the former ridge lines allowed streams to develop and a new phase of down-cutting occurred; Rodds Creek being one of these streams and Cadiangullong Creek another. With continued erosion and stream down-cutting, the basalt and underlying paleo alluvium and low density residual soils were completely removed in some areas and are thin in others.

The current situation is depicted in Figure 4-8, where remnants of Tertiary basalt remain where it is thickest along the former paleo-valleys. The basalt in these areas overlies paleo alluvium and low density FRV protecting it from further erosion except around the periphery. The location of the NTSF centreline and position of the embankment failure is shown on Figure 4-8.

These types of sketches illustrate the usefulness of paleo reconstruction to unravel geological and geotechnical complexity, and hence should guide site investigation.

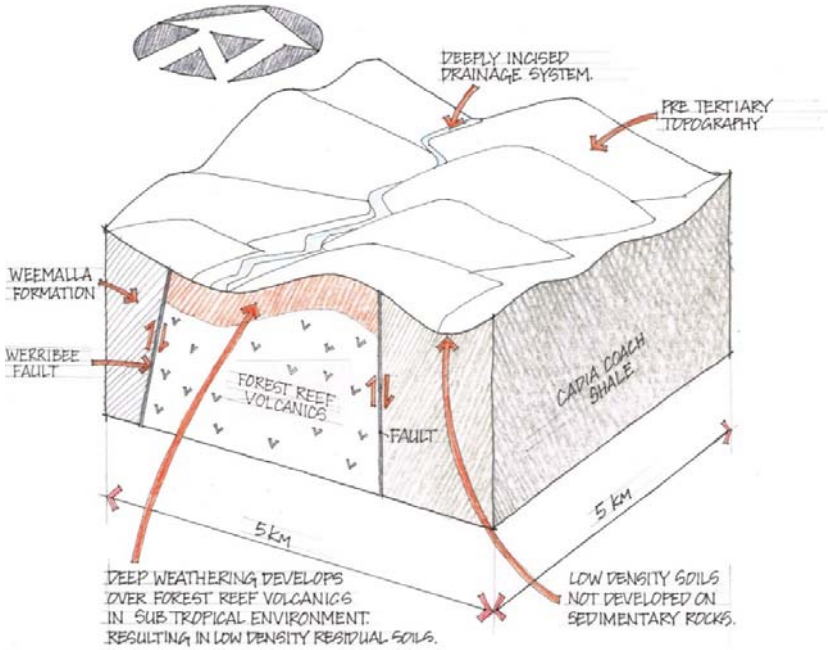


Figure 4-5: Low density soils develop on FRV under a sub-tropical climate

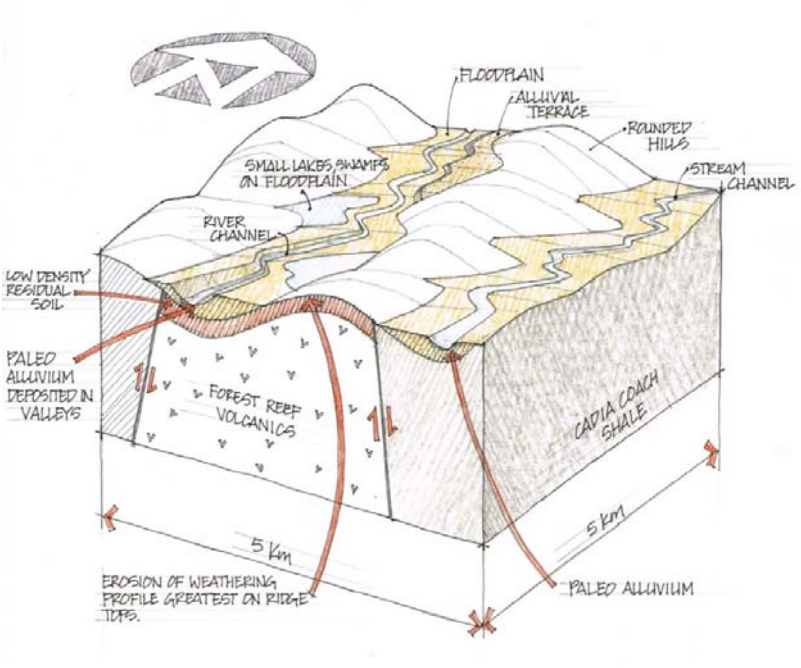


Figure 4-6: Alluvium is deposited along paleo valleys

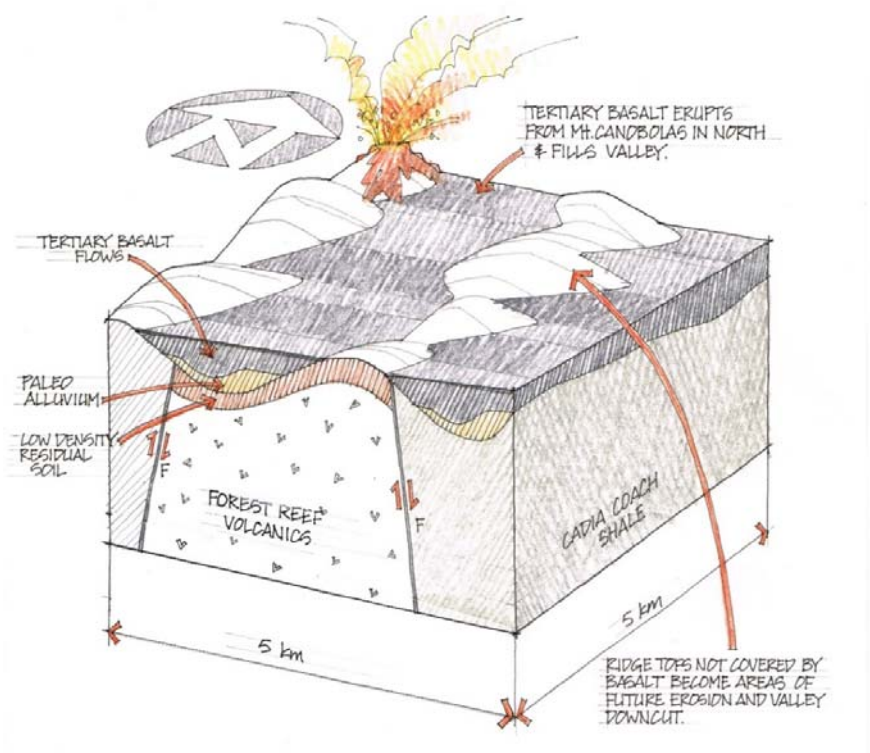


Figure 4-7: Basalt flows down valleys and covers paleo alluvium

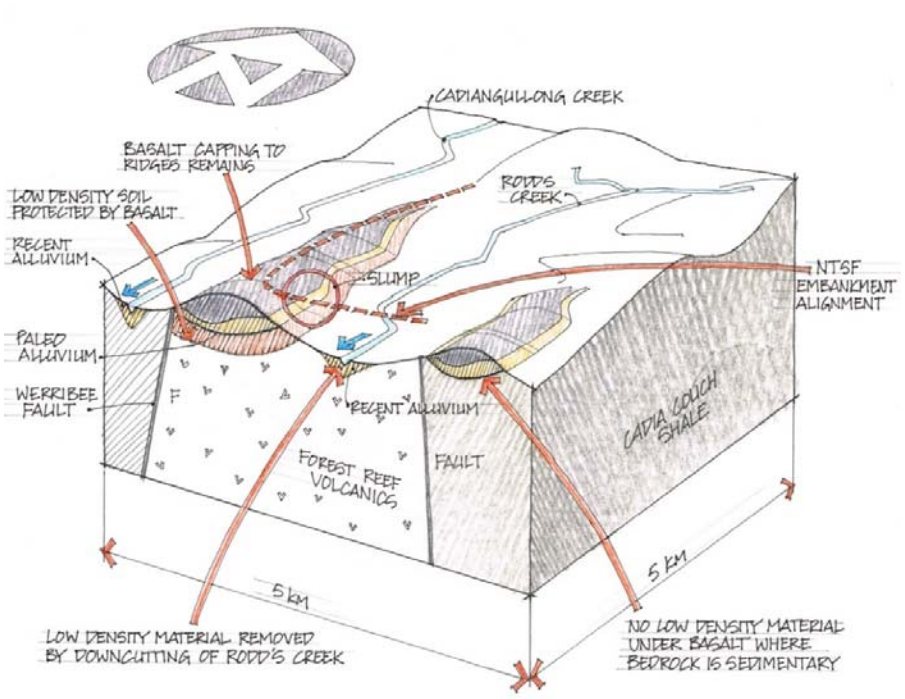


Figure 4-8: Stream downcutting results in the formation of Rodds Creek

5. Material Properties

5.1 Introduction

This section of the report focuses on the advanced laboratory studies undertaken to assess the physical response of foundation material and tailings to loading with differing effects from confinement (consolidation) to distortional (shear) loading – and whether there was sufficient time for pore water to move (drained behaviour) or not (undrained behaviour), and the transition between these two modes. Several testing laboratories have been used, in some instances, where deemed necessary, two laboratories carrying out duplicate tests as a check on the measured behaviour. The testing used modern equipment with computer control and data logging. Some of the advanced testing was commissioned by the ITRB while other advanced testing had already been started by some of the design consultants.

The entire stress-strain behaviour of the foundation material and tailings, not just their strength or ultimate resistance, are of principal importance to the NTSF because a central mechanism in how the embankment failure developed was load redistribution within the dam and its foundation as zones became over-stressed. Thus, while the testing provides strength values, the evaluation of this more comprehensive data goes much further into understanding why and how strength developed.

5.2 Foundation Materials

5.2.1 Material Types

Standard index tests have been carried out on both disturbed and undisturbed samples to assess the characteristics of these materials. The results are summarised on a plasticity chart presented on Figure 5-1. A range of material are evident within any of the four strata previously identified in Figure 4-4. FRV Unit A is distinctly higher plasticity than FRV Unit B, symptomatic of its likely reduced strength.

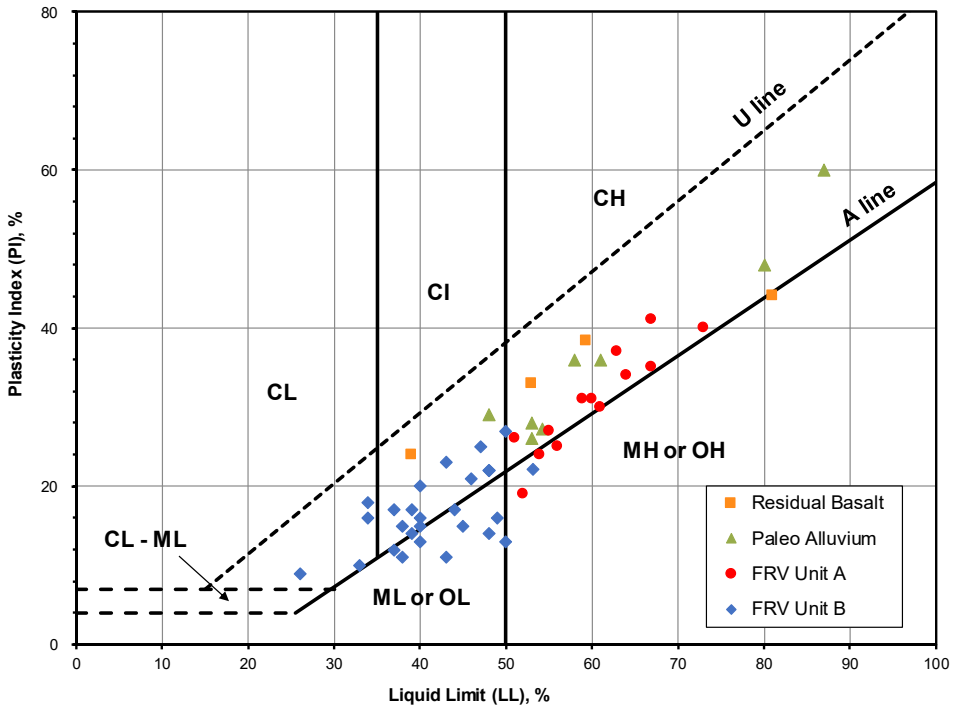


Figure 5-1: Plasticity of NTSF foundation materials

5.2.2 *Insitu Void Ratio*

As summarised on Figure 4-3, the insitu void ratio and density of undisturbed samples of the FRV deposit have been determined, and as indicated in the figure, the FRV Unit A is the least dense deposit with the highest void ratio.

The void ratio or moisture content of a saturated soil can be related to the plasticity classification indices shown in Figure 5-1 by means of the Liquidity Index (LI). This references the potential strength of the soil to the bounding plasticity indices; a high LI indicates a weak soil, whereas a low LI indicates a stronger soil. This data is shown on Figure 5-2. There is variability in the LI in all strata, but the FRV Unit A displays both the greatest values and the greatest proportion of high values.

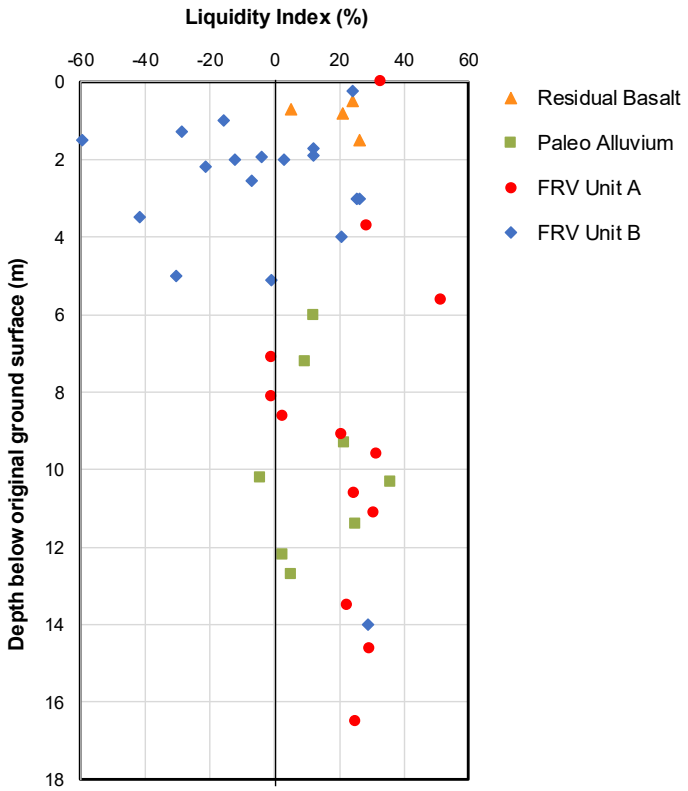


Figure 5-2: Liquidity Index vs depth

5.2.3 *Laboratory Testing*

Five types of mechanical tests were used for the foundation soils: triaxial compression, direct shear, ring shear, direct simple shear, and confined compression (oedometer). The first four test types investigate strength while the fifth investigates compressibility.

Triaxial compression (TX) is the reference procedure for measuring soil strength properties. However, although this test measures the complete details of soil behaviour it does so under particular conditions of symmetry and loading direction. This test is more aligned to investigating failure under vertical loadings, rather than horizontal deformations in horizontally bedded strata.

Direct simple shear (DSS) deforms the soil in a manner that is a close analogue to that of the NTSF foundations and is widely used in practice for such cases.

Direct shear (DS) and ring shear (RS) tests constitute convenient methods for determining the residual strength developed along shear planes associated with large deformations. This is a characteristic of the potential failure mode associated with the foundation materials after yielding has been initiated.

Conventional Oedometer (OED) and Constant Rate of Strain (CRS) tests have been used to document soil compressibility.

The testing undertaken for the ITRB has been biased towards DSS with some supporting testing by TX, DS and RS, consistent with the foundation conditions at the NTSF and the nature of the loading by the dam. Both types of tests have been carried out undrained (and with measurement of pore water pressures), partly because the time during which the slump developed was such that drainage would have been inhibited. Drained testing was more characteristic of Phase 1 deformations. DS and RS testing provide information to account for the low undrained strengths developed at large strains under DSS conditions. Table 5-1 summarises the extent and types of testing undertaken. Details of all tests are provided in Appendix D.

Table 5-1: Summary of advanced foundation testing program

Stratum	Number of Tests				
	TX	DSS	DS	RS	OED + CRS
Residual Basalt	---	6	---	---	2
Paleo Alluvium	3	5	---	---	4
FRV Unit A	10	12	4	1	2
FRV Unit B	6	6	3	---	4

5.2.4 *Compressibility*

Compressibility is the behaviour of these foundation soils in confined compression, which captures their response to the loading by the weight of the dam in the absence of shear forces. The plot shows the void ratios versus vertical effective stress, it indicates that the compressibility of the FRV Unit A is generally among the highest of the residual soils tested, this is reflective of its relatively low density. The data for FRV Unit A foundation material are summarised on Figure 5-3, while the remaining foundation materials are presented in Appendix D .The disturbance during sampling and test preparation can significantly affect compression data and the comparisons between specimens do not have high resolution.

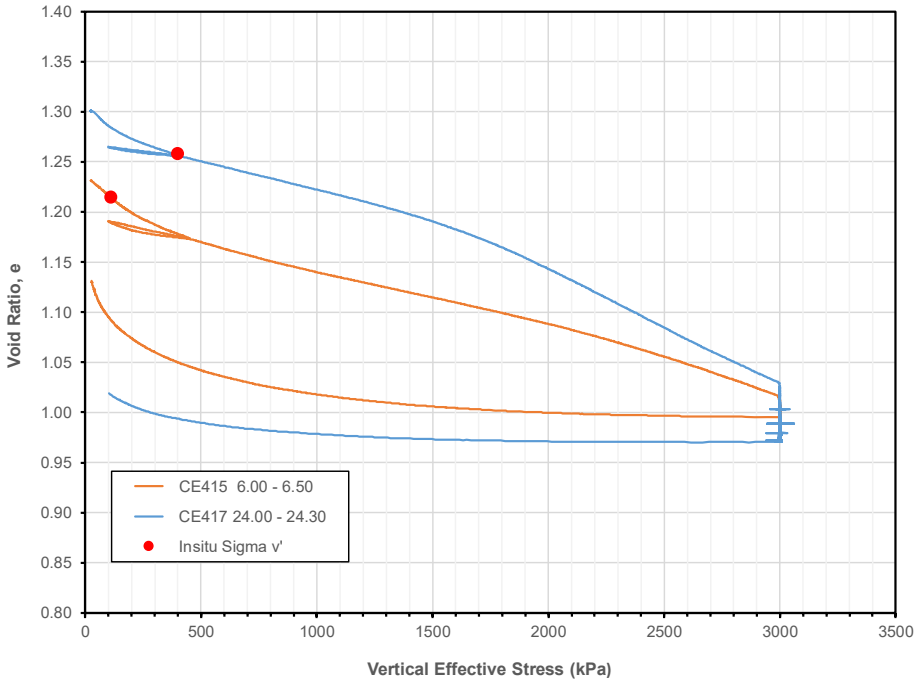


Figure 5-3: Confined compression (oedometer) data for FRV Unit A

5.2.5 Consolidation

The rate at which clays gain strength under increasing load depends on the coefficient of consolidation (C_v), which is the ratio of their hydraulic conductivity to their compressibility. This property also controls the soil's response to transient changes in water pressures. The property is measured as part of the confined compression testing.

The data from testing the NTSF foundation materials are summarised on Figure 5-4. All strata show a marked decrease in C_v with confining stress, with about an order of magnitude reduction moving from conditions near the toe of the embankment to those under the Stage 10 crest. There is also considerable difference between the strata. Overall, the FRV Unit A will be the faster unit to reflect drainage conditions under the imposed boundary loading of the OED test.

These tests are on intact samples and, as such, do not account for preferential water movement in the relic structure reflective of the parent rocks.

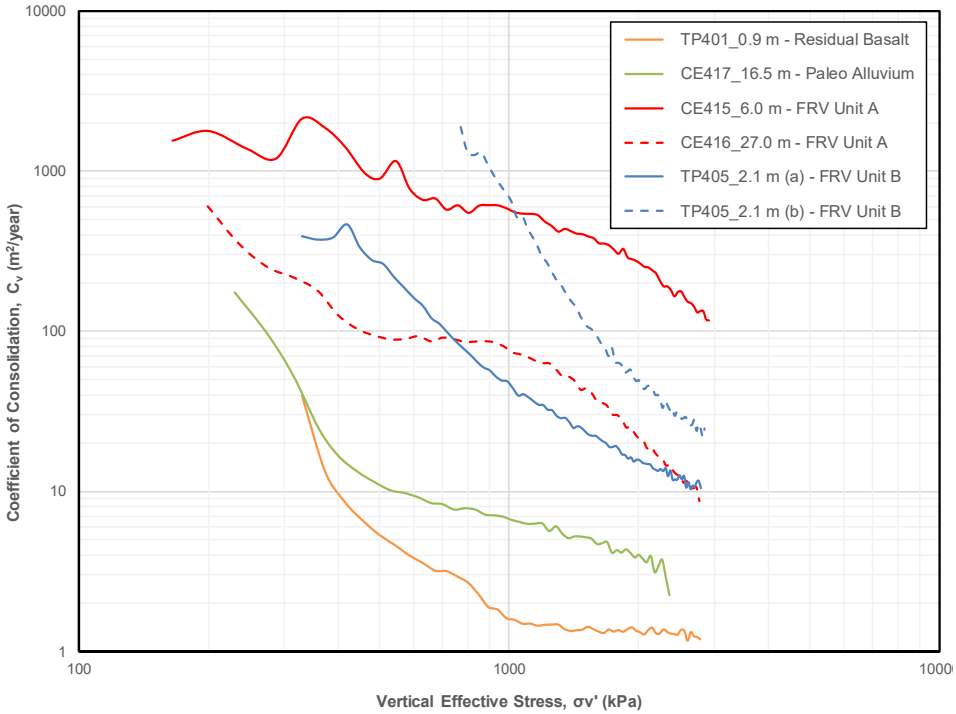
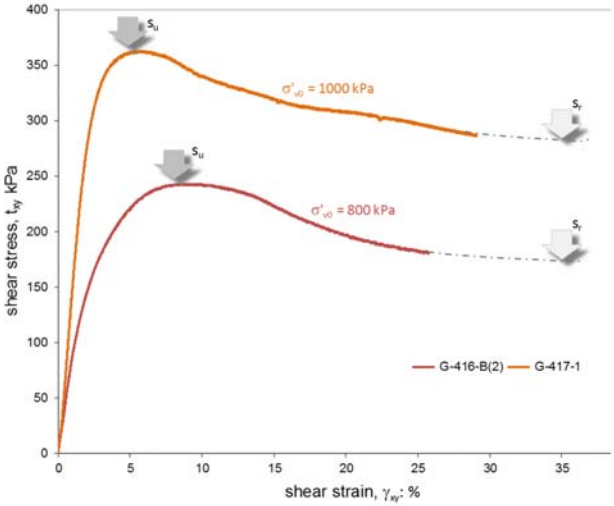


Figure 5-4: Coefficient of consolidation in confined compression

5.2.6 Stress-Strain Behaviour

The stress-strain behaviour of all foundation materials was measured. An example of the measured behaviour is shown on Figure 5-5 for the direct simple shear tests on the FRV Unit A soil. Both the peak undrained strength (denoted as S_u) and the large deformation residual undrained strength (denoted as S_r) are indicated. The tests indicate that an increase in effective vertical stress results in an increase in strength, which is usual. Overall, peak undrained strength develops at a shear strain of about 8 - 10%. The simple shear tests generally did not develop their ultimate residual undrained strengths within the displacement limits of the test equipment, with the estimated trends for residual undrained strength developing at about 40% strain. These strains do not appear to be affected by the initial vertical effective stress.

a) Measured behaviour



b) Example of tested sample



This sample is that of the lower curve plotted to the left

Figure 5-5: Undrained stress-strain data in direct simple shear (FRV Unit A)

5.2.7 *Direct Shear Tests*

As noted previously, the DS and RS tests are used to determine the residual frictional strength in foundation materials at large displacements reflective of the progressive failure developed in the foundation during embankment loading. A summary of test results is presented in Appendix D. Data from FRV Unit A is of particular interest and shear stress vs displacement plots at a relatively high pressure (800 kPa) are provided in Figure 5-6. In this case the mobilised friction $\emptyset'_m$ ranges from a of peak of 26.3° to a residual value of 15.3° after four reversal cycles, while most residual friction values are about 16°. This low value, when coupled with pore pressures induced by construction and yielding, helps account for the low foundation strength estimated from the deformation analyses (see Appendix H).

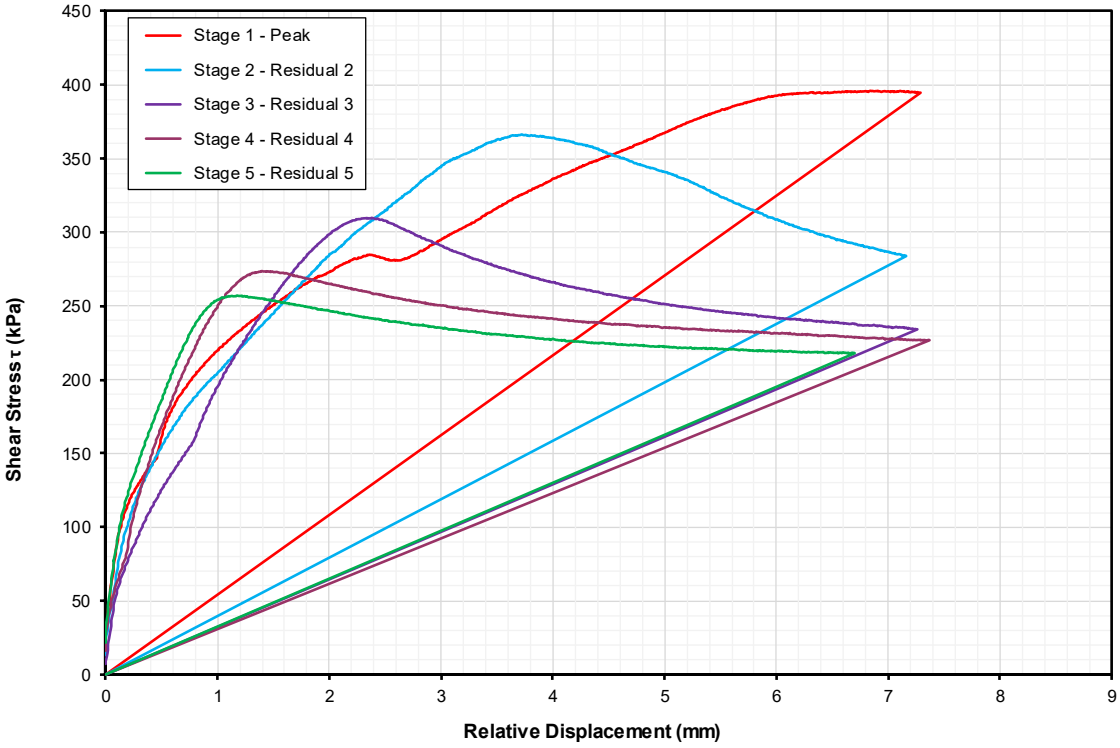


Figure 5-6: FRV Unit A - Drained Direct Shear Test

5.2.8 Strength Trends

It is useful to evaluate the factors controlling the strengths by plotting the strength ratios (S_u/σ_{v0}'; S_r/σ_{v0}') against the initial confining stress σ_{v0}'. There is a considerable range in the peak strength ratios shown on Figure 5-7 and residual strength ratios shown on Figure 5-8. Trends indicated on these figures are discussed below:

- There appears no systematic difference between any of the four foundation materials;
- High strength ratios are reduced by increasing initial confining stress; and
- There is a lower limit to the strength ratio of about S_u/σ_{v0}' ~ 0.27. The residual strength ratio shows a similar pattern of behaviour as peak, but with a lower limit S_r/σ_{v0}' ~ 0.20.

The relationship between peak and residual strengths can be expressed using the Brittleness Index I_B $(1 – S_r/S_u)$, which gives a measure of the proportional strength loss of any sample due to large deformations. I_B versus mobilised peak strength ratio is presented as Figure 5-9. With two exceptions, this figure indicates less than 10% loss in peak strength as deformations continue. In the case of the FRV Unit A, half the tests show substantial strength loss, averaging about 25% loss but in one instance approaching 40%. This material is prone to brittle failure. In the case of the Residual Basalt, which had relatively low peak strength, only one of the five tests shows substantial strength loss, and hence this material appears to be less brittle.

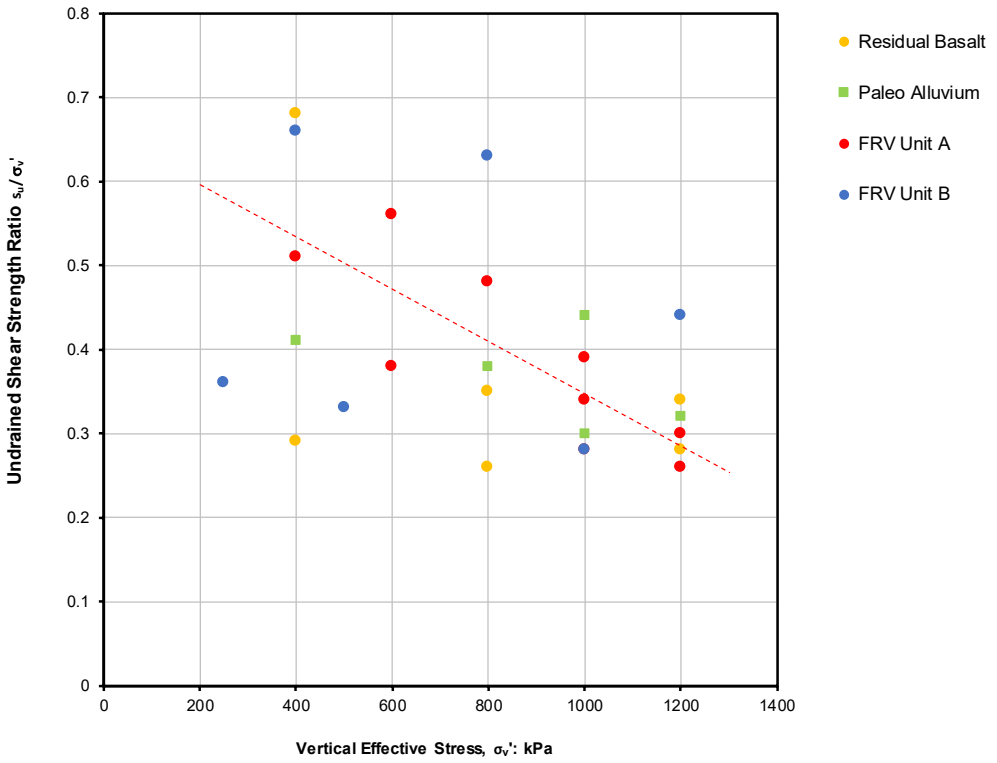


Figure 5-7: Peak undrained strength ratio in direct simple shear

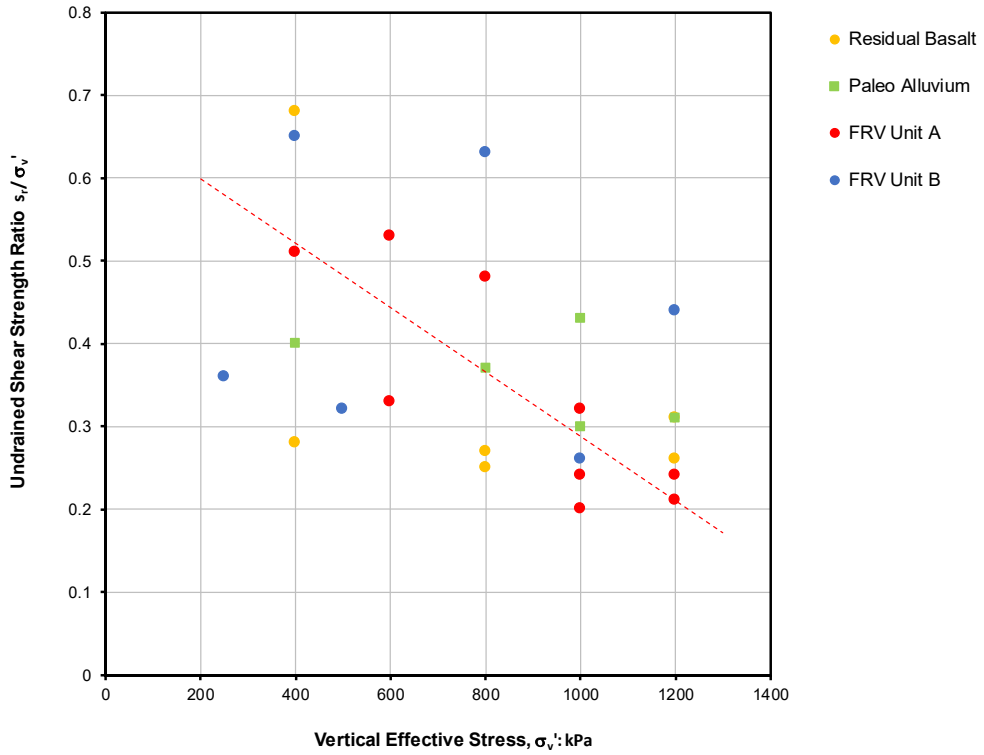


Figure 5-8: Residual undrained strength ratio in direct simple shear

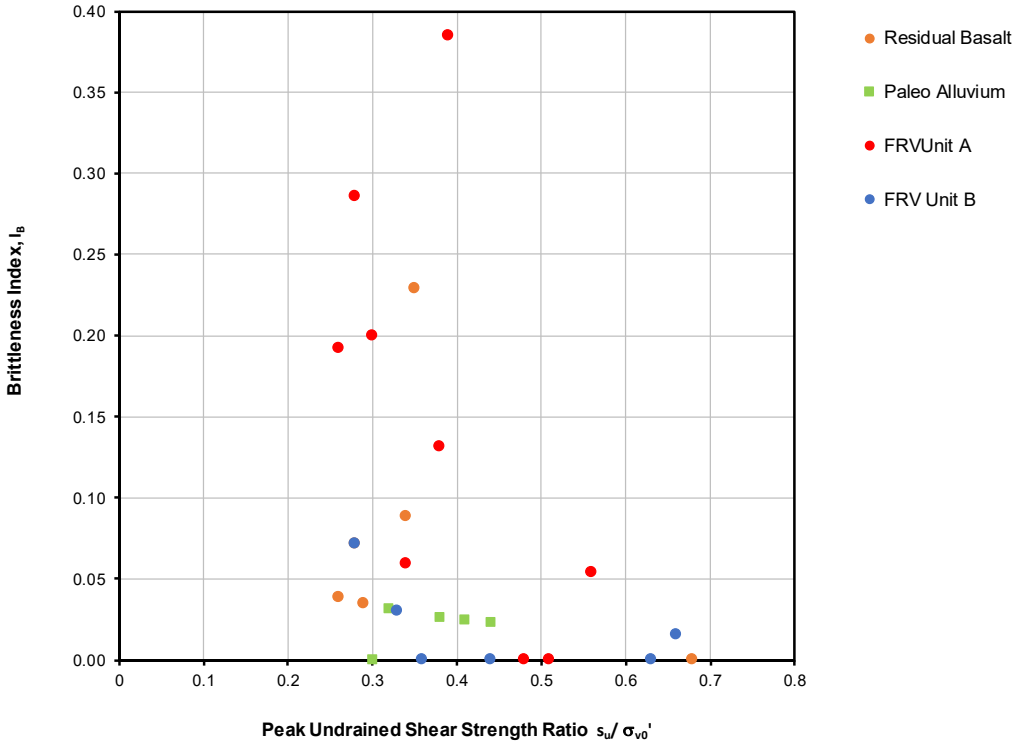


Figure 5-9: Brittle post-peak strength loss in direct simple shear

5.2.9 *ITRB Assessment of Foundation Properties*

The measured confined compression behaviour in the residual basalt, the paleo alluvium, and the FRV is broadly consistent with their soil type as characterised by the standard index tests. There is some scatter in the data, but that is reasonable as weathering is not a uniform process. However, an important trend is that the FRV Unit A has a greater proportion of low density, weak tests than the other foundation materials. Since the distribution of this critical unit is approximately horizontal in the vicinity of the NTSF embankment failure, and the foundation loading approximates horizontal shear, it is this systematically weaker stratum that will control the foundation response. The ITRB therefore focused on the FRV Unit A soils in their assessment of foundation response to embankment construction. The undrained behaviour of the FRV Unit A is an important parameter controlling the development of progressive failure devolved prior to the onset of Phase 2.

The confined compression data as shown earlier (Figure 5-3) revealed trends of void ratio with imposed stress. This same data can be viewed as a confined modulus i.e. change in void ratio with change in stress, with Figure 5-10 showing the data in this form for the two CRS tests on the FRV Unit A samples. This plot is for those parts of the tests where plastic deformation developed (first loading). In this case, there are three trends seen in the data, emphasised by the red lines on the figure:

- Even at very low confining stress there is a significant stiffness with a modulus of ~6000 kPa, likely a reflection of the residual nature of the soil that has preserved some structure from the parent rock;
- As stress increases, so does the modulus, and in direct proportion; and,
- The increase in modulus peaks at a confining stress in the range of 1000 to 1500 kPa before a decrease in modulus with further loading increase develops. This is an unusual behaviour that appears to be caused by crushing of the soil particles or disaggregation.

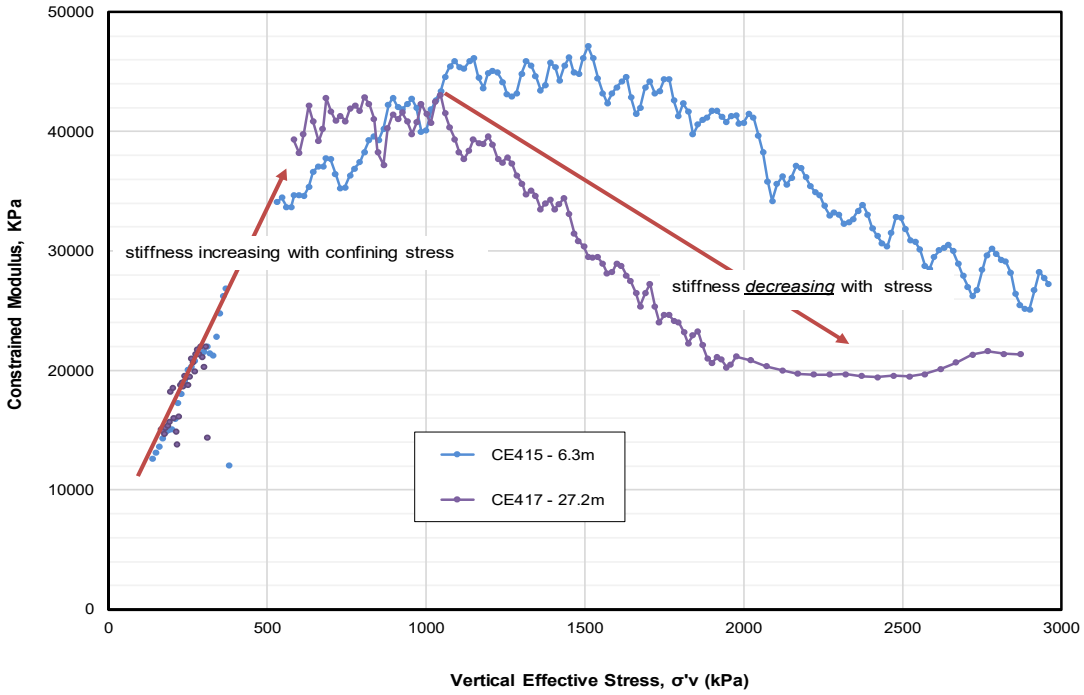


Figure 5-10: Confined compression modulus trends in FRV Unit A

This change in behaviour in the vertical stress range 1000 to 1500 kPa appears important as that stress range applies to the portion of the NTSF embankment that is upstream of the Stage 2 raise. Therefore, all the FRV Unit A present as part of the foundation beneath the upstream raise will have exhibited a reduction in stiffness as upstream construction was carried out.

Turning from confined compression, where the soil is prevented from moving other than vertically, to the more general case where lateral movements depend on the soil's strength, two examples of the measured stress-strain behaviour in undrained TX compression are shown on Figure 5-11. The data shows test data from two samples from different parts of the FRV Unit A that have been tested in two independent laboratories; both laboratories found that most of the post-peak loss of strength develops within about 3 - 5% axial strain from peak strength. Triaxial tests on three undisturbed samples of FRV Unit A all showed comparable behaviour, with details provided in Appendix D.

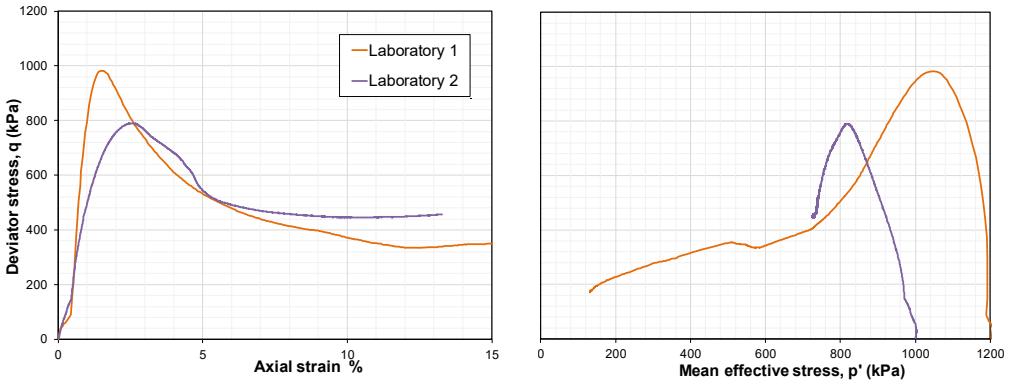


Figure 5-11: Examples of undrained triaxial compression of FRV Unit A

5.3 Tailings

5.3.1 *Introduction*

The framework used here, to evaluate the stress strain behaviour of tailings is known as 'NorSand' (Shuttle & Jefferies, 2002). NorSand is a constitutive relationship that is based on the state concepts discussed above, see Section 4. It is finding increasing usage in geotechnical engineering, particularly for the assessment of liquefaction of loose saturated granular deposits such as tailings (Jefferies & Been, 2016). Modelling with NorSand was used effectively in the analysis of the Samarco Tailings Dam failure which provides a useful precedent for its adoption here (Fundão Tailings Dam Review Panel, 2016).

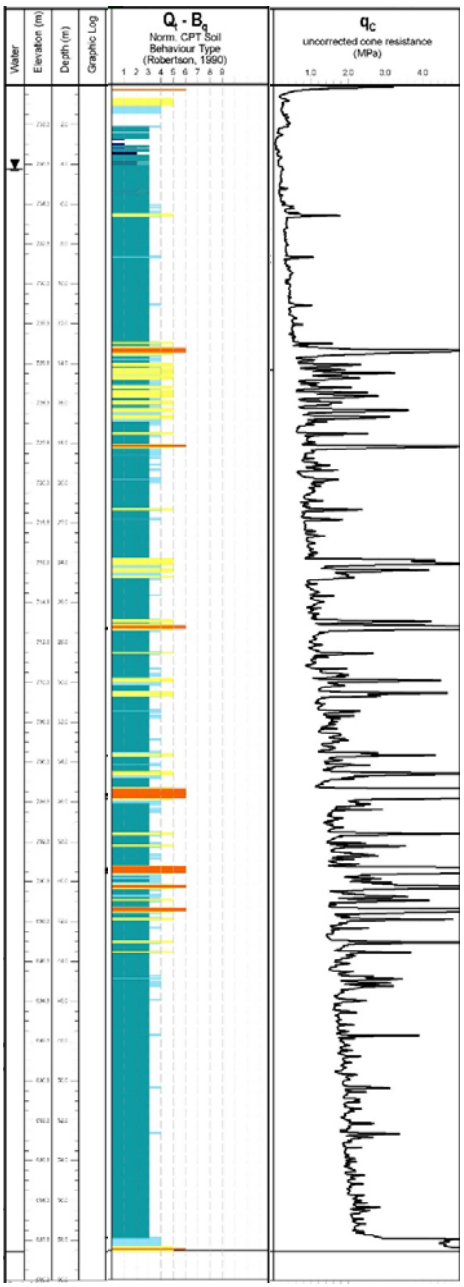
5.3.2 *Sampling*

The ITRB investigation included four drillholes to provide both disturbed and nominally undisturbed piston samples of tailings. The holes were drilled from the Stage 1 Buttress and Stage 10 embankment crest on either side of the slump. Figure 5-12 shows CPT-N04 (2017 CPTu fieldwork campaign) completed in the slump area and a photograph of the recovered tailings in their sample tubes from nearby drillholes. These tube samples were split and air-dried, the drying allowing visual identification of the layering within the tailings because the sandier tailings dried faster than the silty tailings; a photograph of the split tubes during air drying is also shown on Figure 5-12.

Two characteristic tailings samples were produced from examination of the split sample tubes. These were bulk samples, with sufficient tailings of each type for a comprehensive laboratory test program. Bulk sample TC1 was characteristic of the predominant silt material, which is shown as the green soil type on the processed CPTu record of Figure 5-12. Bulk samples TS1 and TS2 were characteristic of the multiple sandy silt layers, which is shown as the orange soil type on the processed CPTu record of Figure 5-12.

Tailings became mixed during the runout of the slump and this changes the particle size distribution of the tailings. Because the particle size distribution affects the critical state, bulk sample HA401 was recovered from the slump run-out zone for testing. HA402 sampled ejecta from the surface of the sand boils on the slump. The particle size distributions for all of these samples are shown in Figure 5-13.

a) Inferred from CPTu sounding



b) Drilling and Sampling

Recovered tube samples



Tube samples after splitting and air drying



Figure 5-12: CPT-N04 and samples adjacent to the NTSF slump

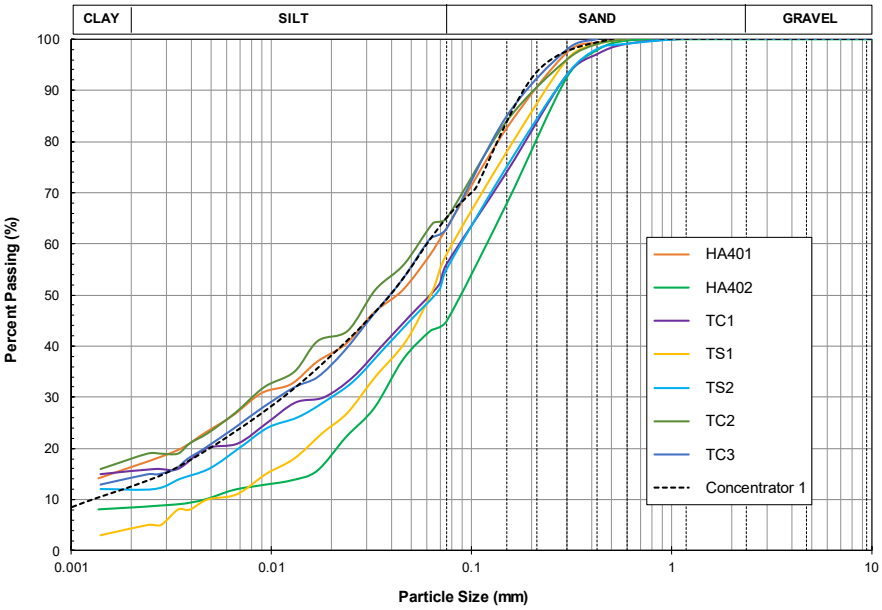


Figure 5-13: Particle size distributions of characteristic tailings tested

5.3.3 *Laboratory Investigation*

The tailings laboratory investigation first focused on determining the critical state, and associated properties, of samples TC1, TS2 and HA401. TX tests were used for this purpose using now standard techniques and with particular attention to accurate void ratio measurement. Both drained and undrained tests were used.

The potential effects of the small earthquakes also needed to be understood. The ability of the tailings to withstand earthquake induced ground motions requires special testing using cyclic direct simple shear (CDSS) tests. This type of testing is the de facto current standard, at least for silty tailings.

The elastic shear modulus is important to assess the embankment response to earthquake motions. The laboratory testing included elastic modulus measurements using bender elements, a well-known technique.

The overall laboratory testing program is summarised in Table 5-2. All laboratory data are provided in Appendix E.

Table 5-2: Summary of advanced tailings testing program

Characteristic Type	Number of Tests			
	CIU/CID Triaxial	Cyclic DSS	Bender Element	Stress Path
Predominant SILT: TC1	8	9	1	2
SANDY SILT: TS1	3	---	---	4
SANDY SILT layer: TS2	8	1	---	---
Run-out SILT: HA401	9	---	---	---
Run-out SANDY SILT: HA402	7	---	----	---

5.3.4 Critical State

The critical state changes with confining stress, with the relation of critical void ratio to confining stress being referred to as the critical state locus (CSL). This CSL was determined for each tailings type using the standard method of triaxial tests on predominantly loose samples, tested both drained and undrained. The critical state is the end point of those tests that reach the condition of continuing deformation at constant deviator stress and constant void ratio. These end points provide clear definition of the CSL for all the tested tailings.

Figure 5-14 shows the CSL determined for each of the characteristic gradations. These CSL relations are all slightly curved in the plot used and are readily represented with a power law relationship.

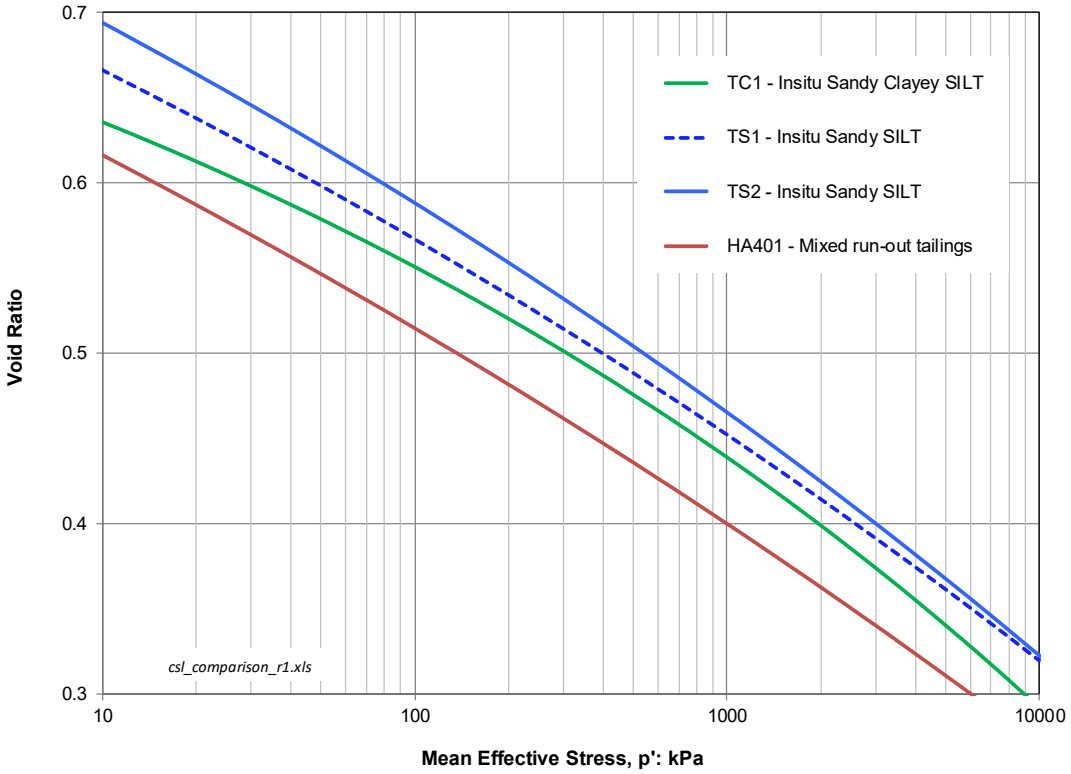


Figure 5-14: Comparison of CSL for NTSF tailings

5.3.5 Strength

The tailings strength was determined using both the TX tests carried out for the CSL determination with additional tests on denser samples. Although the tailings are loose, the additional tests on dense samples allow simple determination of the soil properties by plotting the measured data. The properties so determined apply at all stress levels and all soil densities.

The dilation that develops as soil deforms (shears) is a consequence of the available space for particles to move into, and is thus controlled by the state parameter (ψ). The state parameter is defined as the difference between the actual void ratio of the tailings at a particular stress level and the associated void ratio on the CSL for that tailings at the same stress level. This is shown in Figure 5-15.

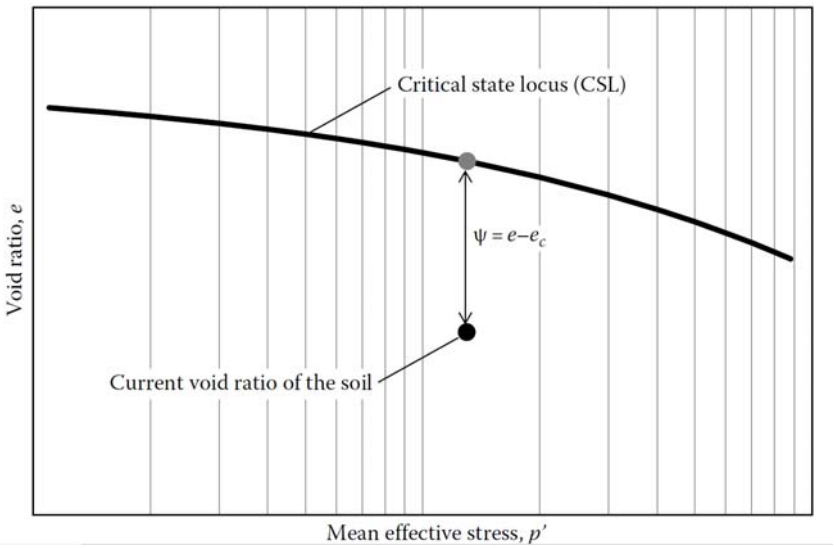


Figure 5-15: Definition of the state parameter (Jefferies & Been, 2016)

The state parameter reflects the tendency of the tailings to either contract in volume when sheared or dilate. Negative values of the state parameter reflect dilation while positive values reflect contractive behaviour.

Three soil properties are associated with relating ψ to soil strength (M, N and χ), and these properties were determined by the laboratory testing campaign (critical state testing) presented in Appendix E. The representative tailings gradations tested exhibited small changes in properties from one gradation to another, but the variation is quite small. For the purpose of analysis in support of the ITRB investigation (Appendix H), a single set of properties were considered sufficient and the determination of these properties is discussed in Appendix E and presented in Table 5-3.

Table 5-3: Adopted critical state parameters for tailings

M	N	χ	H	G_{max}	υ	a (1)	b (1)	c (1)
1.49	0.25	8.5	50-450ψ	(2)	0.2	0.906	0.355	0.119

Notes:

(1) $e_c = a - b * \left(\frac{p\prime}{100}\right)^c$

(2) $Gmax = 17 * \left(\frac{p\prime}{100}\right)^{0.76}$

5.3.6 *Earthquake (cyclic loading) Response*

Eight cyclic DSS (CDSS) tests supplemented by two cyclic triaxial tests (CTX) were used to assess the response of the tailings to cyclic loading. In addition, two monotonic DSS were carried out to directly benchmark the cyclic data against the soil properties measured in the standard triaxial testing. Tests were carried out mainly on the predominant silt sample (TC1), with the samples being prepared to a loose state (ψ ~ +0.1) comparable to that insitu. Some tests were somewhat looser, which makes their behaviour trends conservative compared to insitu conditions.

Various static and cyclic load combinations were used so as to define trends in the tailings behaviour with changes in the loading conditions. Most of the testing was for conditions underlying the upstream crest of the dam. However, the numerical analysis of slump development (Section 8.4.4) identified a potentially critical zone where dam construction changed to the

upstream method; three tests focused on the conditions in this potentially critical zone, simulating the stresses (static bias) predicted by the numerical analysis.

The cyclic response of the tailings has been assessed using the pore pressure ratio parameter r_u.; the excess pore pressure generated as a fraction of the initial vertical effective stress. This pore pressure response depends on both the number of loading cycles as well as the cyclic stress ratio imposed. The number of cycles experienced by a soil in an earthquake depends on the earthquake magnitude, with 15 uniform cycles being an industry standard measure and equivalent to the average duration of a M7.5 earthquake with its actual 'random' ground motion.

The test data presented on Figure 5-16 has also been plotted for five load cycles and 15 load cycles. The five load cycle data is slightly more severe than experienced in the ground motion at the site for which the imposed cyclic stress ratio was about $\tau_{cyc}/\sigma'_{v0} \sim 0.05$. As soil "liquefaction" in an earthquake typically occurs at $r_u > 0.9$; the data on the NTSF tailings show a very substantial capacity under low-level cyclic loading. There appears to be minimal effect of confining stress or static bias.

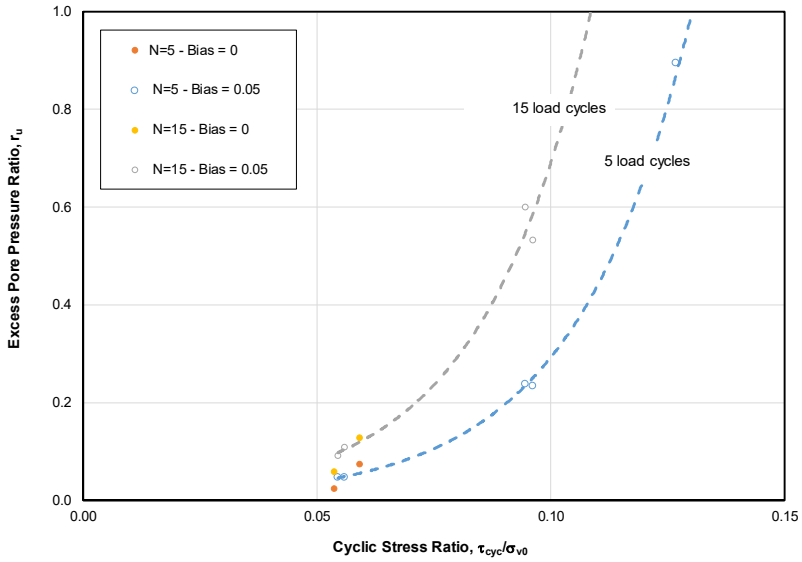


Figure 5-16: Measured cyclic response of NTSF tailings

In addition to the above testing, which utilises sinusoidal loading, cyclic testing simulating the actual ground motion of the March 8, 2018 seismic events, was undertaken and is discussed in Section 8.4.6.2.

5.3.7 Insitu State

The strength of tailings depends on both the soil properties and the state parameter. The state parameter of the tailings must be measured insitu, usually done with the CPTu. The 2017 CPTu campaign provided appropriate data and it is this data that has been used to assess the state of the tailings prior to the Event. CPT-N04 being particularly appropriate as it was within the tailings that subsequently slumped.

5.3.7.1 Processing Method

The CPTu does not measure any soil property directly, the measurements being stress/pressure that result from the CPTu probe being forced into the soil and which depend on the stress level, the geological stress-history, and the soil density. Recovering the engineering information from CPTu data requires processing the data (commonly called interpretation), and there are three types of data processing approaches: screening, calibrated, and precedent. The screening method assumes typical soil behaviour (an average response) and gives a quick appraisal of the

deposit, typically implemented as response charts that are used to assess soil type and density (approximate amount of dilation). It is not normal practice to rely on screening methods for engineering design/assessment. The calibrated method uses, as the name suggests, specific calibration on the CPTu in the strata of interest. The precedent (or case history) method directly relates CPTu measurements to engineering performance, commonly though studies of past failures that have been analysed in terms of operating strength at failure etc. and indexed to CPTu data. In all of these applications, CPTu data is utilised to determine the insitu state of the tailings, see Figure 5-17 for the interpretation of CPT-N04.

The specific approach followed here has been developed over the past decade as discussed by (Shuttle & Cunning, 2007) and (Shuttle & Jefferies, 2016). An alternate approach that is commonly used in practice was developed by Robertson (2016) and this has also been adopted for purposes of comparison.

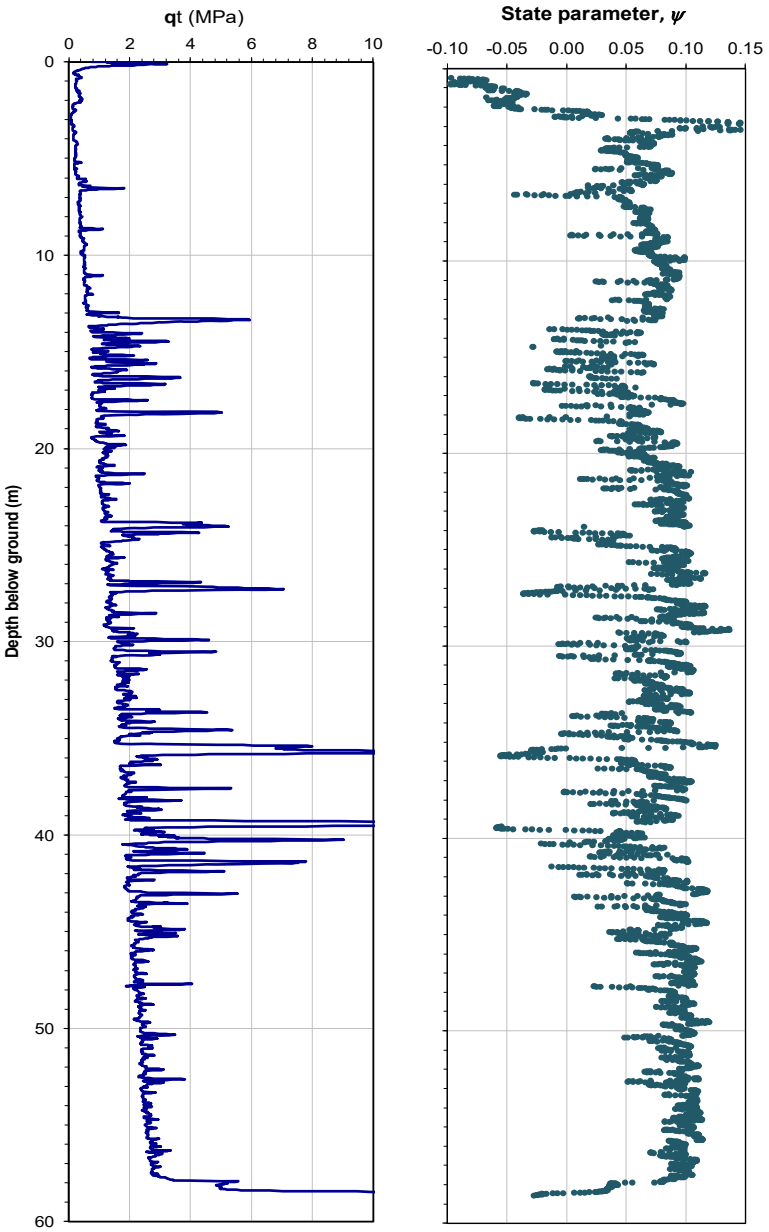


Figure 5-17: Insitu state parameter at CPT-N04

5.3.7.2 Application to CPT-N04

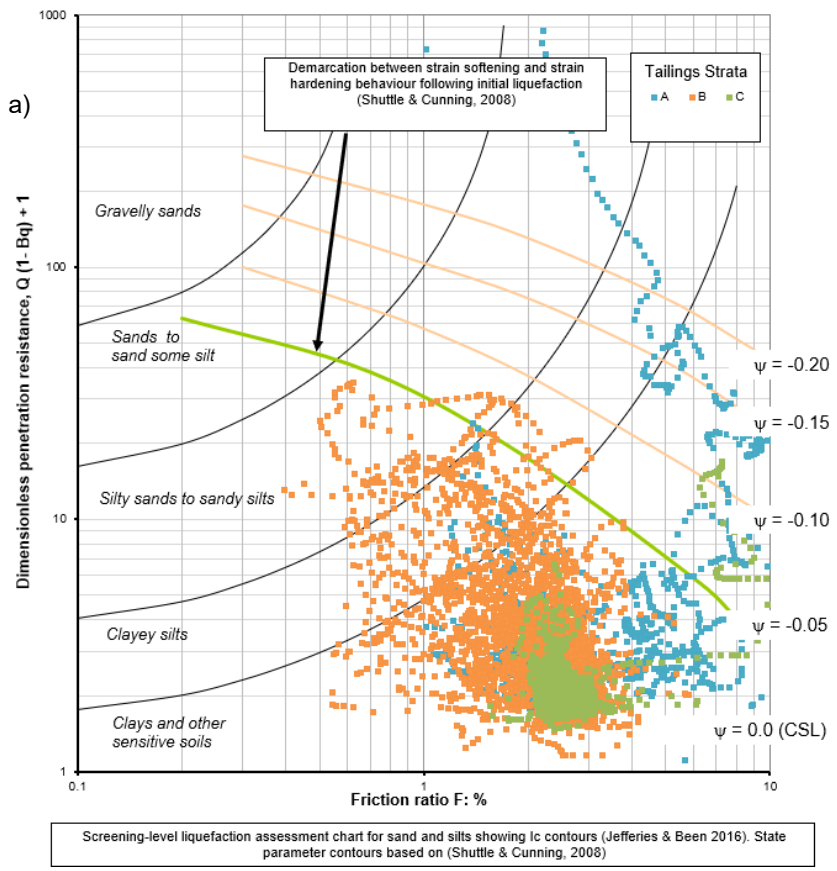
The derived calibrations have been used in processing the data from CPT-N04 and is shown in Figure 5-17. The left-hand plot shows the measured tip resistance as a visual aid in comparing the results with the features of this sounding discussed elsewhere; the right-hand plot shows the computed ψ. Details of the interpretation process are presented Appendix E.

In general, the deepest tailings appear to be slightly looser. The characteristic state parameter lies in the range +0.08< ψ_k<+0.10, with the sandier layer between 13 m and 18 m depth being rather stronger.

From a detailed evaluation of CPT-N04 three zones have been distinguished as having some variation in soil type and density, they are Zone A (0-13 m), Zone B (13-45 m), Zone C (45-59 m).

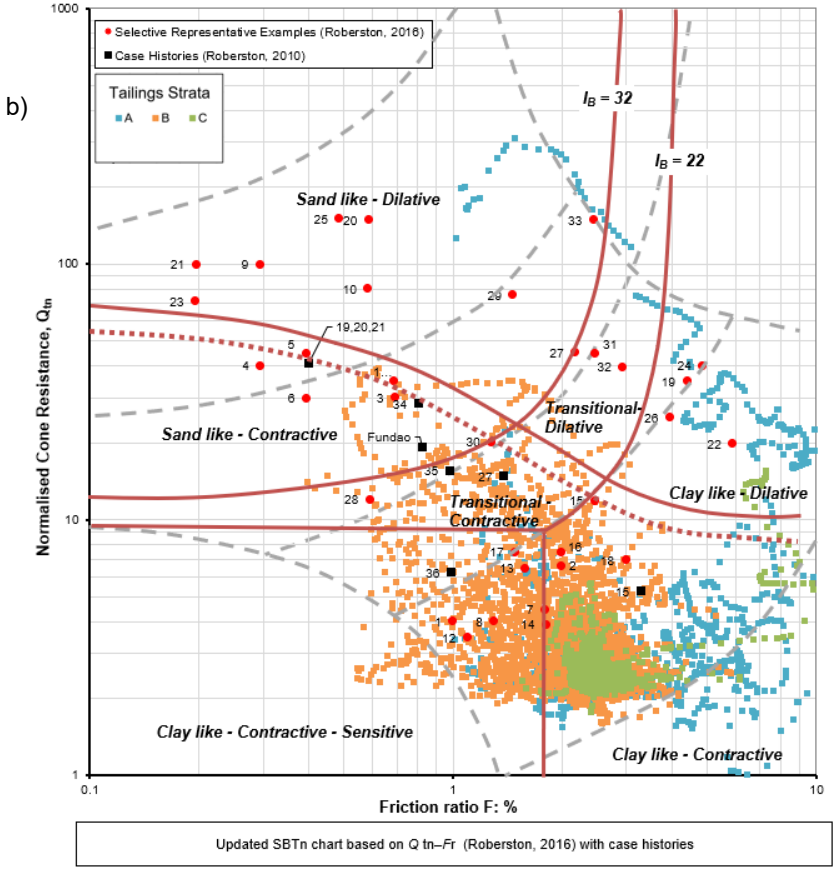
5.3.8 ITRB Assessment of Tailings

Tailings state plots are presented for CPT-N04 on Figure 5-18 using Shuttle & Cunning (2008) and Figure 5-19 using Robertson (2016). Both approaches lead to the conclusion that the NTSF tailings, as a whole, were contractive and rather weak with a clear propensity for flowslide behaviour.



Screening-level liquefaction assessment chart for sand and silts showing Ic contours (Jefferies & Been 2016). State parameter contours based on (Shuttle & Cunning, 2008)

Figure 5-18: CPT-N04 –Shuttle and Cunning tailings state plot



Updated SBTn chart based on Q tn–Fr (Roberston, 2016) with case histories

Figure 5-19: CPT-N04 – Robertson tailings state

5.4 Embankment Dam

5.4.1 Fill Zonation

Three classes of material were used in the NTSF embankment: rockfill, which provides the main strength of the dam; clay core, which primarily provides a hydraulic barrier to retain tailings water and is supported by the rockfill; and, filters to prevent the very small clay particles migrating into the void space of the rockfill.

5.4.2 Rockfill

Rockfill (both Monzonite, and Silurian sedimentary rock), was sourced from the initial stripping and mining operations for the open pit. The sedimentary rock was initially regarded as inferior strength rockfill by the original designer, a view that they subsequently changed to 'complying with design requirements' based on some (unreported) shear tests.

Rockfill placement depended on the zone within the dam. In the zones where rockfill strength was of particular concern to the designers, it was placed in layers of less than 1m thickness with some compaction. Other zones where rockfill strength was a lesser concern, end-dumping was used for placement.

Due to the difficulty and cost of performing large-scale tests on rockfill, no strength tests were completed for design nor were any insitu density tests carried out during construction. The rockfill bulk density used in design ranged between 19 kN/m^3 and 20 kN/m^3, while drained strength parameters of c' = 0 kPa and ϕ' = 40° were adopted for the main rockfill with slightly higher values (c' = 0 kPa and ϕ' = 42°) were assumed for the finer transition zone.

These rockfill placement choices, associated design strengths, and level of quality control testing are common for rockfill dams of this type.

5.4.3 Clay Core

Potential clay borrow for the core was investigated in two campaigns before construction. Drained strength tests were carried out on samples compacted in accordance with the planned construction specification. A further round of testing followed shortly after construction started.

The construction quality assurance records show the Stage 1 and Stage 2A clay core materials generally conformed to the construction specification.

As part of the ITRB investigation program, one drillhole (CE407) was completed specifically to intersect and sample the Stage 1 embankment clay core. Three undisturbed samples were recovered, with two undrained triaxial tests then carried out on the sampled core.

Figure 5-20 compares the ITRB strength results with those from pre-construction testing. The new data (CE407 samples) shows a generally weaker core.

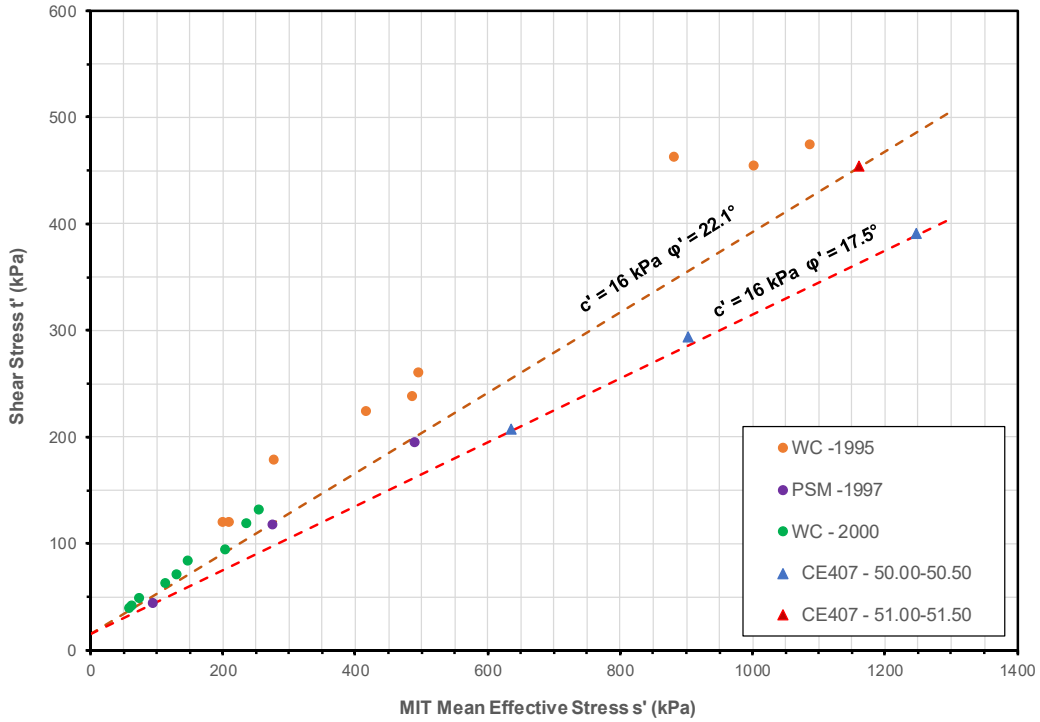


Figure 5-20: Compacted core strength in triaxial compression

5.4.4 *Filter Materials*

Stages 1 and 2 of the NTSF were designed as water retaining structures, with filters provided between the clay core and the downstream rockfill. Filter design appears to have been entirely focused on adequacy of hydraulic purpose, rather than strength, and there appear to have been no strength tests. This design intent was transferred into construction as a gradation envelope specification for the filters.

A change to the embankment filter design during the construction was the inclusion of a transition zone between the filter and the core to improve the compatibility of these two materials. Also, where potentially permeable material was identified in the downstream side of the core trench, the core trench was widened with filter material.

Quality assurance procedures for the filter focused on the as-placed gradation. Concerns were raised as the contractor consistently had difficulties in achieving the specified material grading, with the records indicating compliance on average but with shortfalls overall (Appendix D). A physical test of filter adequacy was carried out and which confirmed that the as-used material met the design intent.

5.4.5 *ITRB Assessment of Embankment Properties*

In the case of the rockfill, the strength was checked using Leps (1970), who assembled published laboratory test data on rockfill strength and reported the friction angle as a function of normal pressures. This is a well-cited and widely used study. The Leps data set was screened to include only fine grained igneous rocks similar to that which was used in the NTSF, and is reproduced in Figure 5-21. It indicates that for a normal stress of 1000 kPa, which is a representative stress level on a failure wedge for the current embankment height, a friction angle of 40° is appropriate. The original design choices are consistent with this estimate.

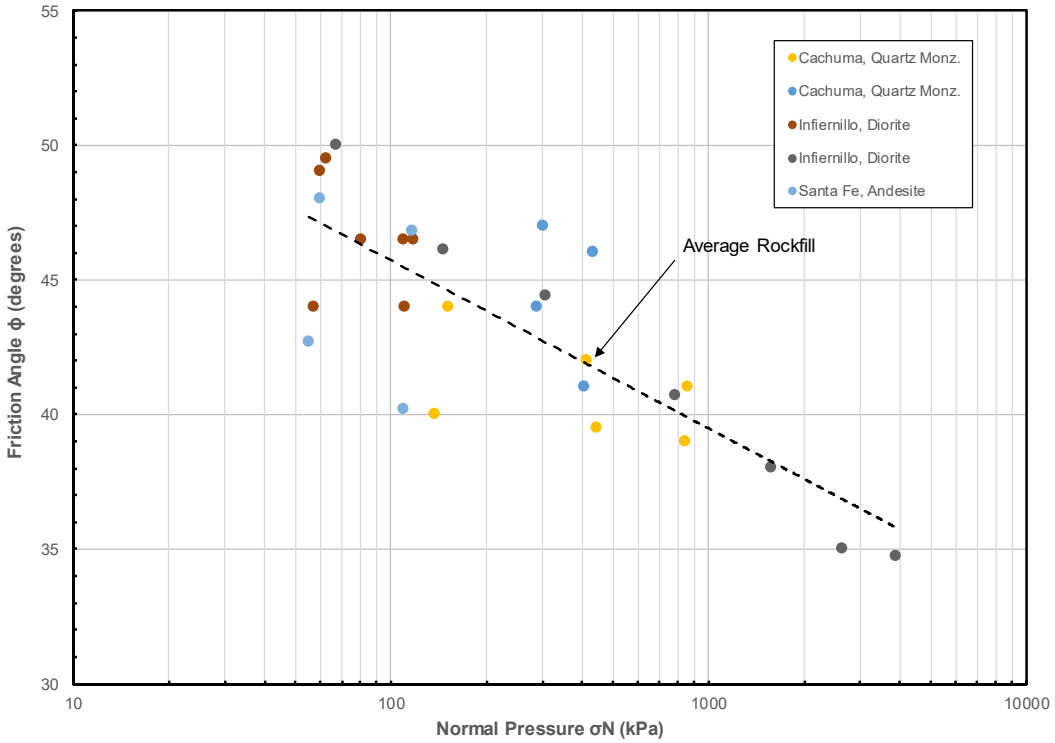


Figure 5-21: Leps (1970) data including fine grained igneous rocks

The rockfill stiffness was also estimated using data obtained from the 2018 GHD geophysical investigation using Multi-Channel Analysis of Surface Wave (MASW). The MASW method provides a profile of shear wave velocity with depth, which in turn can be interpreted as a profile of the elastic shear modulus. Appendix D compares this geophysical data to stratigraphy in adjacent drillholes. However, rockfill deformation will involve irrecoverable plastic strains and the elastic modulus will over-estimate the apparent rockfill stiffness to foundation movements. A widely used rule of thumb is that the operating stiffness is about one-third of that measured by geophysical methods. Overall, a shear stiffness of about 250 MPa is a starting point for the numerical studies; but, this NTSF-specific modulus is double what might be inferred from some correlation in the literature, so some stiffness reduction could be viewed as reasonable.

In the case of the compacted core, the ITRB's investigation shows systematically less strength than was expected when construction started. It is likely that part of the strength reduction is due to softening that might have happened under operational conditions. In practical terms, these reduced strengths are not a concern as the strength of the larger part of the dam (the downstream constructed part) derives from the rockfill.

In the case of the filter, hydraulic deficiencies of filters are a known cause of trouble with water retaining dams. Checks on the filter gradations indicate that although the filter material used met their design criteria they do not comply with modern criteria for adequate prevention of fines movement. As the embankment has not been a water retaining dam for most of its life, the ITRB has neglected fines migration as a mechanism that should be modelled. In terms of strength, the compacted filter would be marginally weaker than the rockfill based on their soil type, gradation, and placement. However, in practical terms, given the uncertainty in rockfill stiffness, there is no need to explicitly represent the filters within numerical models.

6. Failure Hypotheses

6.1 Introduction

The most common causes of failure of tailings dams include overtopping, piping, operational error or mischief, and instability of the slope and/or foundation. A forensic investigation would normally assess each in turn in order to rank the hypotheses for the cause of failure. However, in this case the exclusion of all but one of these causes is straightforward. The NTSF decant pond was too small and far away to directly affect the integrity of the TSF. Operations prior to, and at the time of failure were conventional, and there was no evidence of mischief. Moreover, direct observation of the deformation within the NTSF prior to collapse and immediately afterward support the view that the Event was triggered by instability of the slope and/or of the foundation.

6.2 Causes of Instability

While it is evident that instability of the NTSF arose from geomechanical failure of the slope and/or foundation, the contributing causes of the failure are multiple and complex as indicated by the timeline of the failure summarised in Section 2 above and in Appendix B, and the analyses presented in Appendix H.

Surface deformation monitoring prior to the collapse indicated above average embankment displacement in the failure zone some time before the Event. They were not so large, given the observational procedures being used, that they were regarded as alarming. In the months preceding the Event they were accelerating, particularly evident in the InSAR data that was discovered subsequent to the Event. The explanation of the failure has to capture this history. As revealed in Section 4 above, the site investigation discovered a zone of exceptional weakness beneath the failure zone, and it will be shown that the pre-cursor movements within Phase 1 before the Event are attributable to yielding in this zone. The mechanism for Phase 1 will have to account for the acceleration of movement that occurred as well as the timing and location of the cracks that were identified prior to Phase 2 movements.

Phase 2 movements that resulted in the substantial displacement of a portion of the embankment can only be explained by an increase in loading on the embankment due to the liquefaction of the loose, saturated tailings. Under these conditions, the analyses have illustrated that the driving forces on the embankment exceeded the resisting forces at that time, in order to account for the ensuing movements.

There are two different processes that can initiate liquefaction that need to be considered. The first is static liquefaction. This arises when the yielding of the saturated loose tailings occurs in such a way that they are brought to a collapsing state. The movement of the embankment on its weak foundation is one such process that could induce static liquefaction.

The other process is cyclic liquefaction. There is abundant evidence from earthquake-induced failure of tailings dams that the cyclic dynamic stresses from the earthquake ground motion can result in liquefaction of loose saturated tailings. As noted in Section 3 above, just the day before the Event, the NTSF experienced two small earthquake shocks, just a few seconds apart, hence extending the duration of significant shaking. Under normal circumstances, these small earthquakes would not be regarded as consequential. However, in the failure zone, the structure was already exhibiting some distress due to the accumulating foundation movements and may have become increasingly fragile. The analyses needed to distinguish if the earthquakes induced the liquefaction, whether liquefaction resulted from static loading alone, or whether it is too difficult to distinguish between these two mechanisms.

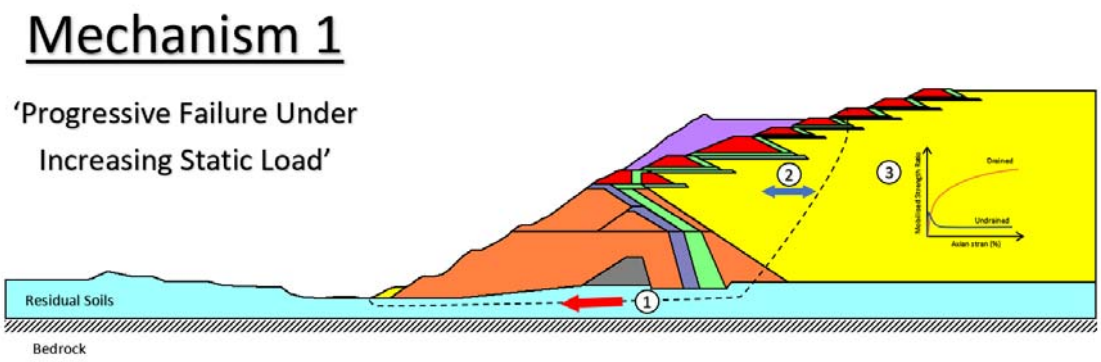
Hence the explanation of the failure must account for this sequence of events while being consistent with the site and laboratory characterisation data as well as the integrated seepage database summarised in Appendix F .

6.3 Failure Mechanisms

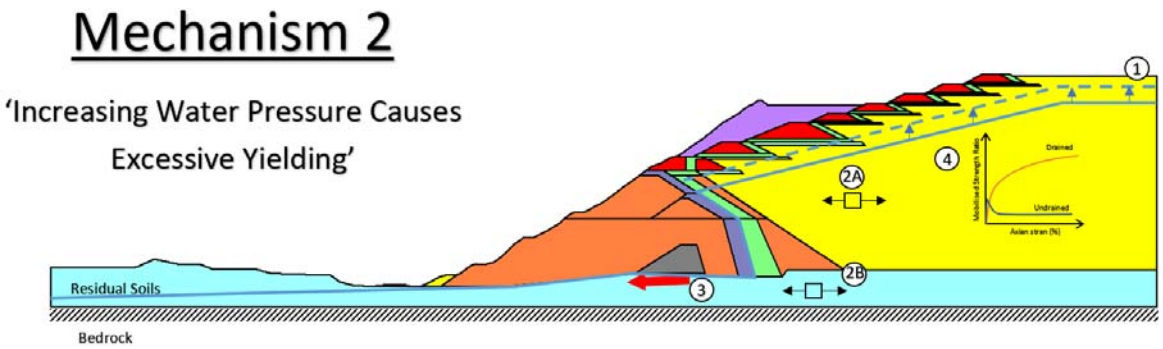
The NTSF embankment was stable on March 8, 2018 and the piezometric data strongly suggests that drained conditions prevailed in the tailings. The rate of Stage 1 Buttress construction was also such that the foundation likely behaved in a drained manner (there were no relevant foundation piezometers to provide data). The issue for the ITRB was then: what processes or events could have led to the tailings becoming stressed beyond their instability locus. Three mechanisms were identified for analyses and which are now described briefly before discussing what was found when analysing each of them. The mechanisms are illustrated on Figure 6-1.

All three mechanisms lead to the condition where the undrained strength of foundation is insufficient for the applied tailings loads and Phase 2 initiates.

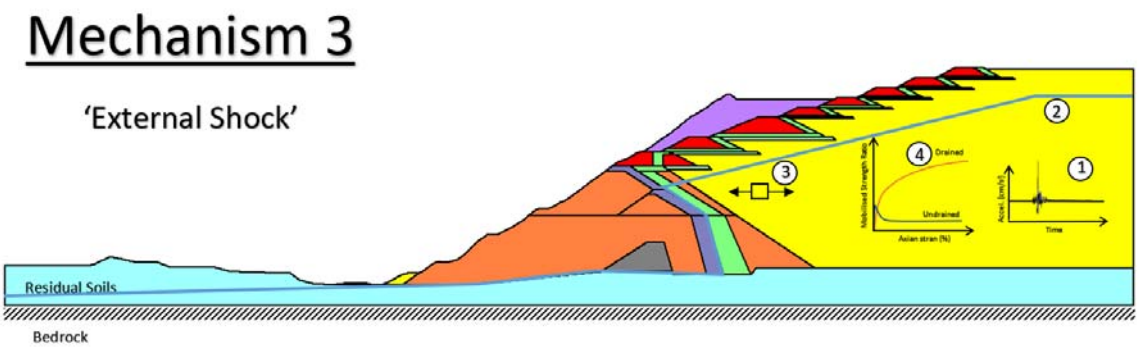
The ITRB's investigation was thus to simulate the dam condition at the end of the Stage 10 raise as closely as could be done, using the key observations and measurements to condition the model. Then, each of these mechanisms was evaluated by further assessment and supported by advanced laboratory tests where appropriate.



(1) Progressive failure in the foundation as upstream raises cause outward horizontal movement in foundation.
(2) Foundation movements reduce support to tailings while increasing yielding in the tailings.
(3) When yielding in tailings progresses to the instability locus tailings rapidly switch to undrained response losing about 2/3 of their strength (Gens & Alonso, 2006).



(1) Water table rises in the TSF as tailings level rises.
(2) A: Rising water pressure reduces effective confining pressure in tailings.
B: Rising water pressure reduces vertical effective stress in residual soils.
(3) Decreasing effective stresses accelerate yielding because the shear stresses remain constant.
(4) When yielding in tailings progresses to the instability locus tailings rapidly switch to undrained response losing about 2/3 of their strength (Eckersley, 1990).



(1) Earthquakes cause increase on pore pressures within the tailings as the particles move under the applied ground motion.
(2) These pore pressures can trigger liquefaction on their own or can dissipate by pore water moving horizontally because of the sandier layers within the tailings and trigger liquefaction at a later time.
(3) Migrating pore water reduces effective confining stress under the upstream raises causing yielding in these tailings.
(4) When yielding in tailings progresses to the instability locus tailings rapidly switch to undrained response losing about 2/3 of their strength (Ishihara, Post-Earthquake Failure of a Tailings Dam Due to Liquefaction of Pond Deposit, 1984).

Figure 6-1: Schematic illustration of potential failure mechanisms

7. Stability Analyses

7.1 Introduction

The safe design of tailings dams conventionally employs Limit Equilibrium Analyses (LEA) to demonstrate stability. LEA considers the static equilibrium of a potential sliding mass and compares the resistance of the ground required to equilibrate the potential failure mechanism with the strength available. It does this through the calculation of the Factor of Safety which is the factor required to reduce the strength(s) of the soil units to bring the mass into a state of limiting equilibrium. The method of analysis presented by Morgenstern and Price (1965) is generally regarded as the most suitable procedure for analyses restricted to two dimensions and is adopted here for screening purposes. This and other more simplified methods are available in well-established computer programs used commonly in professional practice. Appendix G provides more details.

Design requirements for the Factor of Safety are generally prescribed by design guidelines and regulations. Appendix B summarises the design Factors of Safety for the NTSF throughout its various stages and cites reports that indicate compliance with Australian National Committee on Large Dams (ANCOLD) requirements throughout the evolution of the structure.

The Event demonstrates that the NTSF was not in compliance at that time. At its location, the Factor of Safety had reduced with ongoing raising of the structure, as progressive failure in the foundation propagated. It was likely just above unity at the end of Phase 1, when movements were still modest. Subsequently, the Factor of Safety fell to unity or below when Phase 2 occurred, with likely rapid translation of the structure. As summarised in Section 6, above, the failure mechanism was exceedingly complex, involving progressive failure due to strain-weakening in the foundation, the mobilisation of the undrained residual strength of the foundation, and finally the triggering of liquefaction of the loose, saturated tailings that had been contained until Phase 2 occurred.

LEA is not capable of addressing the number of complex physical processes involved, except by making gross assumptions about the available strengths of the NTSF and its foundation at various stages of its construction. This is more appropriately addressed by means of a comprehensive deformation analysis that can follow more closely the stresses and deformations of the NTSF and its contents through the sequence of behavioural changes. Such a sequence is discussed in detail in Section 8 of this Report with supporting documentation presented in Appendix H. However, LEA is still useful in undertaking screening analyses to explain the sensitivity of the stability of the structure to assumptions of strength consistent with observed behaviour. Information from these analyses provide guidance for the selection of material properties to be considered in the more complex deformation analyses. LEA can also be performed to study three-dimensional restraints to failure in an economical manner, before committing to the challenge of undertaking three-dimensional deformation analyses.

7.2 LEA (2D)

LEA in terms of a two-dimensional model (2D) are most commonly adopted in the design of both tailings and water dams. The 2D model assumes that the potential failing mass is infinitely long and hence the extra end resistances to failure can be neglected. The assumption of 2D conditions is intrinsically conservative. All design analyses in support of the NTSF were conducted assuming 2D conditions.

Figure 7-1 is an example of a 2D LEA analysis conducted early in this study for screening purposes. Many others are presented in Appendix G. In this case, sliding failure is assumed to occur within the relatively shallow weak FRV Unit A foundation revealed by the field investigation, and then projected upwards to the location on Stage 7 and Stage 8 where cracking was observed on the day of the Event. In this particular case, peak strengths are assumed in the foundation, ignoring its strain-weakening behaviour. The pore-water pressure distribution reflects piezometric readings and pond level measurements taken before the Event. The more comprehensive assessment of the conditions presented in Appendix H were not yet available when these calculations were undertaken. In this case, the tailings were assumed to be in a liquefied state, but not at their residual undrained strength. All other properties presented in the table were consistent with the summary of material properties presented in Appendix D.

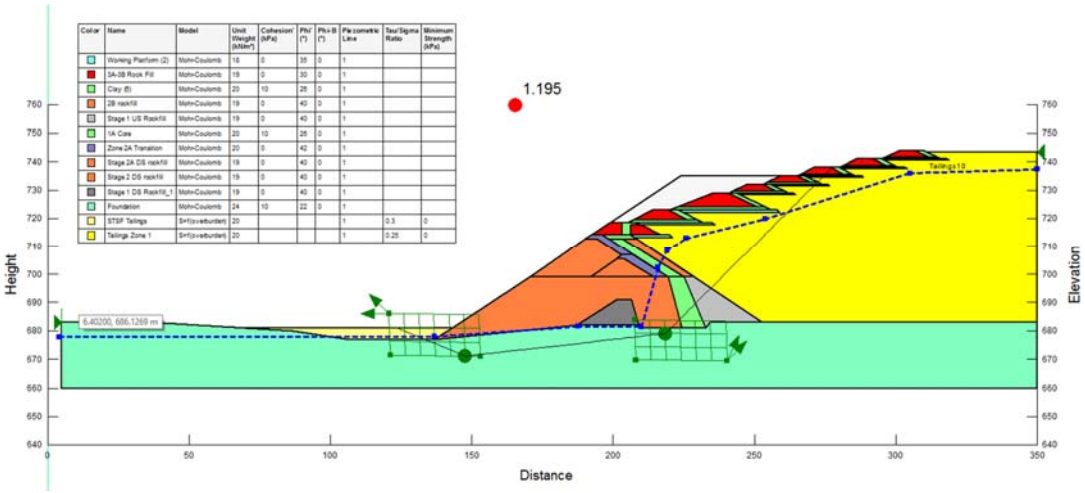


Figure 7-1: Stability section model geometry

It can be noted that a Factor of Safety of 1.2 is indicated for this case. This and many other screening calculations revealed Factors of Safety significantly less than the likely design objective of 1.5 mandated by ANCOLD, and were often close to unity. The specific numbers are not consequential to meeting the objectives of this study. However, the screening analyses did lead to several conclusions that facilitated more focused analyses such as:

- The block sliding mechanism adopted for the failure provided the lowest Factor of Safety for the design section, and a failure surface geometry that closely replicated the observed pre-failure cracking;
- The calculated Factor of Safety at the slump location is relatively insensitive to both the clay core and rockfill shear strength parameters, varying by 0.02 and 0.05, respectively, over the range of shear strength parameters analysed; and
- The calculated Factor of Safety was relatively insensitive to small variations in the assumption of the bedrock level.

It is likely that at the time of the Phase 1 observation of cracking and thrusting at the toe of the structure, the Factor of Safety was close to unity, say 1.1. Having screened out the significance of variation of some of the material properties, it became possible to assume a Factor of Safety and calculate the properties of the foundation material consistent with the assumed Factor of Safety. Given the slow rate of construction, for this analysis it is reasonable to assume that pore-water pressures in both the tailings and the foundation reflect fully drained conditions consistent with the piezometric observations. The range of material properties adopted in these analyses is presented in Table 7-1.

Table 7-1: Material parameters adopted for foundation parametric back analyses

Material	Bulk Density γ (kN/m³)	Drained Parameters	
		Cohesion c' (kPa)	Friction ϕ' (°)
Tailings	20	0	34 to 40
Clay Fill	20	10	22 to 26
Transition	20	0	42
Rockfill	19	0	40

Using the combination of material parameters provided in Table 7-1, the drained parameters required to achieve a Factor of Safety equal to 1.0, 1.1, 1.2 and 1.3 were determined. The case assuming a frictional resistance for the tailings of 34° is presented in Figure 7-2. Focusing on the Factor of Safety of 1.1 results, one can infer that the average mobilised strength is less than the peak drained strengths attributable to the foundation material in Section 5 of the Report, and that little cohesive resistance was available. This implies that the lower undrained strength was likely being mobilised at this time and that progressive failure was advanced. This conclusion is helpful in guiding the formulation of the deformation analyses that one requires to demonstrate the evolution of progressive failure in more detail.

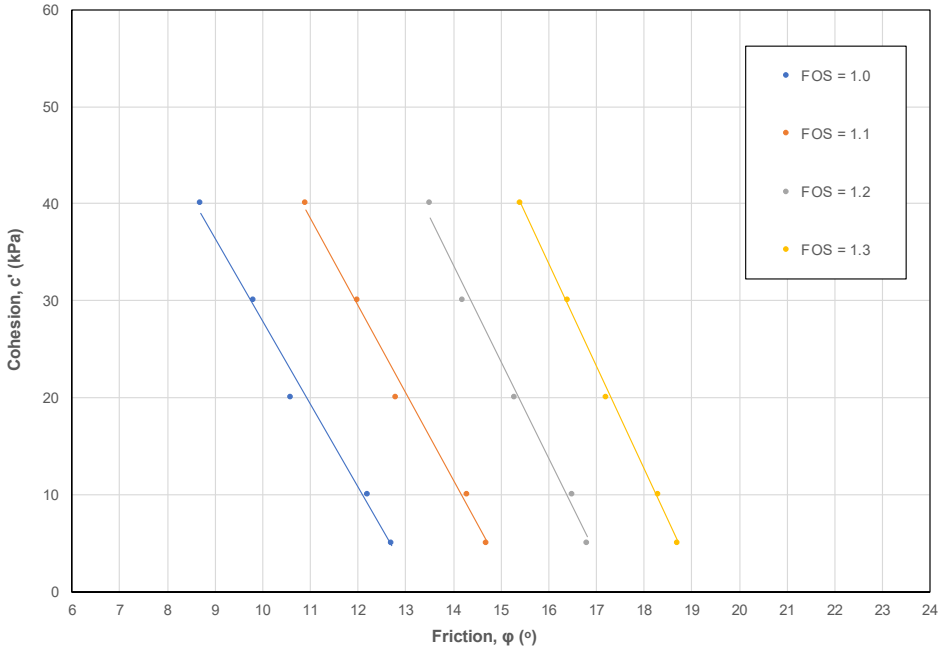


Figure 7-2: Foundation back analysis, drained tailings φ' = 34°

7.3 LEA (3D)

The observed length (L) of the slump parallel to the NTSF crest was approximately 300 m while the height at the slumped section to the level of infilling (H) was approximately 68 m. This provides an L/H ratio of about 4.4 symptomatic of the need to also consider three-dimensional (3D) restraints associated with the failure mechanism. Simple visual examination of the morphology of the slump (see Figure 2-1) provides vivid evidence of the role of 3D edge effects affecting the mobility of the slump. While not commonly used in design, LEA (3D) is not new and has been used increasingly in assessing stability when 3D restraints are evident, as is the case here.

Morgenstern (2017) discusses the increasing role of LEA (3D) in practice and provides an example of dam safety assessment that was flawed by ignoring 3D effects. Chaudhury et al. (2016) provide examples of the use of three-dimensional stability analyses for conditions that arise in mining practice.

The early experimentation with LEA (3D) is summarised in Appendix G. Comparisons at that time suggested that the 3D Factor of Safety may be as much as 20% higher than the 2D value.

A more detailed 3D analysis was subsequently undertaken that honoured field observations in a better manner than the first trial computations. The observed vertical tension cracks were also simulated, and the phreatic surface developed in the comprehensive hydrogeological investigation presented in Appendix H were also incorporated in the analyses. Details are discussed in Appendix G and the modelled failure surface geometry, together with a cross-section of the slump, are shown in Figure 7-3 and Figure 7-4, respectively.

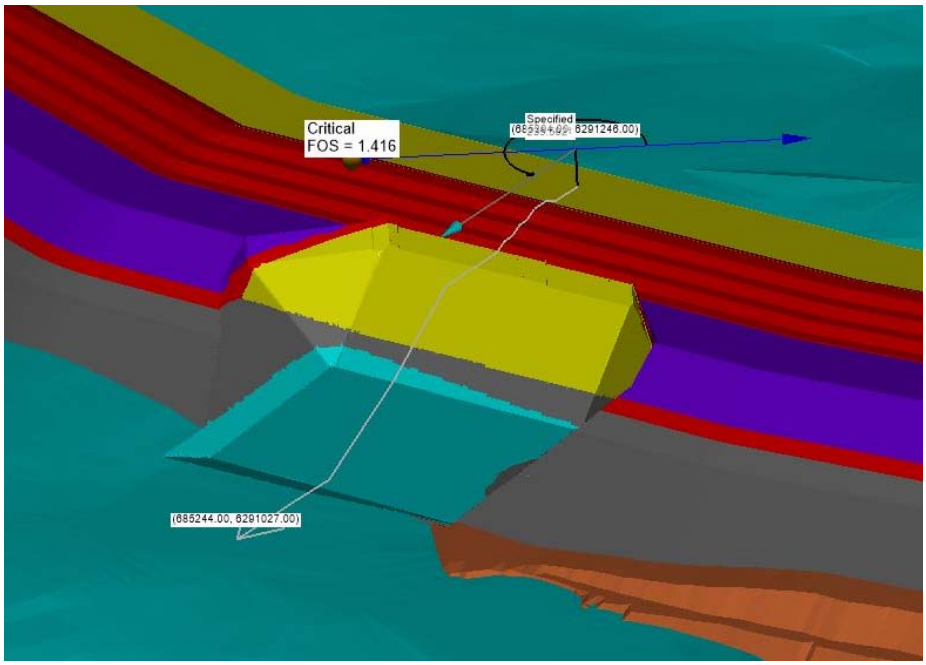


Figure 7-3: Adopted failure surface geometry

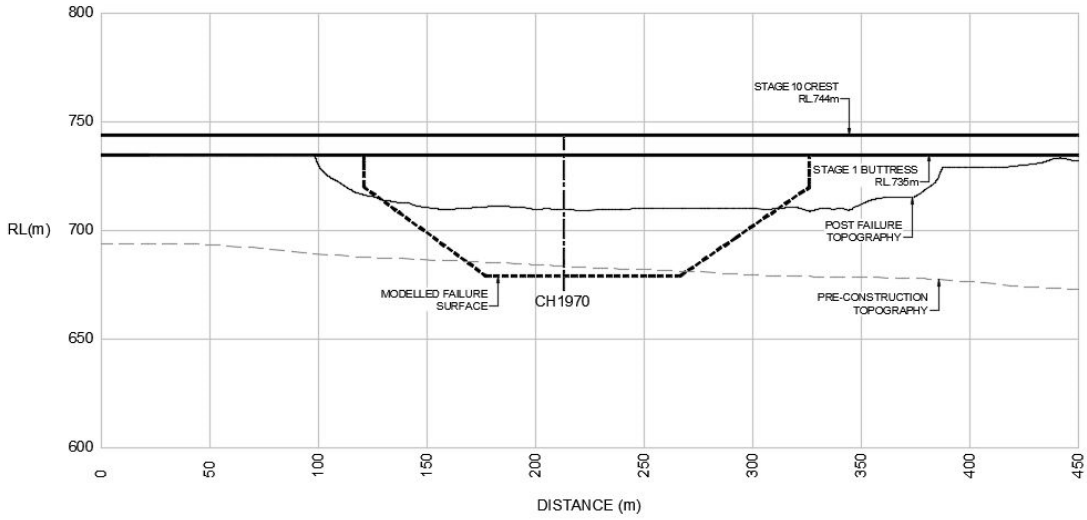


Figure 7-4: Cross-section of slump through Stage 1 Buttress showing modelled failure surface

For fully drained conditions with foundation strength of c' = 0 and ϕ' = 16°, the 3D Factor of Safety approximately 1.39 should be compared with a 2D Factor of Safety of about 1.15 when interpolating from Figure 7-2. This indicates an approximate increase of about 20%, emphasising the need to take 3D factors into account in this study.

Of particular significance is the finding that when the tailings are fully liquefied at their residual strength ratio of 0.06, and the foundation resistance is at an undrained resistance ratio of 0.22, the Factor of Safety is unity, consistent with the conceptual basis put forward for the cause of Phase 2 deformation. If the resistance ratio is put at 0.2, consistent with experimental findings, the Factor of Safety becomes 0.94, indicating the existence of unbalanced forces sufficient to accelerate the failing mass forward.

Of particular significance is the finding that, when the tailings are fully liquefied and the foundation resistance is at an undrained strength distribution consistent with the Phase 1 FLAC 3D deformation analysis, the Factor of Safety is about unity or less. The ITRB is of the view the undrained residual strength ratio of the tailings was about 0.2 at the onset of Phase 2, reducing to lower values as large deformations developed (see Sections 8.6.2.1 and 8.6.2.2). Figure 7-5 plots the Factor of Safety over a range of deduced foundation undrained strength ratios illustrating the potential for Factors of Safety less than unity, consistent with the acceleration that developed at the outset of Phase 2.

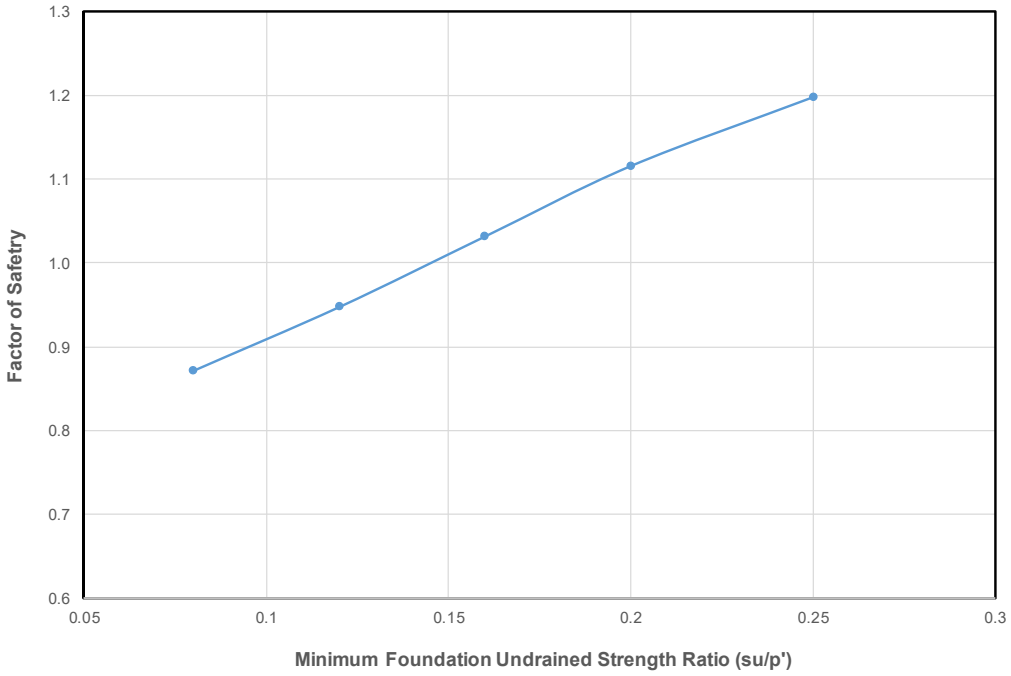


Figure 7-5: Variation in Factor of Safety with undrained strength ratio of foundation

8. Deformation Analyses

8.1 Overview

This section of the report addresses how the Event developed, starting from an apparently stable situation and ultimately generating a mobile slump.

The controlling tailings behaviour is illustrated on Figure 8-1 and is presented here to illustrate why it was necessary to do the analyses presented in this section. Tailings behaviour depends on the loading path and the tailings ψ, with Figure 8-1 being for the approximate loading path of the most vulnerable part of the tailings at their insitu conditions in the NTSF. Figure 8-1 is schematic, but also a fair representation of measured behaviour.

The upper curve on Figure 8-1 (in orange) is the situation where the tailings are loaded sufficiently slowly for the pore water to migrate out of the tailings as they compress under load ie. drained conditions. The design of the upstream raises and Stage 1 Buttress was essentially consistent with this mode of tailings behaviour, with standpipe piezometers deployed to confirm the absence of excess pore pressures.

The lower curve on Figure 8-1 (in blue) is the situation where the pore water cannot migrate quickly enough, and which results in transfer of some load to the pore water, with consequent increase in pore pressure, ie. undrained conditions. This was the mode of the tailings behaviour during Phase 2 of the Event.

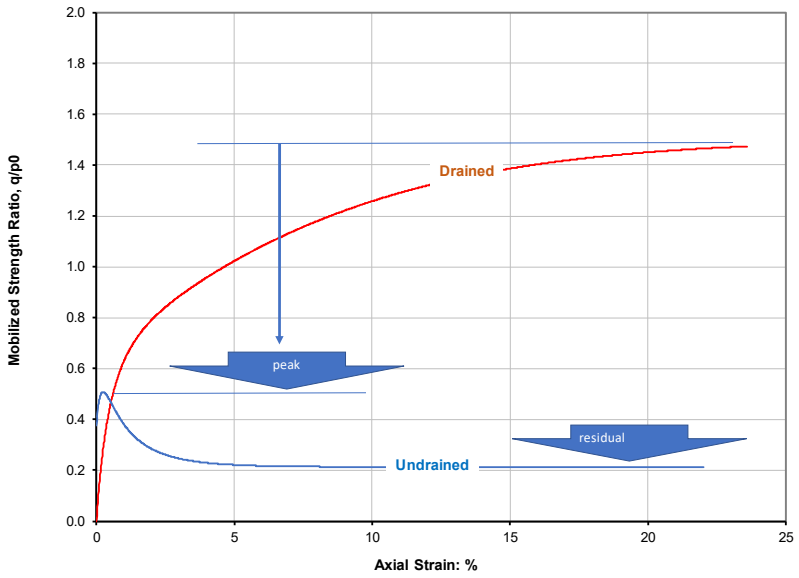


Figure 8-1: Illustration of tailings strength evolution with strain (typical for NTSF)

Figure 8-1 illustrates that the peak undrained strength is about one third of the drained strength, and, if strains develop in the undrained state, the strength can fall even further to a residual undrained value. This is why apparently stable dams designed for drained conditions with supposed conservative Factors of Safety can fail if something causes a change from drained to undrained response; and, because strength falls further as displacements develop, a slump will accelerate.

Evaluating how the NTSF slump developed thus becomes determining why the tailings response changed from drained to undrained behaviour. This switch from drained to undrained behaviour can develop in a few seconds, and with minimal warning. The switching from drained to undrained response arises if the stress state exceeds the instability locus and drainage is inhibited.

The instability locus is most easily explained by test data. Figure 8-2 shows the behaviour of a loose sample loaded in direct simple shear. This test was carried out on a sample of the dominant silt tailings under stress conditions that reflect those operating beneath the downstream crest of the Stage 1 Buttress and at the level where upstream construction started. This is a critical location for embankment stability. Initially, the sample was loaded drained to the stress state reflecting the Stage 1 Buttress as-constructed. Loading then continued undrained. This test is shown on Figure 8-2 (MSS-10).

When undrained loading starts, there is some reserve strength with the sample showing a stiff response until a sudden loss of strength after the shear stress had increased by about 5 kPa. The locus defining this sudden loss of strength is represented by the green line shown on Figure 8-2. The instability locus is usually expressed as the ratio η_{IL} ($\eta_{IL} = \tau/\sigma_v$ at this condition). This test had an equivalent Factor of Safety against static liquefaction of approximately 1.05 at the end of drained loading. For other stress conditions, different stress variables are utilised, see Appendix E.

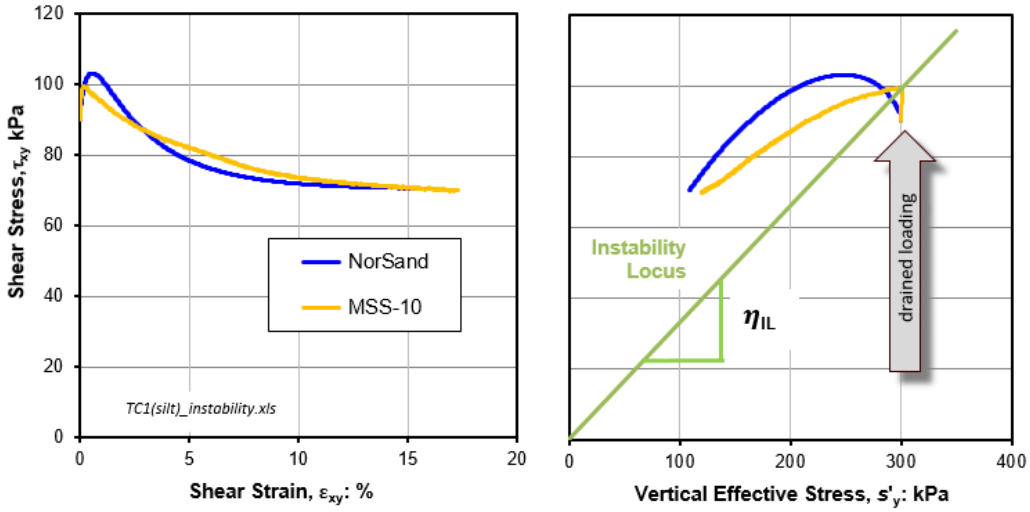


Figure 8-2: Definition of Instability Locus

The blue line shown on Figure 8-2 is computed (using NorSand) for monotonic simple shear with the tailings properties determined in triaxial compression (see Appendix E). The computed behaviour is a reasonable match to the test, especially in the case of the stress-strain behaviour. The instability locus is also much affected by ψ, as illustrated in Appendix E.

If the soil stress conditions exceed the instability locus, the subsequent behaviour depends on the ability of the adjacent soil to accept load that must be redistributed from the over-stressed zone. If adjacent soil cannot accept this redistributing load, progression to failure accelerates and this can result in almost instantaneous collapse of the soil mass. This almost instantaneous failure development can be seen in the video record (2019-01) of the recent Brumadinho dam liquefaction. Based on that video record, liquefaction appears to have developed there in less than five seconds and with no excess pore pressures apparently being indicated by the piezometric monitoring array prior to that event (2019-02). It is of interest to note that this phenomenon was identified by experiments completed by (Eckersley, 1990); the occurrence of excess pore pressure is a consequence, not a cause, of the instability and thus deployment and monitoring of piezometers provides no guidance to the actual embankment stability.

The manner in which the drained to undrained transition develops, and influences the stress redistribution within the dam, depends on the relative stiffness between the various locations. This dependence on stiffness requires that the analysis explicitly represent the stress-strain behaviour, particularly of the foundation and the tailings, and hence excludes the simpler limit equilibrium methods of Section 7. Analysis must use advanced numerical methods. The numerical modelling used was Fast Lagrangian Analysis of Continua (FLAC), with both 2D (plane strain) and 3D versions. The methodology used is documented in Appendix H, and had been previously used in the Fundão Tailings Dam Investigation (Fundão Tailings Dam Review Panel, 2016). The analyses discussed earlier also adopt the stress-strain relations used by NorSand for tailings, see Appendix E.

The existence of the instability locus reflects the balance between the drainage from a contractive loose soil and factors that might impede it. If during shear induced contraction, drainage is totally unimpeded, as might be the case in a gravel, the instability locus will be reflected as a change in rate of volumetric strain. If drainage is fully impeded, i.e. undrained loading, the reduction in resistance when stresses reach the instability locus will be sudden as discussed in the section above. Intermediate cases can develop, both in the laboratory and the field, in which there may be sufficient drainage to inhibit the mobilisation of the instability phenomenon. Under these circumstances alternate laboratory procedures will be needed to explore the influence of drainage on the onset of liquefaction.

Laboratory testing to assess instability is not routine. The results obtained are known to be affected by the nature of the loading arrangement and the ease with which water can move out of the test sample (‘system compliance’; eg Gajo, 2004). The possible effect of laboratory procedures on the assessed instability was evaluated by using two independent laboratories and evaluating this test data within the context of the measured stress-strain behaviour (Section 8.7).

Although Figure 8-1 is presented in terms of measurements in DSS tests, all the analyses reported in this section were carried out using complete representations of stress (ie. the full 3D ‘stress tensor’). Soil behaviour (including that of tailings) is controlled by the ratio of distortional stress (σ_q) to mean effective stress (σ'_m), the parameter η (= σ_q / σ'_m). Because the intrinsic ‘frictional’ strength of soil (M_t) varies with the relative proportions of the principal stresses, it is helpful to use the ratio η/M_t to scale the controlling stress ratio to the available strength. This ratio η/M_t is used throughout this section as it allows direct comparison with the computed stress distributions in FLAC with the supporting laboratory tests (with their special stress or strain conditions) used to investigate the operating instability locus for the NTSF.

8.2 Observations Honoured

Understanding how the Event developed must start with determining the stress distributions within the impoundment and its foundation. The foundation properties have a range of plausible values, the configuration of the foundation strata is known only at the locations of the available drillholes, and the tailings have a variable state. The stress analysis has therefore been used parametrically within the plausible range of these factors, and then followed an optimisation to develop the best match between computed deformations and the following measurements and observations:

- Absence of excess pore pressure in the tailings. (ie drained conditions during Phase 1),
- The CPTu data (particularly 2017-N04 on the upstream edge of the slump),
- Location of crest cracking and the timing of its development,
- Minimal toe heave thrusting,

- Development of deformations over preceding months (terrestrial survey & InSAR data),
- The dam in the vicinity of the slump was stable after completion of the Stage 1 Buttress, and
- Extent of the tailings that failed.

The work reported in Appendix H is thus a series of scenarios where the representation of the embankment, its foundation, and the retained tailings are progressively varied to honour as much as possible (within current computational capability) these observations. The final result is a best-fit stress analysis for the conditions in the embankment, its foundations, and the tailings that is consistent with the key measurements and observations. The final result must also consider the small earthquakes on March 8, 2018 which needed to be considered as a potential trigger for Phase 2 of the Event.

A principal constraint on the deformation analysis was that the simulated embankment deformations should match those measured. Two types of deformation data are available, namely survey prisms measurements (terrestrial) and InSAR derived observations. These are summarised in Section 3.3.4 and discussed in detail in Appendix B.

Piezometric conditions were routinely monitored in the tailings, as is normal for upstream raise construction. This monitoring data are summarised in Appendix B and support the observation that tailings consolidated as fast as the rate of accumulation so that no excess pore pressures developed, i.e. drained conditions. As the tailings height increased with the elevation of the pond, so did the pore pressures which is entirely normal. The CPTu data from the 2017 site investigation campaign revealed a distinct downward hydraulic gradient within the tailings. These monitoring data and trends have been synthesised in a comprehensive hydrogeological study, see Appendix F, and the integrated piezometric data have been utilised in the deformation analyses, see Appendix H.

8.3 Representation of NTSF

8.3.1 Staged Construction

The construction history of the NTSF, summarised in Section 3 and detailed in Appendix B, was incorporated in the FLAC models, see Appendix H. Tailings were placed concurrently with each stage of the construction. Consolidation under incremental loads was taken as rapid with effective stresses updating concurrently as the loads were applied. This is consistent with the measured pore pressure records in the tailings.

The Stage 1 Buttress was split into three substages, all reflecting how the buttress was built as well as allowing the stresses to redistribute and honouring the actual loading path.

As stated in Appendix H, the model geometry was developed using the topographical survey and geological site characterisation data, as well as historical pond elevation data and interpretation of subaerial beach width from GoogleEarth time-lapse aerial photographs.

8.3.2 Material Zones Modelled

The material zones simulated in the dam were slightly simplified from the construction drawings. The internal zonation details of the NTSF dam (rockfill shell, clay core, and the transition zone) were included in Stage 1 and 2, of the model. For Stage 3 to 10, each stage was modelled as rockfill as the dimensions of the transition zones were insignificant compared to the rockfill. Figure 8-3 shows the distribution of the various zones represented; the tailings extend for 500 m upstream of the dam core to allow full development of the extent of liquefaction unconstrained by boundary effects. The fill and foundation elements were grouped to allow sequencing of staged construction and to include inter-stage excavation or deposition downstream of the dam toe.

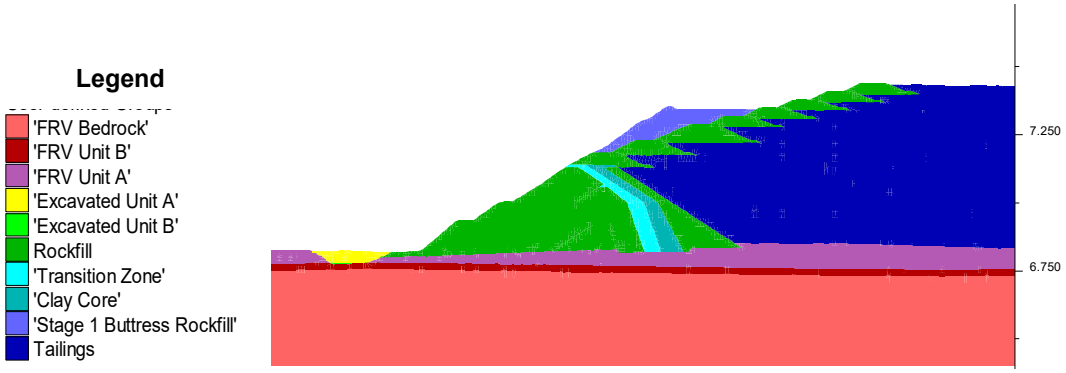


Figure 8-3: Idealisation of the NTSF embankment at CH1950 for numerical analysis

8.3.3 Piezometric Conditions

8.3.3.1 2D Model

The pore pressures for the end of each construction stage were defined using three data sources: the historical piezometric records available close to the upstream edge of the dam; pond elevation; and subaerial beach length.

Some piezometer records were available from the end of Stage 5 construction (2011) while others were available from the end of Stage 9 construction (2016). Pond level records were available from the end of Stage 4 construction (2008). For Stages 1 to 3, where the data were not available, the pond level was estimated.

Beach length information was inferred based on historical time-lapse photography sourced from GoogleEarth; these images were available from December 2003. For the end of construction periods where the beach length was not available, the beach length was obtained by linear interpolation between the available photographs. The phreatic surface was defined by connecting the piezometer levels to the pond level located at the calculated beach length distance. The data indicate that the phreatic surface at the end of Stage 10 and Buttress 1 construction was taken at 4 m below the tailings surface just upstream of the then dam crest.

The 2017 site investigation data shows pervasive downward groundwater flow just upstream of the dam crest, so that the piezometric conditions are not hydrostatic within the tailings adjacent to the dam. This was honoured by using a reduced pore-water unit weight in the tailings below their phreatic surface.

8.3.3.2 3D Model

The results of the hydrogeological study were used in the FLAC 3D analysis (refer Appendix F) and the piezometric data in it were incorporated.

8.3.4 Material Properties Used

The basis for selecting material properties is discussed in detail in Section 5, and is supported by Appendix D and Appendix E.

The properties of the engineered zones of the dam (rockfill, clay core, and transition), were similar to those used in its design, but reflected some changes arising from testing and evaluation conducted by the ITRB.

In the case of the foundation soils, the strengths and stiffnesses were based on laboratory tests, emphasising DSS data over TX data due to the anticipated deformation mode. The testing program is considered sensibly representative of all the materials encountered but involved emphasis on testing of the FRV Unit A and FRV Unit B, and to some extent the residual basalt, due to their special significance in likely controlling the foundation behaviour. While representative, this experimental data does not provide unique parameters, but is open to additional interpretation by the ITRB. There is always unavoidable uncertainty associated with data obtained from undisturbed sampling and testing (eg. sampling disturbance) that provides latitude for the ITRB to exercise its judgement on what are the strengths and deformation properties for analysis. In this study the ITRB places a great emphasis on the goodness of fit between calculations and field observations as evidence to support the operational strength and deformation properties.

In the case of the tailings, there is a range of gradations within the impoundment, which was captured in the laboratory testing. Properties were largely similar regardless of the sand fraction (see Section 5 and Appendix E). This aspect of the tailings was thus well defined. The insitu ψ of the tailings was approached by computing a soil-specific calibration of the CPTu response (using NorSand) and then processing the CPTu data with that calibration. The procedure was independently checked by comparing the results of the CPTu processing with the few direct measurements of insitu void ratio (the 2017 fieldwork campaign supplemented by testing for the ITRB in 2018), a reasonable match being found as shown in Figure E4-5 in Appendix E. However, tailings show natural variation in their state as a consequence of depositional conditions which leaves open the question as to which state within the range of values controls the overall behaviour of the deposit (known as the characteristic value, ψ_k). The ITRB's view was that the characteristic value lay within the range +0.06 < ψ_k < +0.10 with a most-likely value of about +0.08. The tailings state was adjusted in the modelling within the identified range, but only after first iterating to optimised values for the FRV Unit A and rockfill.

The bedrock was modelled with a higher strength and greater stiffness than the overlying residual soils, so as to honour the findings from the investigation that suggested the failure passed through the shallower foundation units.

8.4 2D Analysis (Phase 1)

8.4.1 Models Simulated

The 2D (plane strain) analysis was carried out along the central axis through the slump, see Figure 2-1. Various model iterations were run. These iterations changed the properties of the rockfill, the FRV Units A and B, and the representation of the tailings while the geometry and loading sequence was constant. Only the final best fit is discussed here, the various material properties for which are presented in Appendix H.

8.4.2 State Parameter Evolution

The tailings state parameter was specified concurrently with each raise, consistent with the CPTu data. Subsequent placement of tailings compressed the underlying tailings. More importantly, the embankment deformations somewhat densified (improved) the tailings through their response to distortional stress (shear induced compaction). Figure 8-4 shows the distribution of the state parameter at the completion of Stage 10, which was the situation at the time of the 2017 CPTu campaign. As shown in this figure, this distribution of state varies considerably from that associated with the CPTu campaign conducted in 2017. This distribution of state arises from the stress history imposed upon the tailings and modelled by NorSand. It is of special interest to observe that the CPTu test program was limited in its ability to determine the variation of state that prevailed in the tailings within the affected region prior to the onset of instability.

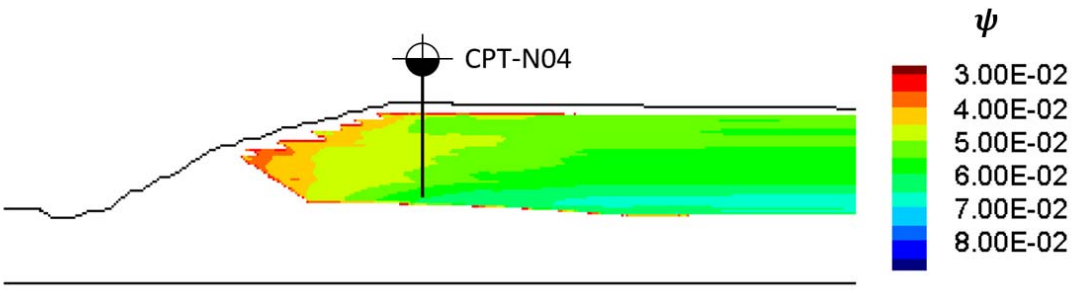


Figure 8-4: Distribution of state parameter in tailings on completion of Stage 10 raise

8.4.3 *Deformations*

Measured displacements at the survey prisms are compared with those of the FLAC model on Figure 8-5. Overall;

- Both FLAC and measured displacement show comparable values on average,
- Within this average trend, FLAC computes less vertical settlement than measured. FLAC is showing predominantly horizontal translation at the Stage 5 crest whereas the data indicate movement at approximately a 45° angle downwards, and
- FLAC displacements accelerate far faster with buttress construction than the InSAR trend indicates.

Overall, this is an acceptable initial match of surface displacement monitoring data allowing preliminary assessment of the underlying processes. Moreover, the calculated surface displacement pattern provides an approximate but rational explanation for the appearance of the cracks that were observed and this is discussed in detail in Appendix H.

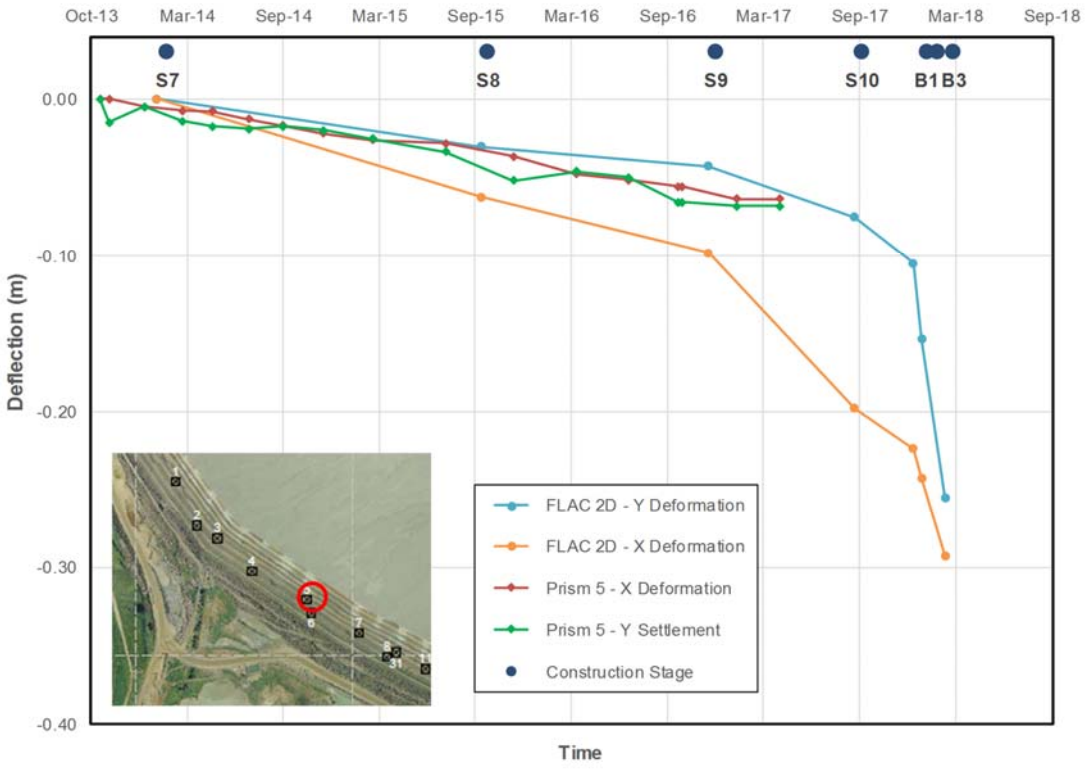


Figure 8-5: Comparison of displacements from 2D best-fit simulations with those measured

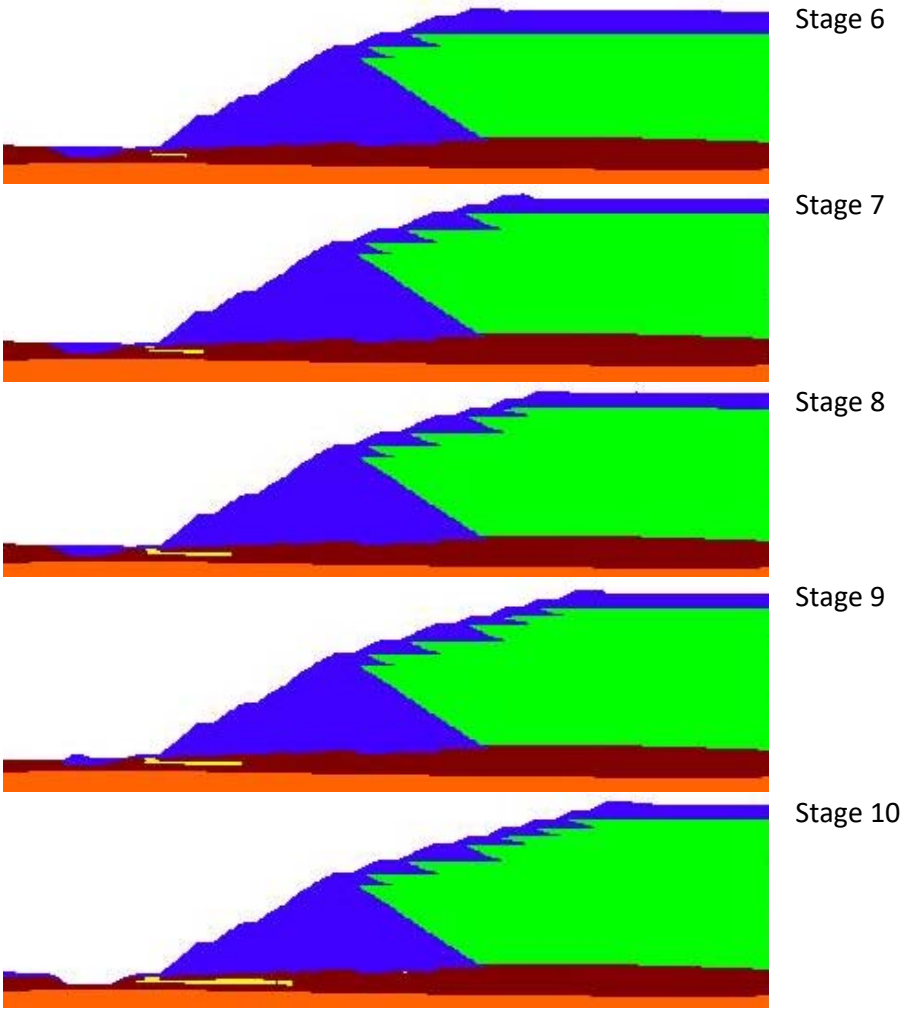
8.4.4 Progressive Failure of Foundation Under Static Load (Mechanism 1)

8.4.4.1 Foundation Response to Loading

An important discovery early in the investigations was the presence of soft and strain-weakening residual soils, discussed in Section 5 and Appendix D. These residual soils have been explicitly modelled, with FRV Unit A constituting the weakest stratum that controls the foundation response. The manner in which strain weakening developed in the best-fit 2D model is illustrated on Figure 8-6.

The zone where the residual soil has been loaded past its peak strength and into the condition of losing strength as displacements develop further (strain weakening) is shown as yellow on Figure 8-6. The first onset of strain weakening began at the toe of the embankment after the Stage 5 raise and developed upstream throughout the subsequent construction stages.

While the strain weakening process that creates large deformation in the foundation is captured in this analysis as seen in Figure 8-6, it initially appears at the toe of the structure and migrates inwards. This is not in accord with the time of the observation of thrusting at the toe prior to the onset of Phase 2 (see Figure 3-16). Nevertheless, the ITRB accepts the associated deformations and internal stresses as adequate for preliminary assessment of mechanisms.



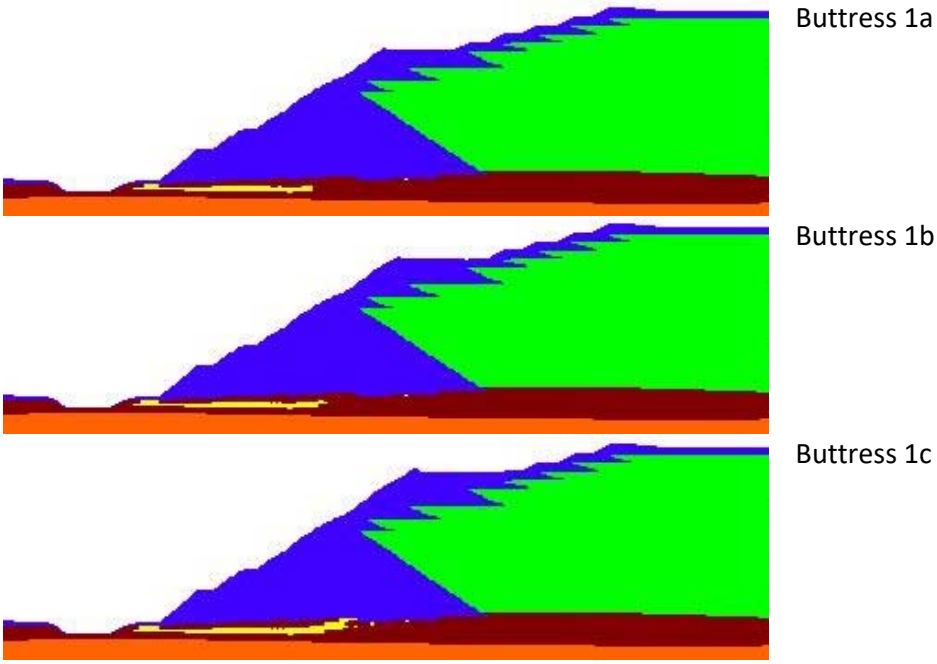


Figure 8-6: Development of strain weakening (shown as yellow zone) in Unit A

8.4.4.2 Tailings Response to Foundation Movement

The foundation movements from strain-weakening propagate upwards into the tailings, and in effect manifest themselves as a loss of support to the tailings. This loss of support then requires the tailings to increasingly mobilise their own strength. That mobilisation is shown in Figure 8-7 at the time that the Stage 1 Buttress had been completed. The figure plots the stress ratio η, which reflects the degree of mobilisation of the strength of the soil. If the soil is in its critical state, a value of unity for this ratio indicates continuous deformations at constant load. If the soil is looser than its critical state, as is the case of the NTSF tailings, the transition to continuous deformation starts at a lower value of this ratio. The important result from the 2D modelling is the determination of the relatively highly stressed zones which are emphasised on Figure 8-7. The loading path associated with these zones has been explored with specific laboratory tests. In this figure, the failure mechanism initiates in the red zone and propagates outwards.

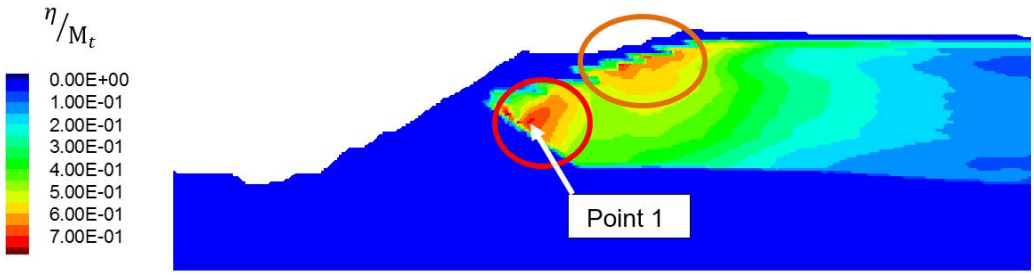


Figure 8-7: Distribution of controlling stress ratio in tailings after berm construction

If liquefaction were to result only by movements associated Phase 1 of the Event which included up to and including Stage 1 Buttress construction, the stress path associated with the tailings would intersect the instability locus, undrained response would result with a reduction in strength initiating Phase 2.

Laboratory tests to evaluate this hypothesis were conducted to represent the insitu state of the tailings and its variation when subjected to the loading path associated with the construction as indicated.

Three load controlled triaxial compression tests (stress path tests) were undertaken to investigate the instability locus and these are shown on Figure 8-8. Two of these tests were duplicates, using two independent laboratories to confirm that the data did not contain an unappreciated artefact caused by some particular aspect of the test apparatus. The data is annotated by the path followed and presented in terms of the stress-path followed (top plot), the associated axial strain (middle plot) and the volumetric strain (bottom plot). All these samples were slightly looser than thought to be the case insitu.

Blue vertical arrows have been drawn on Figure 8-8 to indicate how the different aspects of the measured behaviour in each of the three plots link together. The axial strain data, the middle plot of Figure 8-8 is the key indicator of the soil response. These strains are small (< ~2%) throughout the loading along the computed stress path, which are consistent with the strains computed in FLAC. When the stress path is extended, whether along A or C direction, strains continue to be small until a sudden acceleration in the strains develops. The acceleration is indicated by the vertical blue arrows. Some judgment is involved here, as it could be argued that the transition strain is either 3% or 4%. Notwithstanding this, the acceleration has developed at less stress than that of the soil's critical state which is shown as the green line in the upper plot. The acceleration point is inferred to be the instability locus (blue line, upper plot) as the much faster increase in strain with small increase in load is a direct consequence of a sudden reduction in plastic hardening.

Path A represents the peak loading of the Stage 1 Buttress. With this path, the deviator stress at the 'most affected' tailings remained constant while the foundation continued to yield, thereby reducing the support offered by the embankment and allowing the tailings to move outward.

Path C represents the scenario where there is approximately linear loading vector over the last two lifts of the Stage 1 Buttress, a situation indicated by FLAC.

The instability tests were carried out drained and with load control. Under some circumstances this technique can produce a transition into undrained liquefaction, depending on the soil properties, the inertia of the loading system, and the hydraulic resistance in the drainage line (Gajo, 2004). The effect of drainage could be tested experimentally by introducing a needle-valve or similar in the drainage line of the triaxial cell, but was considered unnecessary to confirm the findings. Rather, a further direct test (Path B) was carried out by simply forcing undrained conditions at the end-stress of the computed loading path.

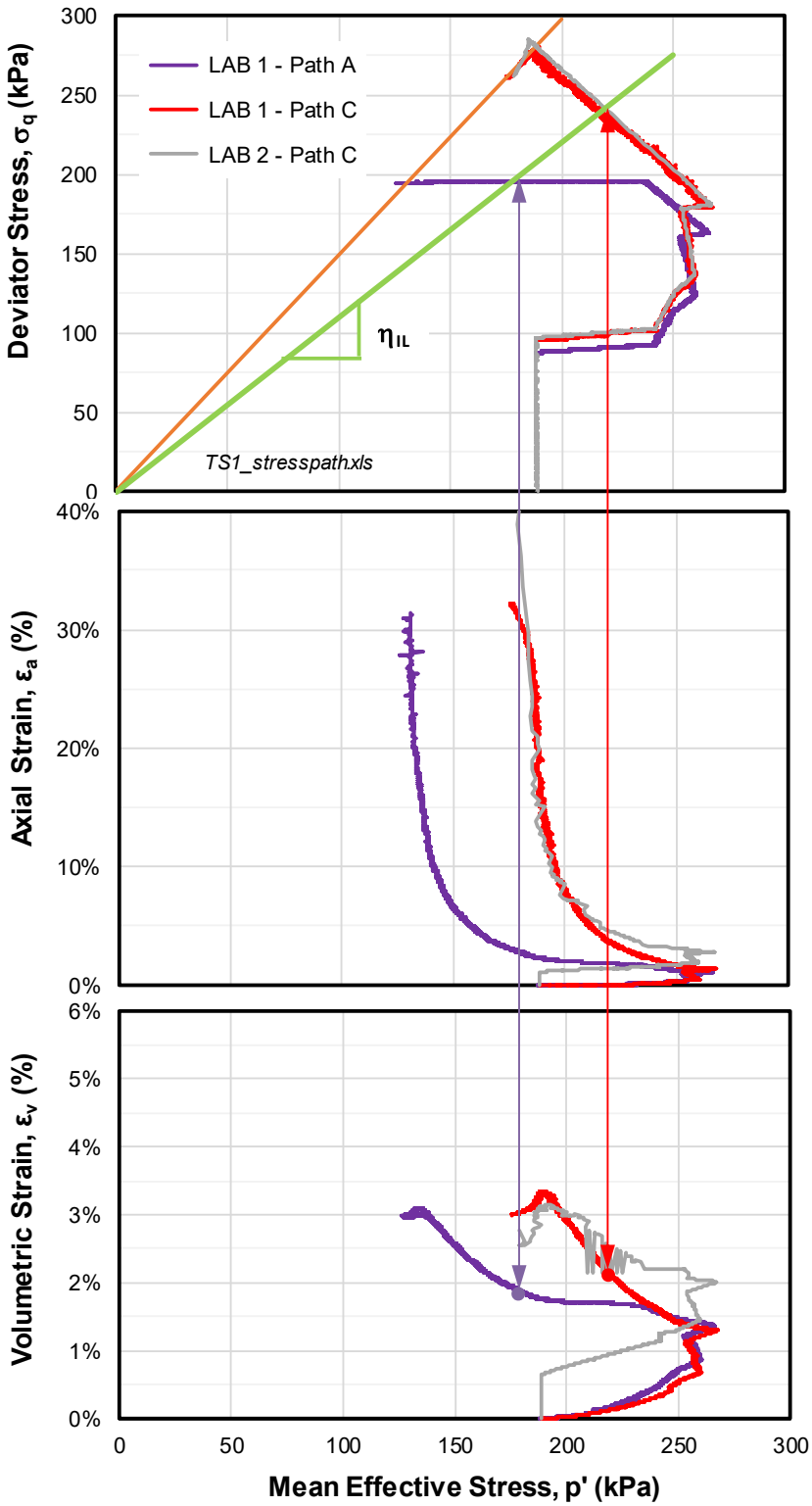


Figure 8-8: Measured soil behaviour at 'Point 1' along computed stress path

Path B is shown on Figure 8-9. This sample was loaded drained (shown in brown) to the end-stress of the FLAC load stress-path before closing the drain line and continuing with the loading (shown in blue). When subject to a small undrained increment of shear stress, the sample collapsed essentially instantaneously (see the video in Appendix E, Annexure ER), at the same instability locus as identified in Path A and Path C loadings.

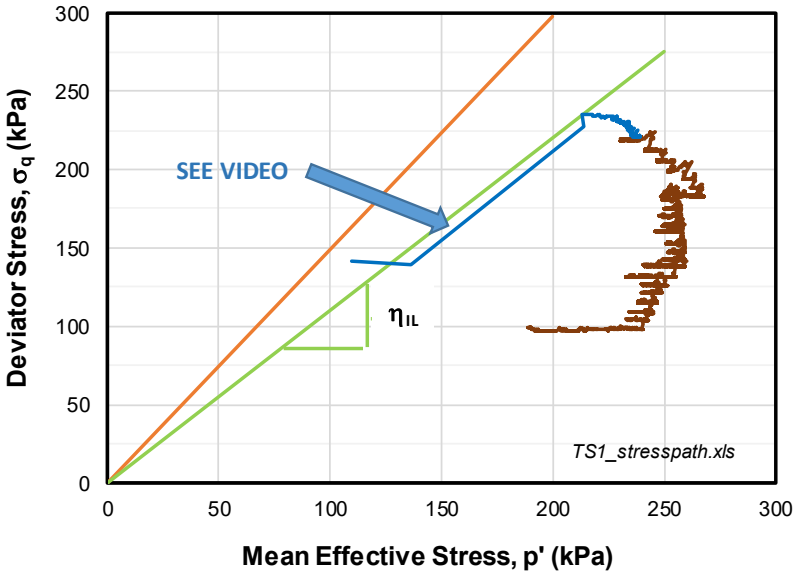


Figure 8-9: Undrained instability following drained loading

Based on the laboratory data presented above, it is the view of the ITRB that Mechanism 1 was initiated by an increment of rapid deformation, leading to an increment of undrained loading in the tailings contained by the NTSF embankment. This rapid deformation would be seated in the already weakened FRV Unit A foundation.

8.4.4.3 Commentary on Mechanism 1 Results

The principal result of this 2D modelling has been to reveal the interplay between the tailings behaviour and the strain-weakening strength loss in the FRV Unit A foundation, with each contributing to the behaviour of the other. In particular, the implication of rate of movement of the foundation which influences the triggering of liquefaction has been highlighted. However, some key observations have not been honoured even with the best-fit model.

One shortfall is in the rate of increase in the deformations during the Stage 1 Buttress construction. FLAC predicts a greater acceleration into apparent failure from the Stage 1 Buttress construction when compared with the InSAR data. Another related shortfall was the deformations at the toe, with the heave computed by the FLAC model being significantly earlier than that observed at the site. Therefore, the ITRB commissioned the development of FLAC 3D modelling.

8.4.5 Rising Ground Water (Mechanism 2)

Figure 8-10 presents laboratory data that illustrate Mechanism 2. The changes in stress at Point 1 with the various stages to construction are presented to the end of Stage 1 Buttress construction. It is seen, that at this time, the local stresses are far from the instability locus. If one envisaged a local rise of pore pressure generated by a rise of ground water, the stress path would migrate in a horizontal direction as indicated. When it intersects the instability locus, liquefaction results. However, it is seen that prior to this intersection, strains are accelerating. For this mechanism to occur, pore water pressures that have not been embraced in the hydrogeological synthesis around the NTSF (Appendix F), would have to be evident.

The ITRB found no evidence for pore pressures that have been omitted from consideration in Appendix F. The ITRB discussed in some detail whether high pore pressures caused by buttress construction might have prevailed for a while, but this was discounted on the basis of the high local C_h determined by dissipation testing as part of the 2017 CPTu testing campaign. The ITRB concluded that local transient high pore pressures were not present and did not contribute to the onset of Phase 2. Therefore, Mechanism 2 was discounted.

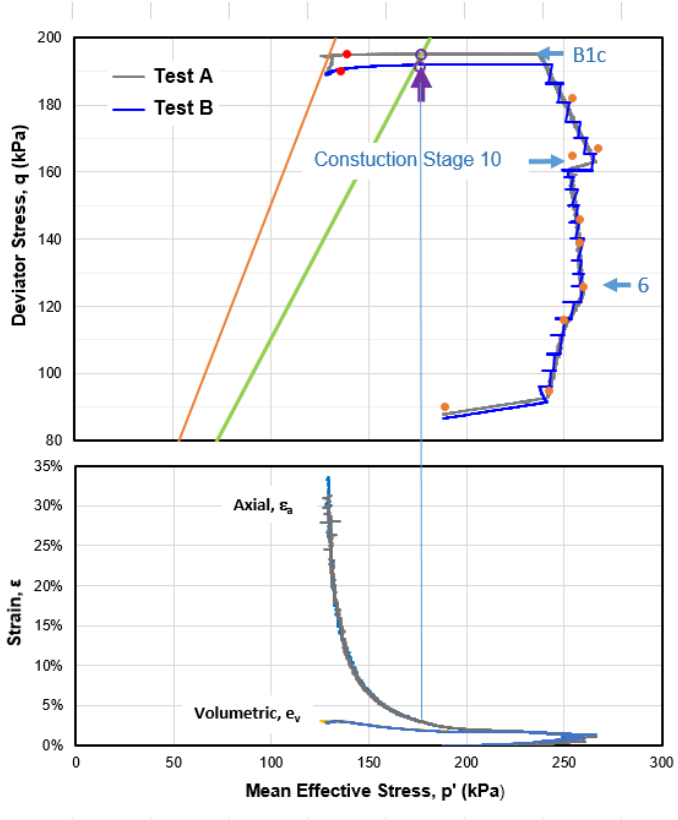


Figure 8-10: Results of laboratory test for Point 1 under rising ground water pressure

8.4.6 Seismic Triggering of Liquefaction (Mechanism 3)

8.4.6.1 Occurrence

There were two small earthquakes on March 8, 2018, the pulses being short bursts with a duration of about a second each separated by about 10 seconds. The instantaneous peak ground motion was about 0.15 g, which is a significant shock even though the duration of motion was very short The origin and nature of the ground motions are presented in Appendix I, and recommendations for seismic response are also included in this Appendix.

There are no known other instances of vibrations imposed on the embankment in the period of interest for slump triggering. However, larger magnitude shocks did occur previous to and subsequent to the Event with no known consequences to the NTSF.

Earthquake motion can cause excess pore pressure in saturated soils almost regardless of the soil density. These excess pore pressures generally subsequently dissipate. However, as discussed in Section 6.3 - Mechanism 3, these excess pore pressures can also trigger liquefaction.

8.4.6.2 Tailings Response to Earthquakes of March 8, 2018

In order to calculate the response of the tailings to the earthquakes experienced on March 8, 2018, was necessary to do the following;

- Based on the recommended source ground motions for the design earthquake (see Appendix I) calculate the dynamic response of the tailings as the earthquake ground motion propagates upwards. This required a dynamic analysis which was conducted in both 1D and 2D conditions with the details presented in Appendix H.

- Apply these calculated ground response results to create imposed cycling loading on tailings samples at representative insitu conditions at that time.
- Conduct these cyclic loading tests under undrained conditions to determine whether the earthquake generates pore pressures that accumulate over time.
- Evaluate whether the accumulations of pore pressures under the design earthquake loading are consequential and could have contributed to the initiation of liquefaction and the onset of Phase 2 of the event.

Figure 8-11 illustrates the dynamic loading that was utilised in the cyclic testing of the tailings specimens. It differs from routine testing by simulating the actual ground motion computed within the structure. Often uniform cycles are used as opposed to more complex realistic ground motion. Because the test is undrained, and because of test equipment limitations the duration between the two shock was reduced from about ten seconds to one second. The ITRB does not regard this as consequential.

The testing was based on cyclic direct simple shear tests (CDSS), documented in Appendix E. which is the best analogue for the way in which earthquake motions propagate in soil, and this testing is now standard. Since it is not possible to get undisturbed samples in the test cell, reconstituted samples are used. The reconstituted samples were created to reflect the state of the tailings as well as the estimate of these stressed that existed at a point at that time. The development of stresses due to the related deformation constitutes what is nominally called *static bias*. For loose tailings the greater the static bias, the greater the propensity for the tailings to liquefy under imposed cyclic loading. Hence, the deformations developed in the structure during Phase 1 of the Event, resulted in enhanced fragility with respect to potential earthquake loading. The extensive program of investigations summarised in this report recognised this enhanced fragility and responded accordingly.

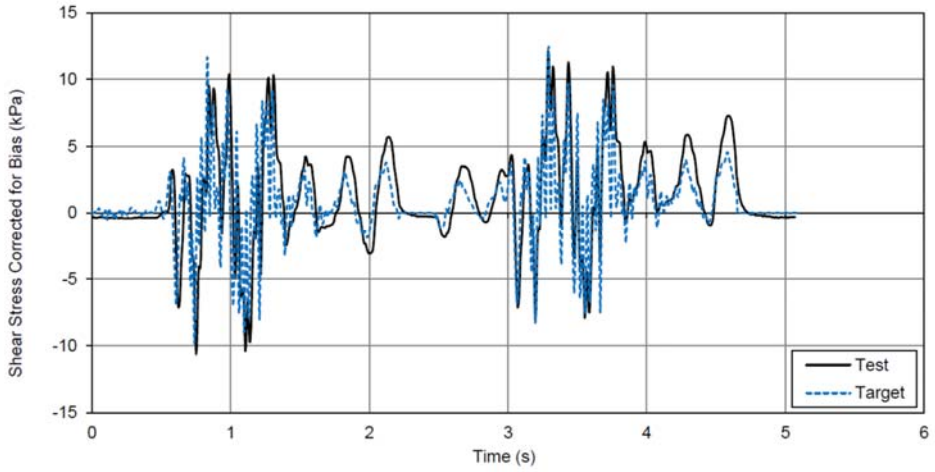


Figure 8-11: Ground motion input to CDSS test simulating earthquake motion at Point 1

The stresses developed within the tailings were determined from the FLAC 2D analysis and Point 1 is reflective of the highest mobilised strength, as illustrated in Figure 8-7. Details of the stress distribution within the dam are given in Appendix H. The state of specimens adopted reflected the calculated state at Point 1. Both sandy and silty tailings were used in the laboratory program because of somewhat greater tendency for liquefaction in the sandy deposits. The results from the cyclic testing on the specimens are presented in Figure 8-12. It is evident that the imposed cyclic loading has had no significant effect on the specimens. The ITRB concludes

that the earthquakes did not contribute to the onset of Phase 2. Therefore, Mechanism 3 can be discounted.

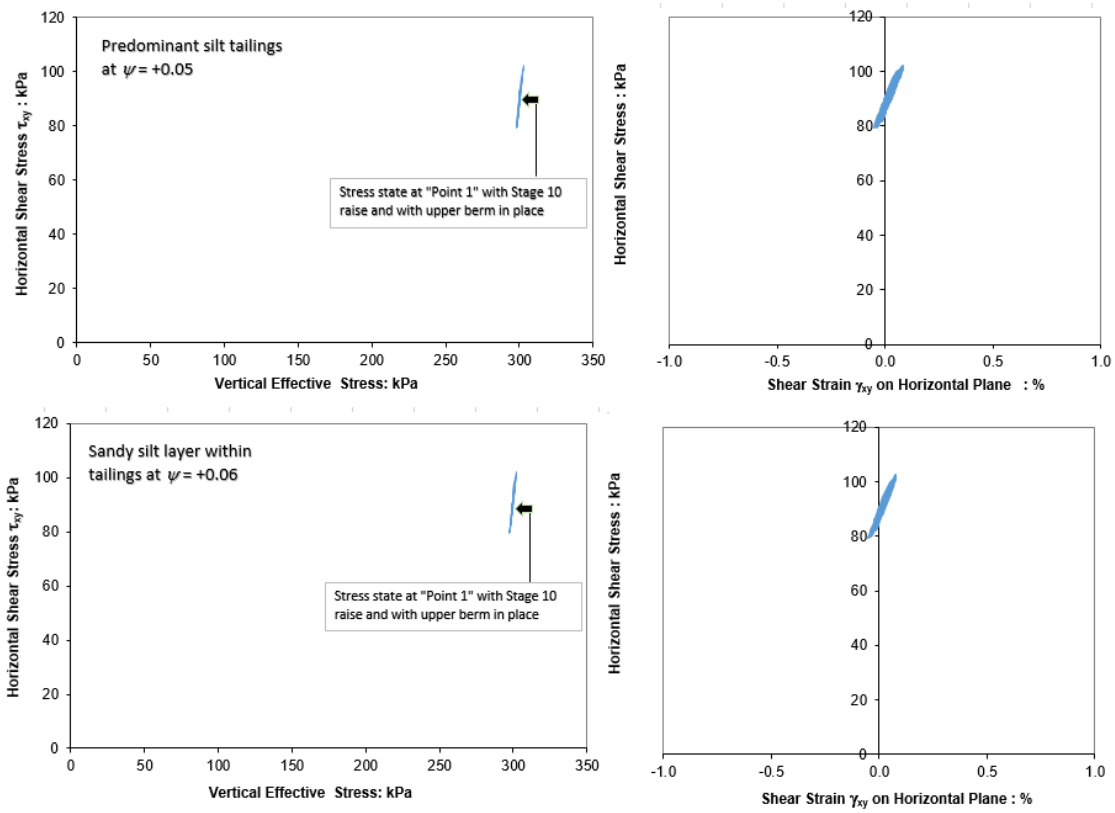


Figure 8-12: Response of Point 1 tailings to 8 Mar 2018 earthquake in cyclic simple shear

8.5 3D Analysis (Phase 1)

8.5.1 Objectives

The FLAC 2D modelling captured some aspects of the failure, but the ITRB was of the view that analyses should embrace full 3D simulation because of the following considerations:

- Observations of the shape of the failure that occurred indicates the presence of 3D effects,
- LEA revealed that the 3D resistance was significantly greater than that calculated with 2D LEA methods,
- The geological understanding was that the FRV Unit A was of limited extent which would affect the location and shape of the failure,

Details of formulation of 3D modelling and related computational methodology are presented in Appendix H. The analysis focused on Mechanism 1, the mechanism that emerged from the FLAC 2D modelling as the most plausible explanation as to how Phase 1 developed.

This section presents the best-fit FLAC 3D model, illustrating the extent to which it captures the key 'truths' discussed in Section 8.2. The parameters required for this best-fit simulation are then discussed in terms of the measured foundation and tailings strengths. The progress of scenarios to develop the best-fit FLAC model are documented in Appendix H.

8.5.2 Description of 3D Model

The location of the 3D model on the embankment is shown in an oblique view on Figure 8-13, the 3D model extends beyond the slump zone sufficiently so that the edges of the model do not influence the situation in the slump. This figure also shows the location of the section used in the 2D analysis just discussed.

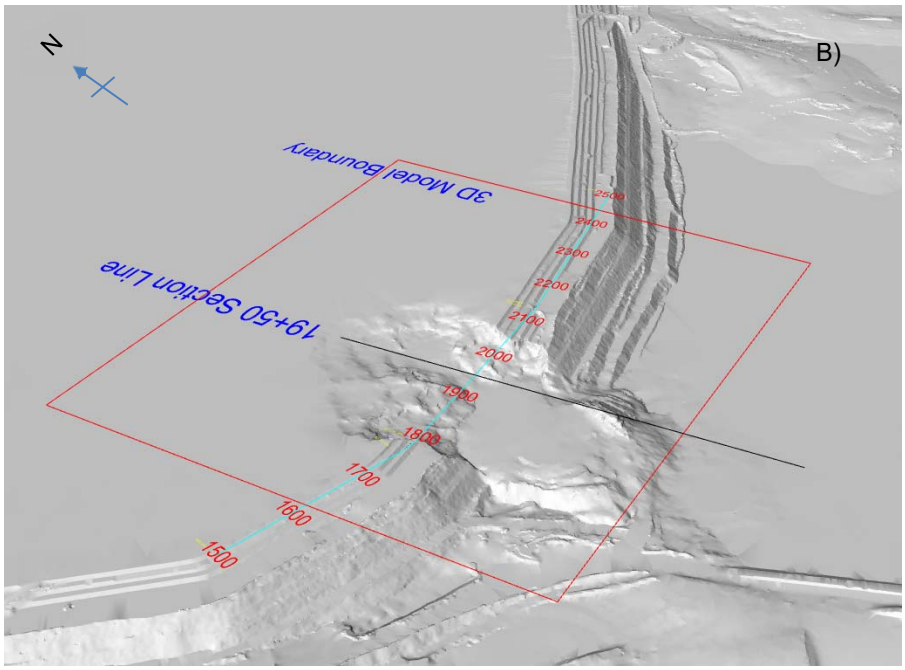


Figure 8-13: Oblique view of slump illustrating extent of 3D model

One purpose of the 3D model was to capture the geological details of the foundation beneath the embankment. This was a challenging undertaking given the complexity of the geology (Section 4) and the results are summarised in Appendix H.

8.5.3 Deformations

As discussed in Section 8.2, the measured deformations at or near the embankment crest (prisms and InSAR) were a principal constraint for optimising the FLAC simulations. These deformations were supplemented by honouring the observed (but unmeasured) minimal toe heave and the extent to which deformations propagated upstream to mobilise tailings strength.

Two FLAC 3D scenarios, which differ in the state parameter adopted for the tailings, closely match the key observations. The scenarios are discussed in Appendix H and are briefly described below as:

- Scenario 33. (ψ_k = +0.06) This scenario is slightly denser than that inferred from the CPTu but remains stable during the Stage 1 Buttress construction
- Scenario 34. (ψ_k = +0.08). This scenario most-closely honours the inferred state parameter from the CPTu but failed to converge during the simulation of Stage 1 Buttress construction

For Scenario 33, FLAC 3D displacements are compared with measured displacement at survey prisms in Figure 8-15 and InSAR data in Figure 8-15. Overall:

- Both FLAC and measured outward displacement are very similar;
- FLAC develops crest settlement in a similar range to the measured data;

- FLAC displacements increase with buttress construction as indicated by the InSAR trend;
- FLAC computes displacement gradients consistent with crack locations; and
- The limited toe heave in FLAC is reflected in the Nov/17-Feb/18 InSAR trend.

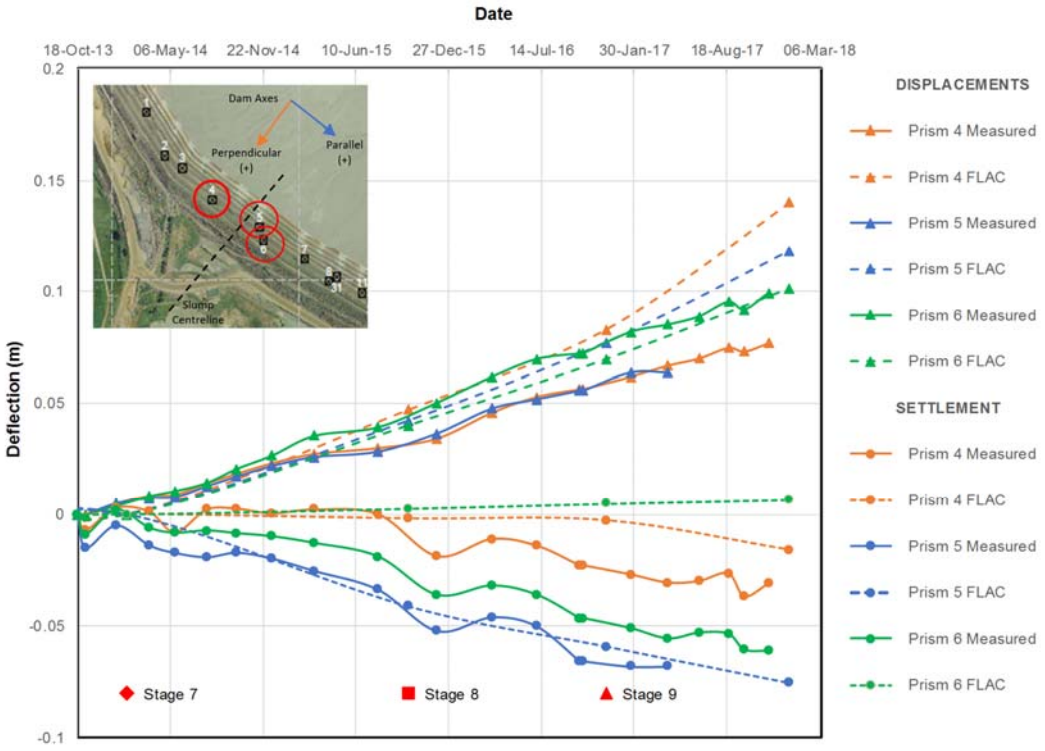


Figure 8-14: FLAC 3D computed and measured prism displacements perpendicular to the dam axis

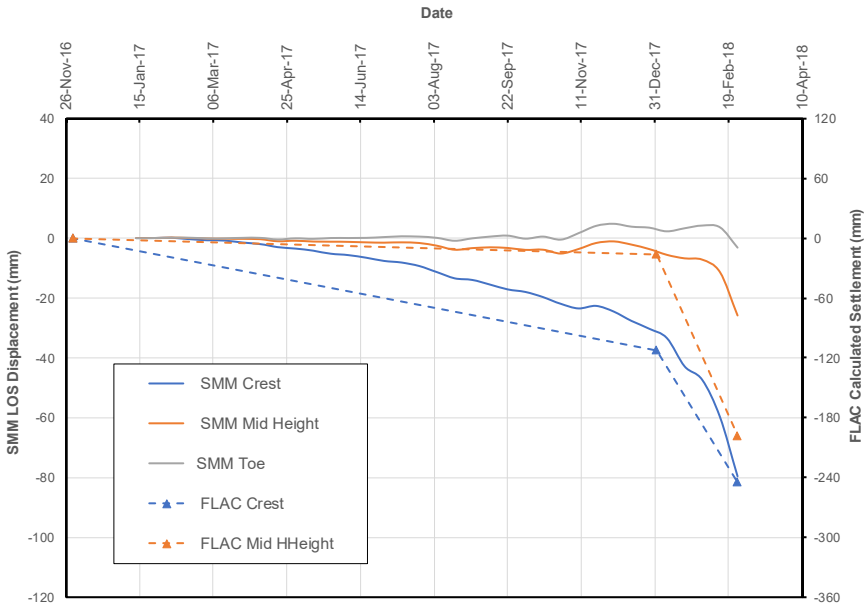


Figure 8-15: FLAC 3D computed and InSAR SMM trends

It should be noted that InSAR SMM presented in Figure 8-15 are in the direction of the satellite LOS and scales have been adjusted to demonstrate the trend rather than absolute values

The heave at the toe of the NTSF was computed using FLAC 3D. Figure 8-16 indicates that the heave at this location was negligible at the end of the Stage 10 raise (before buttress construction). However, Figure 8-17, an isometric view with the toe excavation, indicates a heave of about 0.25 m developing at the edge of the excavation on completion of the Stage 1 Buttress. Although there were no heave measurements at the toe, the results are consistent with the InSAR trend at the toe and witness statements on the day of the Event.

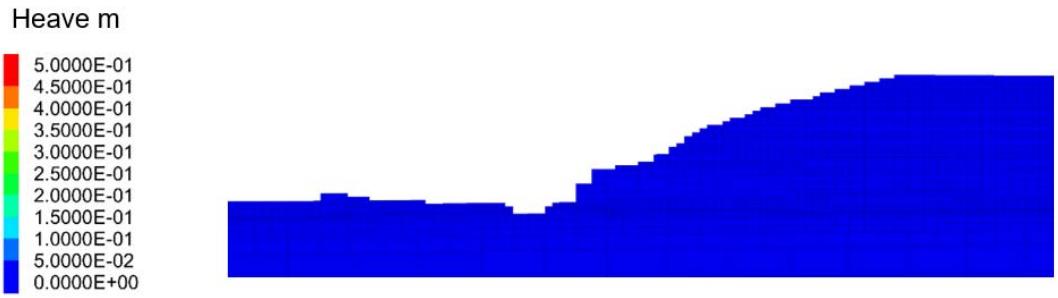


Figure 8-16: Heave computed at end of Stage 10 raise

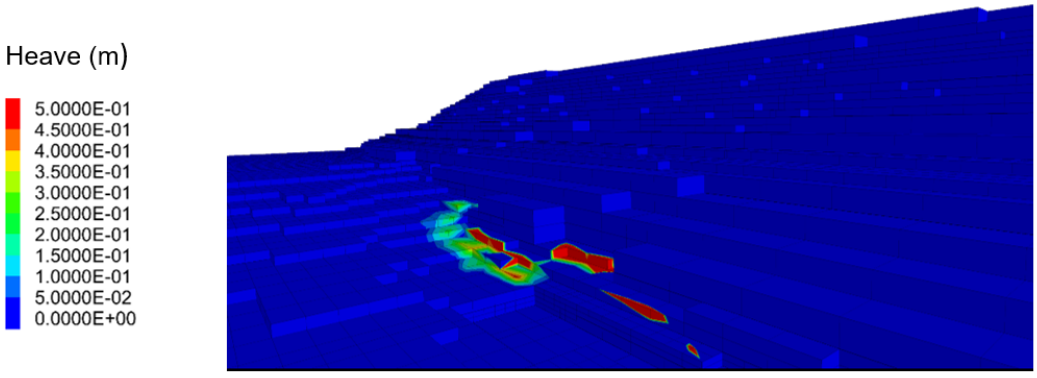


Figure 8-17: Heave computed after Stage 1 Buttress construction

Further insight is gained from horizontal displacement contours at the end of the Stage 1 Buttress construction, shown on Figure 8-18. The computed displacements developed across the width of the slump are similar to those developed during March 9, 2018. The subsequent development of the flowslide (Phase 2) is not captured in the analysis shown here and thus the simulation neither 'runs-out' at the toe nor regresses at the crest.

Overall, Figure 8-15 to Figure 8-18 show an initial match between the best-fit FLAC 3D model and the key observations. This match allows an assessment of the underlying processes which are discussed below.

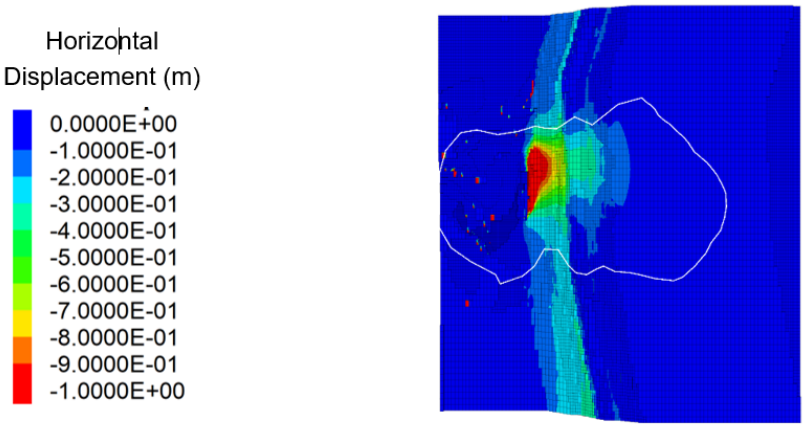


Figure 8-18: Horizontal displacement contours at 8 March 2018

8.5.4 Inferred Foundation Properties

The 3D analysis started with the strengths in the various strata that had been developed through the 2D simulations, but with the strength of the FRV Unit A reduced to account for the 3D analysis including additional restraint at the edges that was not present in the 2D simulations. The initial reduction was based on judgement, conditioned by the limit equilibrium analysis (Section 7). This scenario failed first in the toe of the slope, which is contrary to observations. The FRV Unit A strengths were then adjusted to reflect the very substantial change in vertical effective stress between the toe and beneath the crest of the embankment; this adjustment was still a judgment, but one reflecting the change in compressibility measured in the oedometer tests (Figure 5-10). There were three aspects to this judgment: i) at low stress levels, there was clear evidence of inherent structure from the parent rock; ii) at intermediate stress levels, strength became more soil-like and increased with stress level; and, iii) at stress levels greater than about mid-height of the dam, that initial inherent structure, and its associated contribution to strength, was progressively lost even as the soil-like aspect increased.

The scenarios simulated in the FLAC 3D modelling had to provide sufficient strength in the FRV Unit A to allow the construction to proceed through to the Stage 1 Buttress but with sufficient brittleness to allow the development of the progressively increasing deformations. The effect of the tailings state was investigated as well as the behaviour of the FRV Unit A. No scenarios were found where the tailings, even when simulated as significantly looser than indicated by the CPTu, provided sufficient increase of stress on the embankment to develop a failure mechanism in the absence of strain-weakening in the FRV Unit A. Conversely, no scenarios were found where the tailings, when simulated as significantly denser than indicated by the CPTu, were sufficiently stiff to compensate for weak strengths in the FRV Unit A. It was the FRV Unit A that largely dominated how the FLAC model could be optimised to honour the key observations (as per Section 8.2).

The optimised FRV Unit A strength from the FLAC modelling, expressed as the available undrained strength as the foundation transitions from a drained situation during the embankment raising into incipient undrained strength loss as the slump developed, is shown on Figure 8-19 plotted against distance upstream from the toe of the dam. Also shown on this figure is the inferred operating strengths synthesised from the laboratory testing as summarised on Figure 5-8.

The strengths shown in blue on Figure 8-19 comprise a peak strength, up to which the FRV Unit A shows drained behaviour, followed by a transition into an undrained strength loss. This loss in undrained strength is a result of pore pressures increase due to foundation movement, not a response to embankment vertical stress. This transition was referred to earlier as ‘strain weakening’ and its effect on the operating strength is indicated by the downward arrow on Figure 8-19.

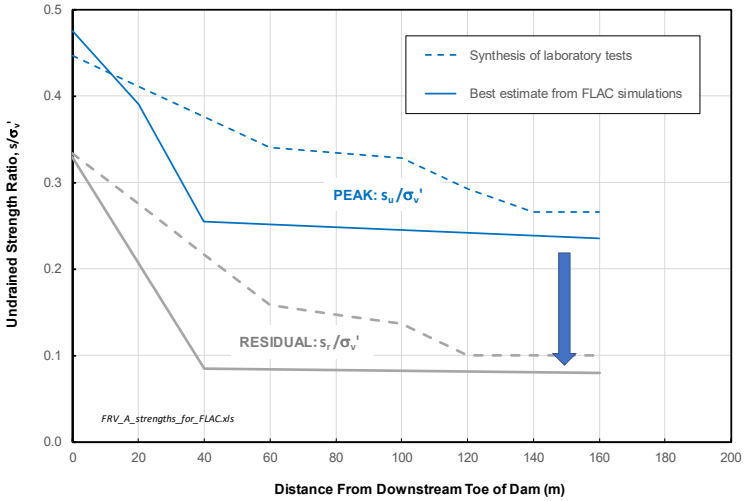


Figure 8-19: FRV Unit A strengths used in best-fit FLAC 3D simulation

Strain-weakening was a central aspect of the FLAC 2D model and it continued to be important in FLAC 3D. The zone where the FRV Unit A has been loaded past its peak strength and into the condition of strain weakening is shown as yellow on Figure 8-20. The first onset of strain weakening began at the toe of the embankment after the Stage 9 raise, and developed upstream throughout the following construction stages. It should be noted that this strain weakening is also accounted for by a significant reduction in available frictional resistance as it converges on the frictional residual strength (see Appendix D).

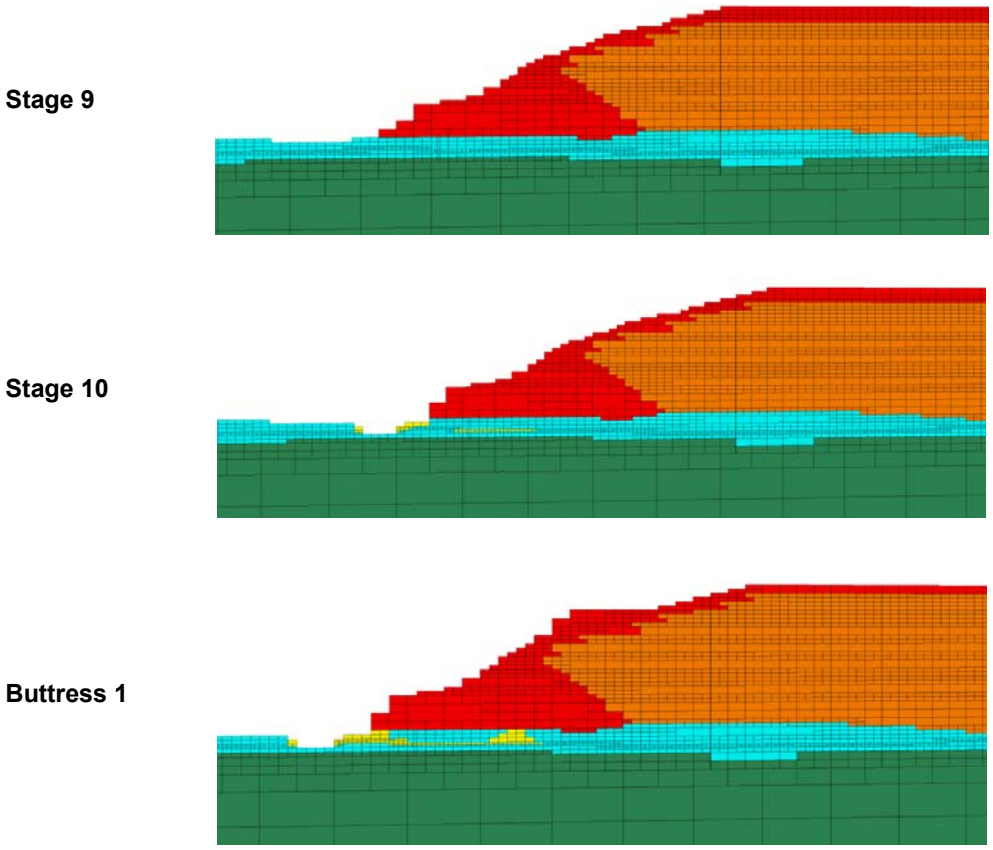


Figure 8-20: Development of strain weakening in best-fit FLAC 3D simulation

8.5.5 *Inferred Tailings Behaviour*

The FLAC simulations involved placing the tailings as an upper layer at the specified state parameter for each stage of the embankment raising, with the state parameter then evolving as subsequent tailings were deposited and as the embankment responded to load by deforming.

The calculated state parameter profile, on completion of the Stage 10 raise, and used in Scenarios 33 and 34, is compared with that assessed from CPT-N04 data on Figure 8-21. As can be seen, the state parameter profile used the FLAC 3D simulation was slightly denser than that inferred from the CPTu data.

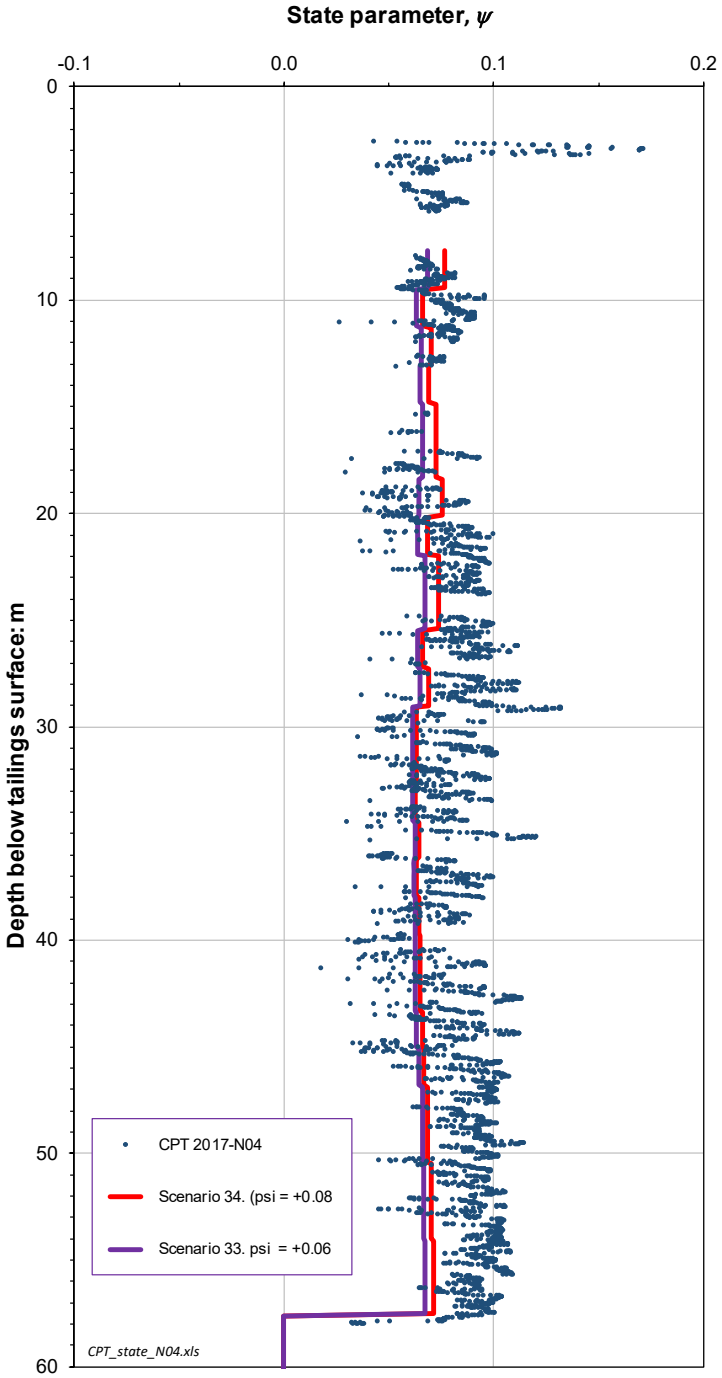


Figure 8-21: State parameter profile at N04 location on completion of Stage 10 Raise

The FLAC 3D simulations were very sensitive to the initial state parameter in the tailings, with the slightly denser scenario appearing a closer match to that which was observed. This is illustrated in Figure 8-22 which shows the contoured mobilised stress ratio (η/M_t) of the tailings, with red approaching the instability limit and a transition to liquefaction. Figure 8-22 a) is for the simulation that was stable with the buttress in place (Scenario 33) while Figure 8-22 b) is for Scenario 34 which failed to converge.

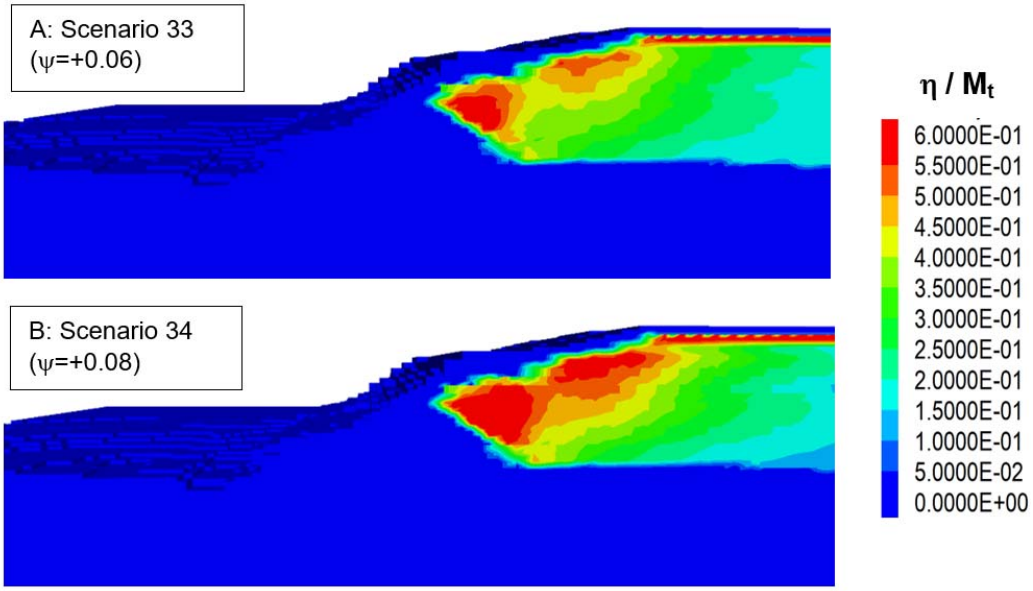


Figure 8-22: Influence of state parameter on extent of mobilised tailings strength

8.5.6 Tailings Instability

8.5.6.1 Framework

As discussed earlier, all evidence indicates that the tailings approached the point of liquefaction in a drained condition without any excess pore pressures. This is a known aspect of soil behaviour, having been investigated experimentally since the early 1990s (eg. Sasitharan et al. (1993); Skopek et al, (1994)). Today, the behaviour is commonly represented by the *instability locus* (also called the *flow liquefaction line*) that was introduced in Figure 8-2. There is a common misunderstanding that this locus is an alternative expression of the undrained strength ratio S_u/p' (eg, Lade & Pradel (1990); Ishihara (1993); and, Yang (2002)). However, the instability limit is the situation in which the soil suddenly exhibits an increase in plastic strains (both distortional and volumetric). If drainage is impeded near the instability locus pore pressures develop and liquefaction ensues in loose tailings. This was demonstrated in the failure investigation for the Fundão Tailings Dam (Fundão Tailings Dam Review Panel, 2016). The ITRB focused testing to establish this stress ratio under drained conditions as appropriate for the Event.

8.5.6.2 Liquefaction

As noted previously, tests to investigate the instability locus were a little denser than indicated by the CPTu testing. Notwithstanding this, the instability locus must intersect the CSL at $\psi=0$ and is also known to be linear with ψ. The instability limit inferred from the various stress path tests (red dots) are shown on Figure 8-23, together with a best-estimate trend for the NTSF tailings instability locus.

The FLAC 3D results for the best-fit model were contoured as values of η_{IL}/M_t on Figure 8-22, with the greatest values being a little in excess of η_{IL}/M_t ~0.6, while the state parameter was contoured on Figure 8-4 with the 'typical' value for the tailings supporting the upstream raise being ψ ~0.05. Comparison of these estimates with the estimated instability locus on Figure 8-23 indicates the tailings were close to their instability condition after completion of the Stage 1 Buttress.

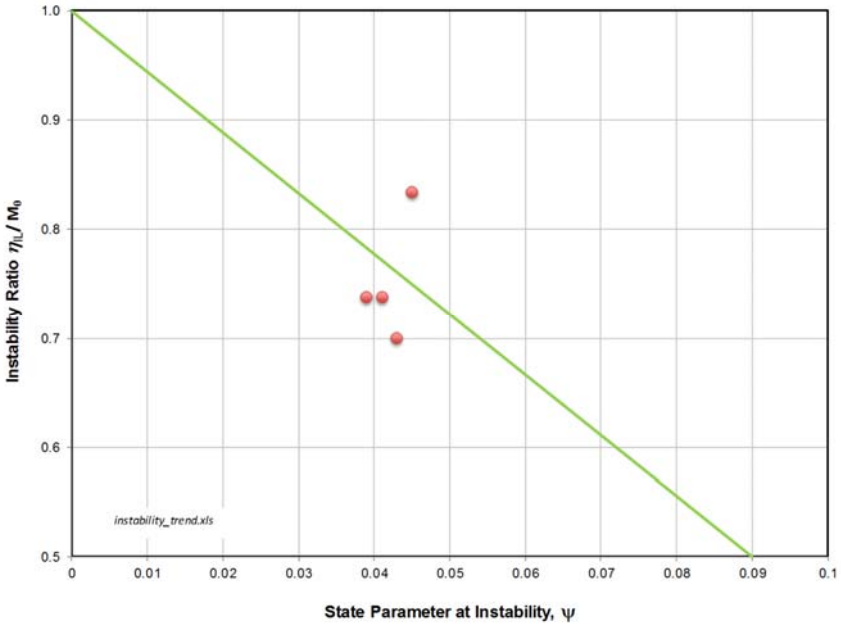


Figure 8-23: Instability locus for NTSF tailings

8.5.7 ITRB Commentary

The FLAC 3D best-fit model has largely honoured the aspects identified in Section 8.2 and which were considered crucial by the ITRB to validate the analysis. A wide range of scenarios were explored to do this, iterating on both the FRV Unit A strengths (both peak and residual) and the tailings state.

What was striking in this iterative modelling was the degree to which the tailings played a secondary role. The tailings acted as a load exacerbating the strain-weakening in the foundation but undrained strength loss in the tailings was not in itself a cause of the Phase 1. The laboratory stress-path tests which investigated the instability locus had both a reserve of undrained strength and a general tendency not to immediately liquefy. It follows from this, that the ultimate trigger was the FRV Unit A behaviour as Phase 1 evolved into Phase 2 of the slump. It was a sudden and large-scale strength loss in the FRV Unit A that caused a rapid increase in deformations that in turn resulted in the liquefaction of the tailings. Whether this is related to a decrease in frictional resistance, or a local increase in pore pressure, or both remains unclear.

The ITRB commissioned three types of tests on the FRV Unit A to determine its behaviour. Overall, the measured strengths were broadly consistent with those used in the best-fit FLAC 3D model. However, it was only the TX tests which indicated a particularly brittle behaviour, both in the magnitude of the strength loss and the small increment of strain over which that strength loss developed. This is a little surprising as the expectation was that the near-horizontal deformation of the FRV Unit A would be most accurately determined using DSS tests.

Earlier, when presenting potential mechanisms for the failure, the Los Frailes dam failure was associated with one such potential mechanism. The conclusion of the ITRB's studies is that this was indeed a comparable dam breach to the NTSF.

8.6 Slump Development (Phase 2)

8.6.1 Transition from Drained to Undrained Behaviour

The deformation analyses, particularly the FLAC 3D best-fit 3D analysis, established that the tailings were approaching (or at) their instability limit after completion of the Stage 1 Buttress. The situation was drained at this time. The nature of the instability limit is illustrated on Figure 8-24 which was computed using Norsand and typical tailings properties (Been, 2016) When soil is stressed to its instability limit, a little above the loading shown as 'B' on Figure 8-24, any 'rapid perturbation' will result in a sharp reduction in the undrained strength as can be seen from this curve 'C'. Therefore, it can be concluded that the NTSF embankment was in a very precarious state at 12:00hrs March 9, 2018.

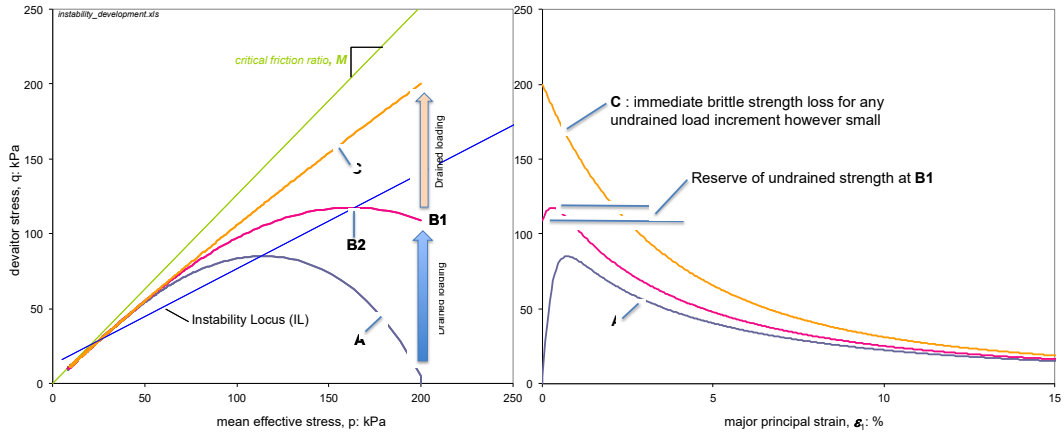


Figure 8-24: Undrained instability of loose soil during drained loading

The ITRB did not enquire into the nature of the 'perturbation'. However, possible explanations could be; a natural acceleration of the foundation movement; excess pore water redistribution within the yielding FRV Unit A or FRV Unit A deformations breaching a strain threshold that caused disaggregation of the structure in that stratum. Rather, the ITRB accepted that the condition of a transition into liquefaction was imminent and then enquired as to how the slump might have transitioned to Phase 2. This was done by switching the tailings from their drained condition to an undrained one; that is, implementing the situation just a little past the stress-strain behaviour shown on Figure 8-9.

Two tailings strengths are needed to assess the evolution of the slump during Phase 2. First, the peak undrained strength of the tailings (S_u) provides a check on the assessed stability. Second, the post-liquefaction strength (S_r) indicates the strength loss allowing the failure to accelerate. Of course, acceleration is not just from strength-loss as a substantial gravitational component would be evident as the tailings dropped a vertical distance of some 50m during the slump.

The assessment assumed that the remainder of the embankment and foundation retained their same properties at the instant of tailings liquefaction.

8.6.2 Available Undrained Strength in Tailings

8.6.2.1 Peak Strength

The available undrained strength at the instant of liquefaction has been estimated from two sources: the CPTu resistance and the laboratory data.

The peak undrained strength estimated from the CPTu data is discussed in Appendix E and has a plausible range $0.15 < S_u/\sigma_v' < 0.19$. This value is based on level ground conditions and assumes undrained failure without any drained 'static bias'.

The peak undrained strength ratio can also be computed from the measured soil properties and the state parameter using the same NorSand model used in the FLAC 2D and FLAC 3D analyses. For level ground conditions at CPT-N04 (using K_0=0.7), an undrained strength ratio in direct simple shear of $S_u/\sigma_v' = 0.19$ was computed using NorSand.

At the 'most affected' location (Point 1), the computed strength ratio was larger ($s_u/\sigma_v' = 0.27$), because a greater portion of the path was drained, and thus less excess pore pressure was generated.

It is apparent from the FLAC 3D analyses that the state parameter varies beneath the upstream constructed embankment, as does the mobilised stress ratio η. A reasonable judgment is that the 'representative' peak undrained strength for a stability analysis at the instant of liquefaction is about $S_u/\sigma_v' = 0.2$ across the entire liquefying region.

8.6.2.2 Post-Liquefaction Strength

The post-liquefaction strength can also be estimated from the CPTu data and from the laboratory data.

The present 'state of practice' is that post-liquefaction strengths should be assessed from a synthesis of the case-histories that are indexed by the CPTu resistance. While these case-histories are viewed as a particularly valuable data set, as they reflect actual full-scale experience, that view overstates the case as there is considerable uncertainty with the raw data underpinning them (Jefferies & Been, 2016). Despite these quite severe constraints, it is possible to honour the uncertainty in each case-history with a single unified trend which is incorporated in the CPTu processing software used by the ITRB. The detailed assessment is presented in Appendix E and indicates a plausible post-liquefaction strength range of $0.08 < S_r/\sigma_v' < 0.10$.

The post-liquefaction (residual) undrained strength ratio can also be computed from the measured soil properties and the state parameter using the NorSand model. For a pre-liquefaction ψ=+0.06, a plane-strain post-liquefaction strength of about $S_r/\sigma_v' \sim 0.12$ can be calculated, while a plane-strain post-liquefaction strength ratio of about $S_r/\sigma_v' \sim 0.09$ can be calculated for the looser sample.

These post-liquefaction strengths would develop quickly, with an increase in distortional strain of ~5%; perhaps no more than a crest movement of 2 m. Thus, the slumping tailings will lose between a third to half their undrained strength at the instant of liquefaction as the slide develops.

8.6.2.3 Effect of Mixing During Slump

A striking feature of the regression events was the obvious mixing of the tailings as they flowed downslope. This mixing is documented in the grading curves, and their consequent effect on causing a shift in the CSL (Figure 5-14). However, void ratio does not change during the slump with the bound pore water only migrating after the slump stabilised as controlled by its post-liquefaction strength (evidenced by the sand boils observed on the slump mass after it set up). This change in CSL at constant water content amounts to a substantial change in the post-liquefaction strength. The effect depends on the proportion of sandier fraction (TS2 tailings) to the dominant silt tailings (TC1 tailings), but a reasonable judgment is that a controlling $S_r/\sigma_v' \sim 0.1$ that existed as the slump started moving could fall to $S_r/\sigma_v' \sim 0.05$ by mid-slump simply because of mixing.

8.6.3 Stability at Liquefaction

8.6.3.1 Elastic-Plastic

The effect of liquefaction was simulated using the FLAC 2D model. Liquefaction was simulated by assigning an undrained strength ratio to S_u/σ_v'~0.20 to the region of tailings adjacent to the Stage 1 rockfill that was identified in the Phase 1 analyses as being close to its instability locus, as illustrated on Figure 8-25. The resulting displacement vectors for the imposed strength change are shown on this figure and provide a visual representation of the failure mechanism.

A distinct concentration of displacements is apparent in the region of undrained strength mobilisation. This zone of concentrated displacements originates at the upstream side of the Stage 1 Buttress and passes through the tailings and into the strain-weakened zone of the foundation. This distinct break in displacement pattern would lead to cracking of the dam surface at roughly the location where it was observed in the field.

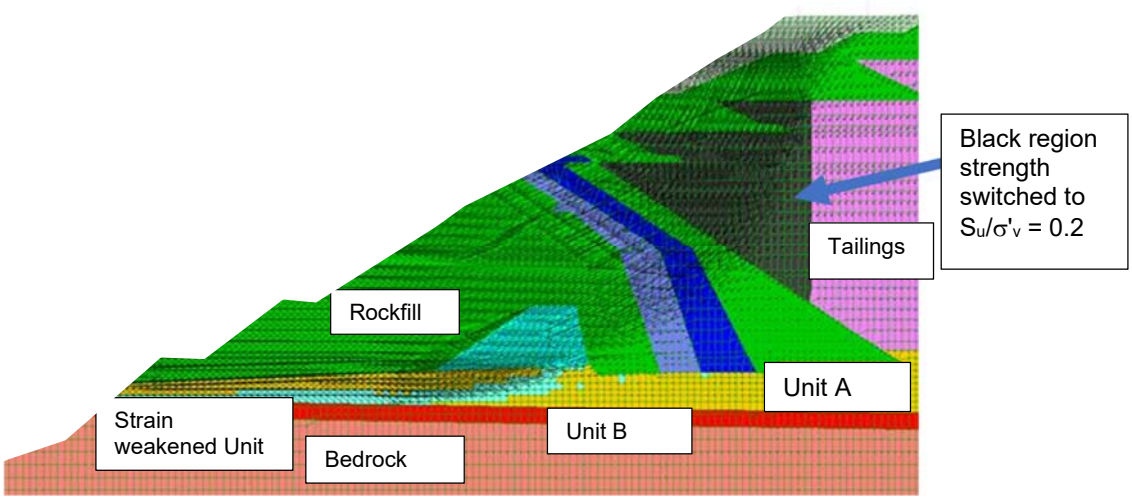


Figure 8-25: Displacement vectors following change from drained to undrained loading

8.6.3.2 NorSand

As illustrated by the calibration to the undrained tests in Appendix E, NorSand works as well undrained as drained (and without changing any soil properties). This provides an opportunity to compute the development of liquefaction directly. The undrained response of the tailings was simulated using NorSand after applying the drained loading to get to the instability locus. To achieve this the following steps were followed;

- The fluid bulk modulus of the tailings zones was switched from a value zero (that was assigned throughout the drained construction loading stages) to 2 GPa. This change causes pore pressures to be generated during shear for any contractive tailings.
- A minor disturbance to the model was created, through a small excavation at the toe, to identify how the undrained response of the tailings would develop.

Contours of the stress ratio η_{IL}/M_t are shown on Figure 8-26. Although this model did not reach numerical convergence, (indicating that the model could not determine a stable solution during this analysis), the partial results that were obtained showed that the region of tailings immediately upstream of the Stage 1 embankment would generate a very high stress ratio. Essentially, the zone of tailings shown in orange/red on Figure 8-26 had already transitioned to their critical state or residual strength. This is the expected behaviour referred to earlier where very little strain is needed to go from peak undrained strength to residual strength.

Most interestingly, if Figure 8-26 is compared to the post-slump survey shown on Figure 2-2 there appears a remarkable resemblance in terms of the loss of most of the original downstream-constructed dam during the Event.

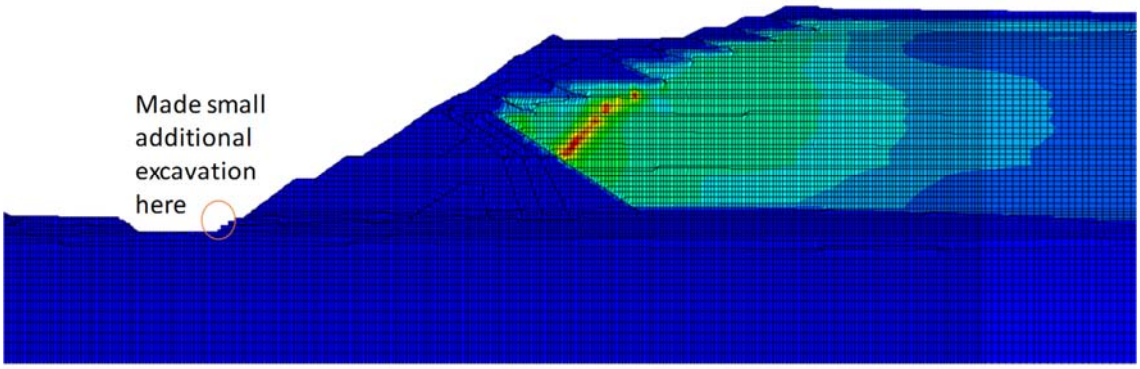


Figure 8-26: Contours of mobilised stress ratio η_{IL}/M_t after a small undrained perturbation

9. Conclusions

9.1 Commentary

The Mount Polley Independent Expert Engineering Investigation and Review Panel (2015) noted the following;

> "*Tailings dams are complex systems that have evolved over the years. They are also unforgiving systems, in terms of the number of things that have to go right. Their reliability is contingent on consistently flawless execution in planning, in subsurface investigation, in analysis and design, in construction quality, in operational diligence, in monitoring, in regulatory action, and in risk management at every level. All of these activities are subject to human error.*"

The Event that resulted in loss of containment of tailings from the NTSF on March 9, 2018, was a complex process. The ITRB has analysed the Event in terms of two Phases. Phase 1 incorporated all of the precursors to loss of containment up to and including the time at which the worksite was evacuated. Movements in Phase 1 were relatively slow. The onset of Phase 2 was not observed since the site had been evacuated, resulting in a period of about two hours without observational data. Upon return to the site, Phase 2 had ended, and its results were evident. A very substantial volume of material had been accelerated southward in a short period of time with associated loss of containment. While the two phases are undoubtedly linked, had movements terminated at Phase 1, the consequences of the Event would not have been so serious.

The technical processes resulting in the Event persisted over a significant period of time. Explaining these processes is included in the Terms of Reference put to the ITRB. Responding to these terms involves a blend of data acquisition from both the field and the laboratory, and invoking theoretical analyses as appropriate. Throughout the integration of new information, forensic investigations such as this must also honour the observations made directly from field behaviour to test the validity of evolving hypotheses. This methodology has been adopted consistently by the ITRB in the conduct of its work. While there are necessarily gaps in detailed information from both field and laboratory investigations, judgement is applied in overcoming these gaps and, where so, this is indicated in the narrative.

The ITRB is satisfied that the conclusions that follow below are adequately supported by the technical analyses undertaken, based on honouring the factual observations in a consistent manner and the exercise of professional judgement to integrate all elements of the process leading to the Event. Initial building blocks that underpin these conclusions are discussed in detail in the Appendices that are part of the Report. They are:

- The History of the NTSF (Appendix B): This contains the timeline of the NTSF from conceptual design through construction and performance to the end of Phase 1. The evolution of the NTSF is summarised, early indications of movement are identified and the structural cracking and deformations prior to collapse are summarised.
- Geology and Field Characterisation (Appendix C): The complicated site geological conditions are summarised. Details are presented related to drilling and sampling of the foundation conditions. The discovery of the relatively weak and compressible FRV Unit A is a critical finding to account for most of the factors that resulted in Phase 1 of the Event.
- Foundation Laboratory Testing (Appendix D): This focusses on the shear strength and deformation characteristics of materials in the foundation of the NTSF and reveals how the FRV Unit A differs from the other materials encountered.

- Tailings Properties (Appendix E): Characterisation of the tailings was undertaken to support the NTSF Phase 1 deformation analysis and to assess the liquefaction potential of the tailings. The mechanics of liquefaction, which is attributed as the dominant factor causing the mobility of the NTSF during Phase 2, have been evaluated.
- Hydrogeology (Appendix F): This summarises all of the hydrogeological behaviour in the vicinity of the Event in a model valid up to Phase 1. This model is used in subsequent deformation and stability analyses.
- Limit Equilibrium Analyses (Appendix G): These analyses are used in a screening manner to identify the range of foundation strengths that might be operable in Phase 1, and to assess the magnitude of 3D restraints affecting the stability of the NTSF.
- Deformation Analyses (Appendix H): These analyses provide a consistent interpretation, with both 2D and 3D considerations, that explore how the weak foundation led to the onset of instability consistent with Phase 1 and the initiation of liquefaction that triggered Phase 2. Advanced analyses, rarely used in professional practice, were needed to reveal these linkages in a quantitative manner.
- Seismology (Appendix I): The site seismicity is summarised and the two small earthquakes that occurred on March 8, 2018 are characterised. This information is used in an analysis of seismic triggering of liquefaction.

The response to the questions put to the ITRB in their Terms of Reference follow below.

9.2 Why Did the Event Occur?

The Event was a mobile slump that resulted in loss of containment of tailings from the NTSF in the vicinity of Ch. 1950. It has been considered as evolving in two phases. Phase 1 involved slow movements up to the time of evacuation of the worksite on March 9, 2018. This was followed by a rapid acceleration of movement (Phase 2) culminating in the slump feature subsequently identified a few hours later. The two phases are intimately linked. Had Phase 1 not developed, Phase 2 would not have resulted. Even if Phase 1 had terminated with only minor movements, it is conceivable that Phase 2 would not have resulted. Phase 2 is entirely the result of the magnitude of movements associated with Phase 1. However, the consequences of Phase 2 dominated the risk associated with the Event. Loss of containment resulted in cessation of production. There was no loss of life due to the timely evacuation of the site and the ITRB was advised that there were no apparent social or environmental consequences as the tailings released were captured in the STSF.

From the observations of cracking in the dam and foundation thrusting at the toe, the primary hypotheses associated with the development of Phase 1 movements considered the likelihood of weakness in the foundation. The drilling and sampling investigation concentrated on foundation conditions which are complex. A major finding of the investigation was the discovery of a low-density zone within the variably weathered volcaniclastic materials (FRV) underlying parts of the NTSF in the vicinity of the slump. This low density zone has been designated Unit A within the FRV. It is relatively weak, highly compressible material and loses strength with deformation (strain-weakening). The presence of FRV Unit A constitutes the most significant controlling feature that led to the Event.

Deformation during construction of the NTSF, especially during the construction of the Stage 1 and Stage 2 Buttresses, accelerated lateral movements as shown in the InSAR data. This movement pattern away from the contained tailings reduces support which is a trigger mechanism for liquefaction of the loose saturated tailings contained by the NTSF. This creates a sudden loss

of strength of the tailings resulting in a sudden increase of load on the dam, already weakened by movements in the foundation. The resulting force imbalance propels the dam outward.

Two small earthquakes occurred the day before the Event, and their role has also been assessed in detail. As a result of a comprehensive laboratory and analytical studies the ITRB concluded that the earthquakes did not contribute to the onset of Phase 2. The Phase 1 mechanism was well-advanced prior to these two earthquakes.

9.3 Why Did the Event Occur Where it Happened?

The dominant factors controlling the location of the Event is the spatial distribution of the FRV Unit A layer, in particular its close proximity to the foundation level. While the data are not abundant, this material has only been found near the failure zone. The geological synthesis presented in the Report provides a rational explanation for the variability of the distribution of the FRV, and the complex geological history that prevailed to bring Unit A close to the surface where it would form the foundation for part of the NTSF.

Other factors also contributed to the localisation of the Event. The height of the dam is a factor, which decreases to the west, and the embankment to the east had been buttressed to a reduced overall slope. The phreatic surface in the failure zone was close to its highest magnitude. In addition, there was an excavation at the toe of the structure, a well-known destabilising act.

Hence, a combination of low resistance of the foundation, and high imposed loading prevailed to localise the movements associated with Phase 1 of the Event. Phase 2 was triggered by Phase 1, and its mobility reflects the substantial imbalance between driving forces and resisting forces that prevailed at the onset of liquefaction.

9.4 Why Did the Event Occur When it Happened?

The NTSF began construction in 1998 and was raised in stages. At the time of the Event, Stage 10 was almost complete, taking the facility to a height of 94 m at its deepest location. All raises since 2005 have involved upstream construction. In the vicinity of the NTSF embankment failure, Stage 10 was essentially complete by the end of July 2017.

As part of the Stage 10 design, the designers concluded that Factors of Safety were too low and recommended the construction of two additional buttresses (see Figure 3-6). The Stage 1 Buttress was completed in the vicinity of the NTSF embankment failure by March 6, 2018. Stage 2 construction had not started in the slump area at the time of the Event, but stripping of more than 4 m had been undertaken at the toe of the dam in January 2018. Hence, considerable activity associated with buttress construction preceded the Event.

Deformation monitoring data analysed by the ITRB from both satellite based techniques (InSAR) and direct terrestrial survey techniques indicated small, but persistent movements continuing through 2017, accelerating in early 2018. Hence, the evolution of Phase 1 is clearly driven by construction of the embankment, with movements intensified by the construction of the buttresses, including the excavation at the toe.

By March 9, 2018, movements had progressed to a degree that cracking was observed along the Stage 5 and Stage 8 crests together with thrusting in the foundation at the toe. These features are all the result of yielding in the FRV Unit A material as it deforms due to the imposed loading.

Liquefaction of the weak saturated tailings ensued, initiating Phase 2. However, two small almost contiguous earthquakes occurred, raising the question whether they contributed to the onset of liquefaction or whether it was the inescapable consequence of continued deformation in the foundation or a combination of the two.

The ITRB has examined in detail with analytical means and special experiments the assessment of potential triggering due to the two earthquakes and has not been able to demonstrate any effects. It concludes that the earthquakes were not consequential to the onset of Phase 2 and that liquefaction was induced by the response of the tailings to the accumulating deformation in the foundation and embankment. Even if the analyses had revealed some influence of the earthquakes, it would have been small and only potentially significant because of the induced fragility of the deformed dam on the tailings.

Hence, this Event occurred when it did because the accumulation of construction-induced foundation deformation was sufficient to trigger static liquefaction in the loose saturated tailings stored by the NTSF.

9.5 Why Won't a Similar Event Happen Anywhere Else?

In the absence of further information, the implicit assumption must be that the remainder of the NTSF embankment and the STSF embankment are at risk to a repeat of the past incident, unless clear differences exist that justify an acceptable Factor of Safety can be demonstrated.

A comprehensive assessment of the level of safety of the remainder of the NTSF and STSF will be required to define the constraints under which investigations, stabilisation measures, remediation and reclamation should proceed.

The following factors play the most important role in establishing differences in the relative safety of different sections on the remainder of the embankment at a screening level;

- State of the tailings,
- Foundation conditions,
- Elevation of the phreatic surface, and
- Height of the embankment and of the dimensions of the downstream raises including buttresses.

The state of the tailings can reasonably be assumed to be similar around the entire embankment since the deposition cycle has been relatively consistent, and the CPTu tests confirm this consistency. This variable can therefore be eliminated from consideration for the purposes of establishing whether significant differences in relative safety can be assumed to exist around the embankment.

Foundation stratigraphy for the NTSF embankment to the east of the failure is similar to the stratigraphy at the failure, insofar as the near surface soils underlying the embankments are of FRV origin. However, FRV Unit A soils were not identified in any of the test pits or drillholes to the east of the failure. As such the foundation shear strength to the east of the failure would be expected to be somewhat better than that at the NTSF embankment failure.

Foundation conditions for the embankment to the west of the failure are also assessed to be more favourable than those at the failure since this segment is underlain by basalt and other geological units. However, it cannot be assumed that all geological units encountered are stronger and less brittle than the FRV Unit A soils and this must be demonstrated consistently at an appropriate scale. In order to do so, it is necessary to undertake drilling and sampling as well as a continual field mapping of as-built foundation conditions, together with development of an integrated geological and geotechnical model to evaluate continuity of units at a field scale, as shown in Section 4.7 above. Although the level of investigations required goes beyond that which is considered adequate for greenfield developments, they are necessary because of the challenge of finding critical anomalous materials of limited extent.

In addition, to demonstrate in an ongoing manner that the embankment foundation is performing as intended, it is necessary to adopt improved instrumentation to monitor deformations insitu such as Shape Array Accelerometer (SAA) inclinometers or other such instruments.

The overall height of the NTSF embankment decreases to the west and east towards the abutments, and more importantly the height of the downstream raise in proportion to the total height decreases towards the abutments. The embankment to the east of the failure has been buttressed and therefore has a much-reduced overall slope. These factors also suggest that the levels of safety elsewhere would be better than at the failure.

In summary, the learnings from the back analysis of the failure indicate that the following factors need to be considered to assess the safety level of the remainder of the embankments;

- Limited drainage within the body of the TSF and a high phreatic surface,
- Storage of a large body of saturated liquefiable tailings behind the starter embankment and upstream raises,
- A foundation that may be both weak and strain-weakening,
- Triggering of liquefaction by local earthquakes, and
- Potential triggering of liquefaction by uncontrolled lateral deformations.

The additional loading arising from buttressing and/or unloading arising from disturbance at the toe of the embankment should also be factored into the design of remedial measures.

The investigations and stability assessments undertaken by GHD on the STSF are set out in their report that was finalised during March of 2019 (2019-003). The report indicates that remedial stabilisation will be required for part of the STSF embankment to deal with current deficiencies and concludes that further stabilisation measures will be required when detailed design of future raises is done.

The ITRB's view of the report is that:

- The investigation provides useful characterisation of the foundation at the scale investigated.
- It is encouraging that low density, high plasticity deposits like the FRV Unit A, have not been encountered; although other weak zones have been found and are being addressed.

In the view of the ITRB, coverage and resolution of the drilling and laboratory testing may not have been adequate to confirm that anomalous weakness in all geological units will have been identified. An illustration of such a gap in coverage is located between drillholes CE402 and CE383 as shown in Figure 9-1. The following additional investigations are therefore advocated:

- Drilling to characterise the zone(s) of concern.
- Laboratory testing to examine the brittleness and large strain strength of the materials sampled.
- Integration of all results into a site wide geotechnical/geological model that should be calibrated whenever new exposures arise.
- The additional investigation can also be coupled with the installation of the additional instrumentation that is required.

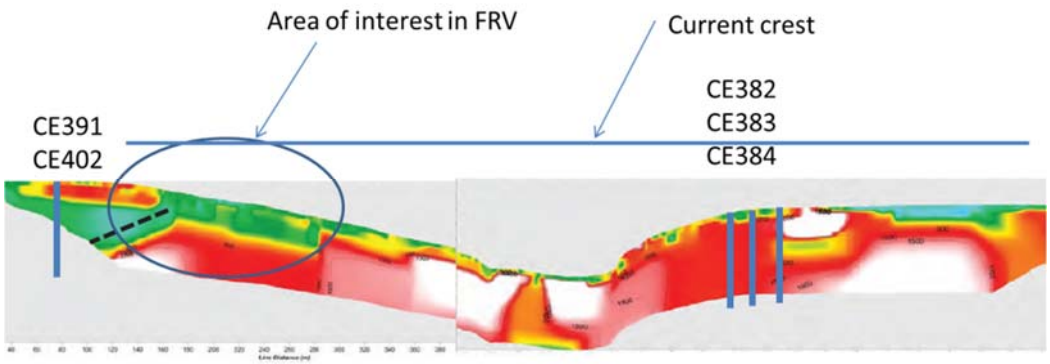


Figure 9-1: Longitudinal section along the STSF showing ERI and drillholes

NML is evaluating the prospect of restoring the NTSF to service as an upstream construction facility and maintaining STSF operations in a similar manner. In so doing, it should recognise that members of the ITRB take a more precautionary view with respect to upstream construction than has prevailed on site in the past (Morgenstern, 2018). The following quote from this reference outlines this more precautionary view in detail which assumes at the outset of a design that liquefiable material be assumed to do so;

> *"However, I side with the views of Martin and McRoberts* (1999) *and others before them (e.g., Lenhart* (1950)*; Vick* (1992)*) that there is nothing wrong with upstream tailings dams provided that key principles are adhered to in the design, construction, and operation of such dams. Some 12 principles are outlined that should be recognised when upstream dams are proposed. In my practice, I advocate for purposes of preliminary design that liquefiable deposits that can liquefy be assumed to do so and that containment be provided by a buttress of non-liquefiable unsaturated tailings and/or compacted dilatant material. In addition, it is essential to continually demonstrate by monitoring that the assumed unsaturated conditions in the buttress persist if relied upon in the design and that the buttress is behaving as intended."*

10. Acknowledgements

The members of the ITRB want to acknowledge the assistance that they received from the Hatch investigation team lead by Mr. Ian Gordon, Principal Investigator. They were devoted in all aspects of this study to responding to the requests of the ITRB and in executing fieldwork, sometimes under difficult conditions. The contribution of CVO personnel in proactively facilitating these ITRB investigations is gratefully acknowledged.

In addition, the ITRB wishes to recognise the contributions made by Mr. Bob Thiele, General Manager, Technical Services, Newcrest Mining Ltd., for his coordinating skills that facilitated the operation of the ITRB.

11. References

Alonso, E., & Gens, A. (2006a). Aznalcóllar dam failure. Part 1: Field observation and numerical properties. *Geotechnique, 56*, (pp. 165-183).

Alonso, E., & Gens, A. (2006b). Aznalcóllar dam failure. Part 3: Dynamics of the motion. *Geotechnique, 56*, (pp. 203-210).

Been, K. (2016). Characterizing mine tailings for geotechnical design. *Australian Geomechanics Society, Sydney, Australia,*, 41-55.

Chaudhury, K., Domingos, V., Gitirana, G., Fredlund, M., & Lu, H. (2016). Three-dimensional slope stability: Geometry effects. *Tailings and Mine Waste.* Keystone, CO.

Eckersley, D. (1990). Instrumented laboratory flowslides. *Géotechnique V40, Issue 3*, 489-502.

Fundão Tailings Dam Review Panel. (2016). *Report on the Immediate Causes of the Failure of the Fundão Dam.* Retrieved from http://fundaoinvestigation.com/wp-content/uploads/general/PR/en/FinalReport.pdf

Gajo, A. (2004). The influence of system compliance of collapse of triaxial sand samples. *Candian Geotechnical Journal 41(2)*, 257-273.

Gens, A., & Alonso, E. (2006). Aznalcóllar dam failure. Part 2: Stability conditions and failure mechanism. *Géotechnique Vol 56, Issue 3*, 185-201.

Independent Expert Engineering Investigation and Review Panel. (2015). *Report on Mount Polley Tailings Storage Facility Breach.* available at https://www.mountpolleyreviewpanel.ca.

Ishihara, K. (1984). Post-Earthquake Failure of a Tailings Dam Due to Liquefaction of Pond Deposit. *International Conference on Case HIstories in Geotechnical Engineering* (pp. 1129-1143). Missouri: Missouri University of Science and Technology Scholars' Mine.

Ishihara, K. (1993). Liquefaction and flow failure during earthquakes. *Geotechnique 43(3)*, 351-451.

Jefferies, M., & Been, K. (2016). *Soil Liquefaction.* CRC Press.

Lade, P., & Pradel, D. (1990). Instability and Plastic Flow of Soils. I: Experimental Observations. *Journal of Engineering Mechanics 116(11)*, 2532-2550.

Lenhart, W. (1950). Control of tailings from wasing plants. *Rock Products*, (pp. 72-80).

Leps, T. (1970). Review of Shearing Strength of Rockfill. *Journal of the Soil Mechanics and Foundations Division*, 1159-1171.

Martin, T., & McRoberts, E. (1999). Some consideration in the stability analysis of upstream tailings dams. *Tailings and Mine Waste '99*, (pp. 287-302). Fort Collins.

Morgenstern, N. (2017). The Evaluation of Slope Stability: A further 25-year perspective. . *Distinguised Lecture, Hong King Insitution of Engineers.*

Morgenstern, N. (2018). Geotechnical Risk, Regulation, and Public Policy (Victor de Mello Lecture). *Soils and Rocks, 41(2)*, 107-129.

Morgenstern, N. R., & Price, V. E. (1965). The anlaysis of the stability of general slip surfaces. *Geotech., London, 15, 1*, 79-93.

Roberstson, P. (2016). Cone penetration test (CPT)-based soil behaviour type (SBT) classification system - an update. *Canadian Geotechnical Journal*.

Robertson, P. (2010a). Evaluation of Flow Liquefaction and Liquefied Strength Using the Cone Penetration Test. *Journal of Geotechnical and Geoenvironmental Engineering, 136(6)*, 842-853.

Robertson, P. (2016). Cone penetration test (CPT)-based soil behaviour type (SBT) classification system — an update. *Canadian Geotechnical Journal*.

Sasitharan, S., Roberston, P., Sego, D., & Morgenstern, N. (1993). Collapse behavior of sand. *Canadian Geotechnical Journal*, 569-577.

Servicios de Ingenieria S.A. Eptisa. (1998). *Investigation of the failure of the Aznalcóllar Tailings Dam.* Summary Report for Boliden Apirsa, November 1998.

Shuttle, D., & Cunning, J. (2007). Liquefaction potential of silts from CPTu. *Canadian Geotechnical Journal*.

Shuttle, D., & Cunning, J. (2008). Reply to the discussion by Roberston on "Liquefaction potential of silts from CPTu". *Canadian Geotechnical Journal Vol. 45*.

Shuttle, D., & Cunning, J. (2008). Reply to the discussion by Robertson on “Liquefaction potential of silts from CPTu. *Canadian Geotechnical Journal, Vol. 45, Issue 1*, 142-145.

Shuttle, D., & Jefferies, M. (2002). Dilatancy in General Cambridge-Type Models. *Géotechnique, Vol. 52, No. 9*, 652-638.

Shuttle, D., & Jefferies, M. (2016). Determining silt state from CPTu. *Geotechnical Research Vol. 3 Issue 3*, 90-118.

Skopek, P., Morgenstern, N., Roberston, P., & Sego, D. (1994). Collapse of dry sand. *Canadian Geotechnical Journal* , 1008-1014.

Vick, S. (1992). Stability evaluation during staged construction – a discussion. *Journal of Geotechnical Engineering, 118*, 1282-1289.
Yang, J. (2002). Non-uniqueness of §ow liquefaction line for loose sand. *Geotechnique 52(10)*, 757-760.

12. Symbol List

Subscripts

cyc	Cyclic
k	Characteristic (in the sense of limit state Codes)
h	Horizontal
v	Vertical; volume
0	Initial condition
1, 2, 3	Principal directions of stress or strain
N	Normal
max	maximum
c	critical

Stress Variables (bar over or ′denotes effective)

$\sigma_{1,2,3}$	[FL^{-2}]	Principal stresses
σ_m	[FL^{-2}]	Mean effective stress $\sigma_m = (\sigma_1 + \sigma_2 + \sigma_3)/3$
σ', *p′*	[FL^{-2}]	Mean effective stress (=σ_m)
q,	[FL^{-2}]	Triaxial deviator stress, $q = \sigma_1 - \sigma_3$ (=σ_q)
t, τ	[FL^{-2}]	Shear Stress
η	[-]	Dimensionless shear measure as ratio of stress invariants $\eta = \sigma_q/\sigma_m$
u	[FL^{-2}]	Pore pressure

State Variables

e	[-]	Void ratio
K_0	[-]	Geostatic stress ratio, $K_0 = \sigma_h/\sigma_v$
G_s	[-]	Specific gravity
γ_d	[FL^{-3}]	Dry unit weight/ Dry density
γ_t	[FL^{-3}]	Total (and generally saturated) unit weight
γ'	[FL^{-3}]	Submerged unit weight
ψ	[-]	State parameter, $\psi = e - e_c$
k, m	[-]	Soil and rigidity specific coefficients in equation relating Q_p to ψ

Laboratory Testing Parameters and Variables

A	[-]	Skempton's triaxial excess pore pressure parameter $A = \Delta u/\Delta\sigma_q$
B	[-]	Skempton's excess pore pressure parameter $B = \Delta u/\Delta\sigma_3$
r_u	[-]	Excess pore pressure ratio
φ, ϕ	[deg]	Mohr Coulomb friction angle (effective implied by context)
ϕ_m'	[deg]	Peak mobilised friction
S_u	[FL^{-2}]	Undrained shear strength
S_r	[FL^{-2}]	Residual (post-liquefaction) undrained shear strength
c'	[FL^{-2}]	Cohesion (Drained)
C_c	[-]	Compression Index
C_r	[-]	Recompression Index
C_v	[LT^{-2}]	Coefficient of Consolidation
γ_{xy}, ε_{xy}	[-]	Shear strain
ε_a	[-]	Axial Strain
η_{IL}	[-]	Instability Locus, $\eta_{IL} = \tau/\sigma_v$
I_B	[-]	Brittleness Index

Elasticity

E	[FL^{-2}]	Young's modulus
G	[FL^{-2}]	Shear modulus
ν	[-]	Poisson's ratio

Critical State

Γ	[-]	Reference void ratio on CSL, conventionally defined at p′ = 1 kPa
λ	[-]	Slope of CSL in e_c – ln(σ_m) space for semi-log idealisation
λ_{10}	[-]	Slope of CSL, but defined on base 10 logarithms
M	[-]	Critical friction ratio, equals η_c at the critical state.
D_{min}	[-]	Minimum dilatancy

NorSand Model Parameters (in addition to those defining the critical state)

χ	[-]	Dilatancy constant
H	[-]	Plastic hardening modulus
H_r	[-]	Plastic softening modulus under principal stress rotation
M_i	[-]	Current value of η *at* $D^p=0$ *(*used in the flow rule)

Insitu and CPTu Parameters and Variables

q_c	[FL^{-2}]	CPTu tip resistance, as measured
q_t	[FL^{-2}]	CPTu tip resistance after correction for unequal area effect
f_s	[FL^{-2}]	CPTu friction sleeve stress measurement
u_2	[FL^{-2}]	Pore pressure measured by CPTu during sounding at shoulder location.
Q	[-]	Dimensionless CPTu resistance based on vertical stress., $Q = (q_t - \sigma_{v,0})/\sigma_{v,0}$
Q_p	[-]	Dimensionless CPTu resistance based on mean stress, $Q_p = (q_t - p_0)/p'_0$
B_q	[-]	CPTu excess pore pressure ratio, $B_q = (u_c - u_0)/(q_t - \sigma_{v0})$
F	[-]	Stress normalised CPTu friction ratio, $F = f_s/(q_t - \sigma_{v0})$
N_k	[-]	CPTu undrained strength factor, $N_k = (q_t - \sigma_{v0}) / s_u$

13. List of Abbreviations

ANCOLD	Australian National Committee on Large Dams
Ashurst	Ashurst Australia
CDSS	Cyclic direct simple shear test
CHPL	Cadia Holdings Pty Ltd
CPT	Cone penetration test
CPTu	Cone penetration test with pore pressure measurement
CRS	Constant rate of strain test
CSL	Critical state locus
CTX	Cyclic triaxial test
CVO	Cadia Valley Operations
DS	Direct shear test
DSS	Direct simple shear test
ERI	Electrical resistivity imaging
FLAC	Fast lagrangian analysis of continua
FRV	Forest Reef Volcanics
gINT	Geotechnical presentation software
GPS	Global positioning system
Hatch	Hatch Pty Ltd
InSAR	Interferometry synthetic aperture radar
ITRB	Independent Technical Review Board
LEA	Limit equilibrium analyses
LI	Liquidity Index
MASW	Multi- channel analysis of surface wave
MDSS	Monotonic direct simple shear
NML	Newcrest Mining Limited
NTSF	Northern tailings storage facility
OED	Oedometer tests
Otus	Otus Intelligence Group Pty. Ltd.
PPI	Piston-pneumatic injection

PWPD	Porewater pressure dissipation tests
RS	Ring shear test
SAA	Shape array accelerometer
SDMT	Seismic dilatometer
SME	Subject matter expert
SMM	Surface movement measurement
SOW	Scope of works
SRT	Seismic refraction traverses
STSF	Southern tailings storage facility
TSF	Tailings storage facility
TX	Triaxial compression test
VWP	Vibrating wire piezometer

14. Glossary of Technical Terms

Alluvium: materials deposited by water

Buttress: fill placed to increase the stability of a slope

Cambridge method: Triaxial test stress path plot using the axes $p' = (\sigma_1' + 2\sigma_3')/3$ (kPa) and $q' = (\sigma_1' - \sigma_3')$ (kPa)

Coefficient of consolidation (C_v): measure of the rate of consolidation of a soil

Colluvium: materials transported downslope by gravity

Cone Penetration Test: standardised penetration test used to measure insitu properties of soils

Crest: the top of a dam or slope

Critical failure surface in stability analysis: the failure surface providing the minimum calculated Factor of Safety

Critical state: State at which a soil continues to deform a constant stress and constant void ratio

Critical state locus: a line defining the critical state void ratio with change in mean effective stress

Deposition: process whereby the products of physical or chemical weathering are laid down

Deposition cycle: discharge sequence of tailings

Dip: angle between a horizontal surface and a planar geological feature measured perpendicular to the strike

Direct shear: test used to determine the shear strength on a plane

Direct simple shear: test used to determine shear strength under conditions of controlled strain or deformation

Downcutting: a natural process of erosion, resulting in lowering of the ground surface

Drained strength: strength defined in terms of effective stress parameters

Effective stress: the stress experienced by a particulate medium after pore water pressure is subtracted

Erosion: process of physical weathering

Factor of Safety: the ratio of available strength to the strength required for equilibrium; a measure of stability

Fines: combined silt and clay fractions less than 0.075 mm diameter

Flowslide: rapid mass movement, where failure mass lacks coherence

Fluvial deposits: materials deposited by rivers or streams

Hydraulic head: the elevation, with respect to a specified reference level, at which water stands in a piezometer

Instability locus: line defining the sudden loss of strength during shear due to the onset of undrained failure conditions

Lacustrine: materials deposited within a lake

Lift: successive layers of fill placement

Liquefaction: rapid loss of strength resulting from an increase in pore pressure under cyclic or static loading of contractive soils

Liquid Limit: moisture content at which soils change from plastic to liquid state

Liquidity Index: measure of natural moisture content of a soil in relation to both the Liquid and Plastic Limits

Loading: the imposition of stresses or weight

Marker bed: a prominent layer of soil or rock used as a reference

MIT method: Triaxial test stress path plot in terms of $s = (\sigma_1' + \sigma_3')/2$ (kPa) and $t = (\sigma_1' - \sigma_3')/2$ (kPa)

Oedometer test: a test for measuring compression of soil under load

Over-consolidation: a state or condition of soil produced by past stresses greater than those that currently exist

Overtopping: water flowing over the crest of a barrier

Paleosoil: a soil formed under previous geological conditions

Paleo alluvium: alluvium formed under previous geological conditions

Paleo geography: land surface developed under previous geological conditions

Phreatic surface: water table

Piezometer: an instrument for measuring groundwater level or pore water pressure

Piezometric surface: level of water measured in a piezometer

Piping: subsurface erosion of soil particles by water

Plastic Limit: moisture content at which a soil changes from a semi-solid to a plastic state

Plasticity Index: the numerical difference between the liquid limit and the plastic limit

Pore pressure: the pressure of water within the voids of a soil or rock

Residual soil: soil formed by the insitu weathering of a rock.

Residual strength: the minimum strength of a soil after having been sheared

Sand boils: material brought to the surface by an eruption of water resulting from excess pore water pressure at depth

Scissor holes: two holes drilled in opposite directions with the purpose of intersecting a geological feature

Seepage: flow of groundwater

Seismic refraction: method for determining the subsurface layering based on the measurement of seismic waves

Shear: force acting in a direction normal to another

Shell/ Shoulder: a zone of material that supports the core of a dam

Slump: rotational or translational mass movement where material maintains coherence

Sonic drilling: drilling method employing both rotation and high frequency vibration

State Parameter (ψ): difference between actual void ratio and the critical state line at a particular stress

Static bias: drained shear stress applied to a sample prior to commencing undrained cyclic shear to simulate field loading conditions

Stratigraphy: systematic layering exhibited by a soil or rock following the Law of Superposition

Substrate: underlying materials

Tailings: fine rock particles remaining after mineral processing or beneficiation

Terrestrial: land based

Tip resistance: the pressure measured at the tip of the cone during CPT testing

Toe: bottom of a slope

Triaxial test: test used to measure strength where axial and confining stresses can be varied independently

Undrained strength: strength based on total stress parameters

Undrained strength ratio: the ratio of undrained strength to confining stress

Vane shear test: test used to assess the undrained shear strength of a soil based on the torque required to rotate a cruciform blade

Void ratio: ratio of volume of voids in a particulate medium to the volume of solids

Weathering: physical or chemical processes whereby minerals and/ or rocks are broken down

Drawings

Drawing 1: Orthophoto Map – March 9, 2018

Drawing 2: Annotated Orthophoto Map - March 9, 2018

Drawing 3: Annotated Orthophoto Map - March 10, 2018

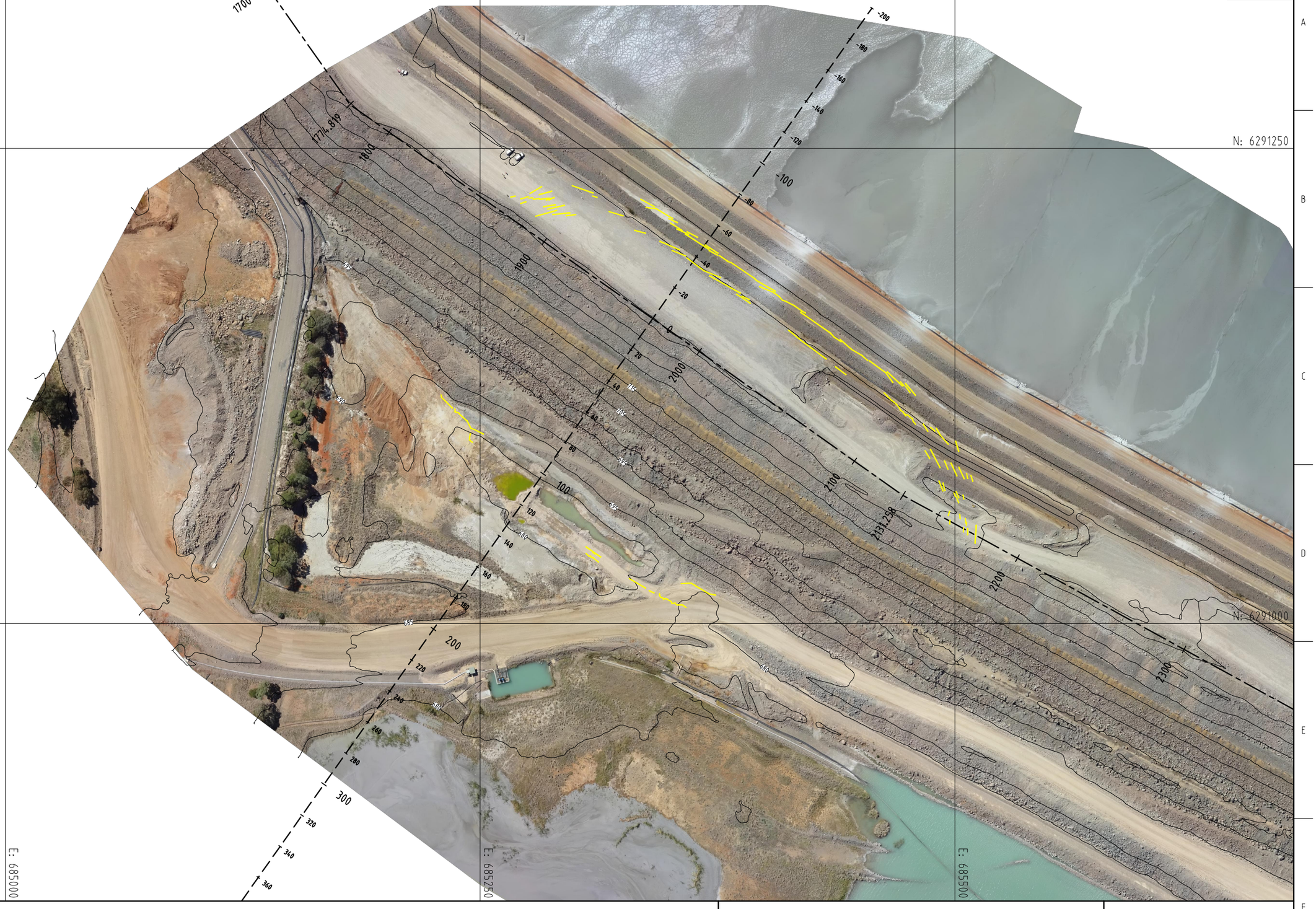
Drawing 4: Annotated Orthophoto Map - March 14, 2018

Drawing 5: Annotated Section Through Slump

Drawing 6: NTSF Geology and Previous Investigation Locations

Drawing 7: NTSF Plan with CPT Locations

Drawing 8: 2018 Investigation Locations



LEGEND

MAPPED CRACKS

1. ALL DIMENSIONS, ELEVATIONS AND COORDINATES ARE IN METERS, EXCEPT WHERE INDICATED OTHERWISE.
2. HORIZONTAL DATUM CORRESPONDS TO GDA 94 MGA ZONE 55.
3. VERTICAL DATUM CORRESPONDS TO AHD.
4. AERIAL PHOTO AND CONTOURS COMPLETED BY NEWCREST ON THE 9TH OF MARCH 2018.

ORTHOPHOTO MAP - MARCH 9, 2018

CADIA NTSF FAILURE INDEPENDENT TECHNICAL REVIEW BOARD

DRAWING D1

DESIGNED	DRAWN	APPROVED
IG	PK	
DATE	DWG. No.	
13-02-2019	H356804-00000-22A-272-0101	

LEGEND

- R_1 STAGE 2 ROCK FILL
- R_2 COARSE ROCK FILL
- R_3 ROCK FILL
- M_1 MIXED ROCKS AND EARTHFILL
- M_2 FILL MIXED WITH TAILINGS
- S_1 SLUMPED TAILINGS 10/03/2018
- S_2 SLUMPED TAILINGS 14/03/2018
- T_1 INTERBEDDED TAILINGS
- T_2 FINER TAILINGS
- MAPPED CRACKS
- TOE OF SLUMP
- BROWN MARKER HORIZON
- SCARP
- PIPES
- PUMP HOUSE
- PONDED WATER
- SEEPAGE
- EXCAVATED SURFACE
- SAND BOIL
- SEEPAGE
- DIRECTION OF MOVEMENT

E: 685000 E: 685250 E: 685500

N: 6291250 N: 6291000

T.N.

SPIGOTS
DRY TAILINGS SURFACE
SPIGOTS
WEST TAILINGS
SPIGOTS
DRAIN 1
BUTTRESS 1
EXCAVATED SURFACE
REMANANT TAILINGS WEDGE
RED SOIL
DRAIN 2
STAGE 6
SEEPAGE
TAILINGS
PIEZOMETER P9
OLD ACCESS RAMP
STAGE 5
ACCESS RAMP
DRAIN 3
BUTTRESS 1
TOE LOCK HAUL ROAD
PUMP HOUSE
PUMP POND
STSF TAILINGS
STSF DECANT
BUTTRESS 2

1700 1774.819 1800 1900 2000 2100 2131.258 2200 2300

R_1 R_2 R_3

SCALE: 1:2000 @A3

NOTES

1. ALL DIMENSIONS, ELEVATIONS AND COORDINATES ARE IN METERS, EXCEPT WHERE INDICATED OTHERWISE.
2. HORIZONTAL DATUM CORRESPONDS TO GDA 94 MGA ZONE 55.
3. VERTICAL DATUM CORRESPONDS TO AHD.
4. AERIAL PHOTO AND CONTOURS COMPLETED BY NEWCREST ON THE 9TH OF MARCH 2018.

ANNOTATED ORTHOPHOTO MAP - MARCH 9, 2018

CADIA NTSF FAILURE INDEPENDENT TECHNICAL REVIEW BOARD

DRAWING D2

DESIGNED	DRAWN	APPROVED
IG	PK	
DATE	DWG. No.	
13-02-2019	H356804-00000-22A-272-0201	

LEGEND

- R_1 STAGE 2 ROCK FILL
- R_2 COARSE ROCK FILL
- R_3 ROCK FILL
- M_1 MIXED ROCKS AND EARTHFILL
- M_2 FILL MIXED WITH TAILINGS
- S_1 SLUMPED TAILINGS 10/03/2018
- S_2 SLUMPED TAILINGS 14/03/2018
- T_1 INTERBEDDED TAILINGS
- T_2 FINER TAILINGS
- MAPPED CRACKS
- TOE OF SLUMP
- BROWN MARKER HORIZON
- SCARP
- PIPES
- PUMP HOUSE
- PONDED WATER
- SEEPAGE
- EXCAVATED SURFACE
- SAND BOIL
- SEEPAGE
- DIRECTION OF MOVEMENT

E: 685000 E: 685250 E: 685500

N: 6291250 N: 6291000

T.N.

BUTTRESS 1

SEEPAGE

DRAIN 1

TAILINGS OUTWASH

TAILING FLOW

EDGE OF SLUMPED TAILING

DRAIN 2 POSITION 09/03/18

PIEZOMETER P9

STAGE 2 MARKER HORIZON

HINGE LINE

DRAIN 3

BUTTRESS 1

PUMP HOUSE 09/03/2018

DRAIN 2

OLD RAMP

SHOVING OF ROAD PAVEMENT

DISCONTINUITY

BUTTRESS 2

PUMP HOUSE 10/03/2018

OLD BORROW AREA

STSF TAILINGS

TAILINGS ERUPTION

STSF POND

SCALE: 1:2000 @A3

NOTES

1. ALL DIMENSIONS, ELEVATIONS AND COORDINATES ARE IN METERS, EXCEPT WHERE INDICATED OTHERWISE.
2. HORIZONTAL DATUM CORRESPONDS TO GDA 94 MGA ZONE 55.
3. VERTICAL DATUM CORRESPONDS TO AHD.
4. AERIAL PHOTO AND CONTOURS COMPLETED BY NEWCREST ON THE 10TH OF MARCH 2018.

ANNOTATED ORTHOPHOTO MAP - MARCH 10, 2018

CADIA NTSF FAILURE INDEPENDENT TECHNICAL REVIEW BOARD

DRAWING 3

DESIGNED	DRAWN	APPROVED
IG	PK	

DATE	DWG. No.
13-02-2019	H356804-00000-22A-272-0202

LEGEND

- R_1 STAGE 2 ROCK FILL
- R_2 COARSE ROCK FILL
- R_3 ROCK FILL
- M_1 MIXED ROCKS AND EARTHFILL
- M_2 FILL MIXED WITH TAILINGS
- S_1 SLUMPED TAILINGS 10/03/2018
- S_2 SLUMPED TAILINGS 14/03/2018
- T_1 INTERBEDDED TAILINGS
- T_2 FINER TAILINGS
- MAPPED CRACKS
- TOE OF SLUMP
- BROWN MARKER HORIZON
- SCARP
- PIPES
- PUMP HOUSE
- PONDED WATER
- SEEPAGE
- EXCAVATED SURFACE
- SAND BOIL
- SEEPAGE
- DIRECTION OF MOVEMENT

E: 685000
E: 685250
E: 685500
N: 6291250
N: 6291000
T.N.
SEEPAGE
BUTTRESS 1
DRAIN 1
DRAIN 2
DRAIN 3
BUTTRESS 2
DRAIN 2 ORIGINAL POSITION 09/03/18
PUMP HOUSE ORIGINAL POSITION 09/03/18
PUMP HOUSE POSITION 10/03/18
PUMP HOUSE POSITION 14/03/18
1700
1774.8°9
1800
1900
2000
2100
2131.28
2200
2300
SCALE: 1:2000 @A3

NOTES

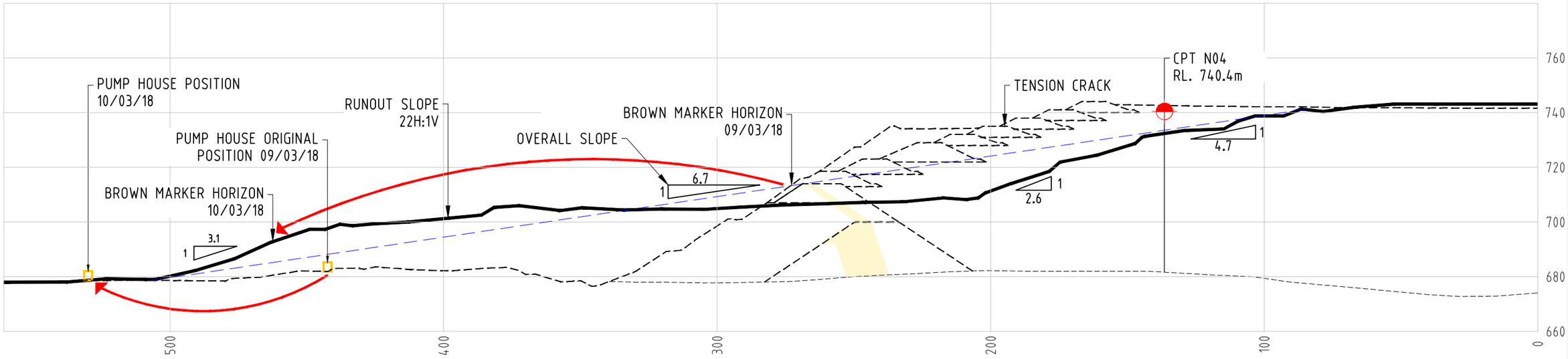
1. ALL DIMENSIONS, ELEVATIONS AND COORDINATES ARE IN METERS, EXCEPT WHERE INDICATED OTHERWISE.
2. HORIZONTAL DATUM CORRESPONDS TO GDA 94 MGA ZONE 55.
3. VERTICAL DATUM CORRESPONDS TO AHD.
4. AERIAL PHOTO AND CONTOURS COMPLETED BY NEWCREST ON THE 14TH OF MARCH 2018.

ANNOTATED ORTHOPHOTO MAP - MARCH 14, 2018

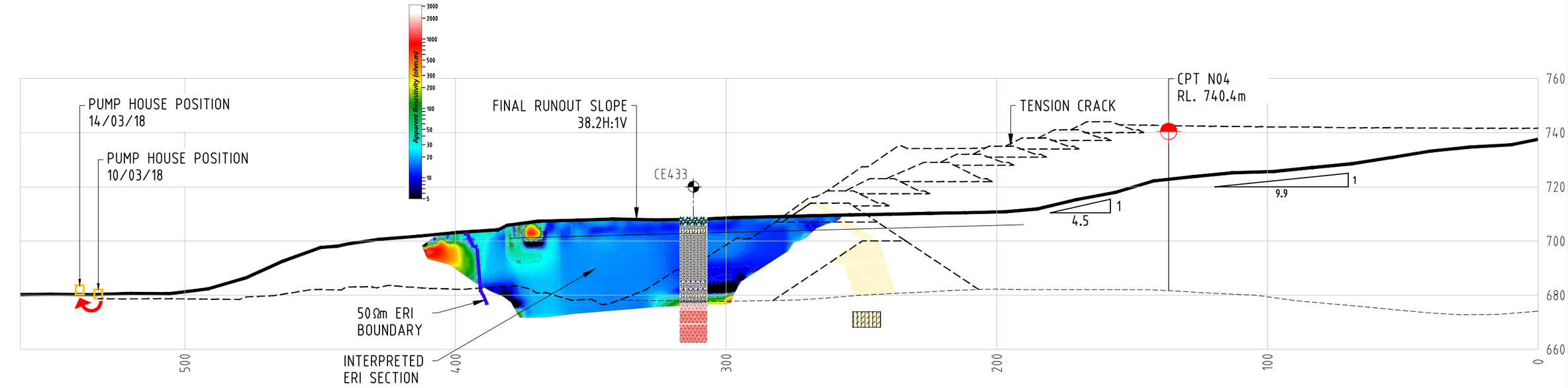
CADIA NTSF FAILURE INDEPENDENT TECHNICAL REVIEW BOARD

DRAWING 4

DESIGNED	DRAWN	APPROVED
IG	PK	
DATE	DWG. No.	
13-02-2019	H356804-00000-22A-272-0203	



ANNOTATED SECTION THROUGH SLUMP - MARCH 10, 2018



ANNOTATED SECTION THROUGH SLUMP - MARCH 14, 2018

0 7.5 15.0 22.5 30.0 37.5
SCALE: 1:1500 @A3

NOTES

1. ALL DIMENSIONS, ELEVATIONS AND COORDINATES ARE IN METERS, EXCEPT WHERE INDICATED OTHERWISE
2. VERTICAL DATUM CORRESPONDS TO AHD

LEGEND

- DRILLHOLE FROM HATCH (2018)
- CPT FROM ATCW TAILINGS INVESTIGATION (2017)
- PRE-CONSTRUCTION SURFACE
- NTSF AS-BUILT
- TOPOGRAPHY ON DATE OF LIDAR

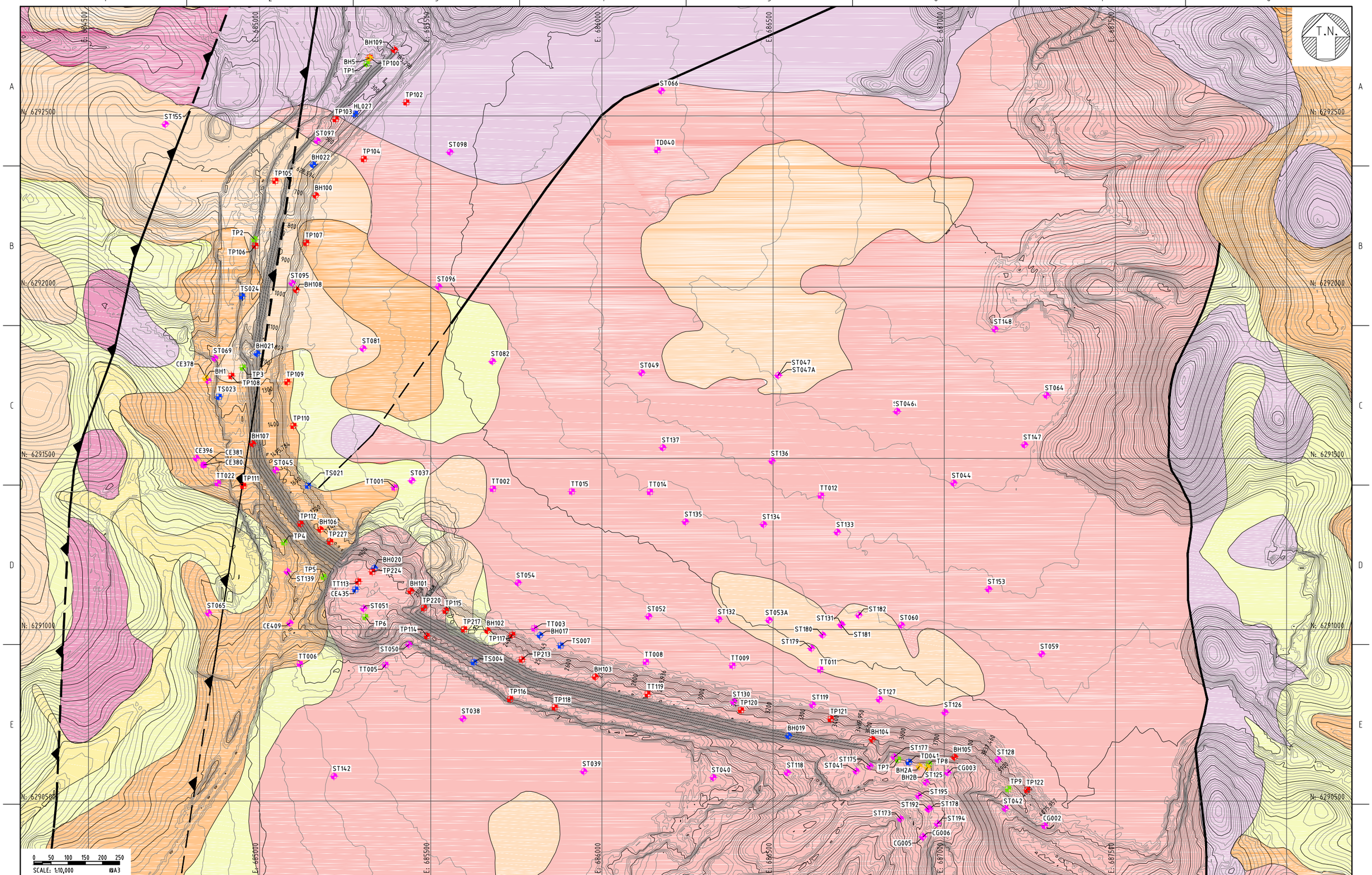
UNIT	DESCRIPTION
	TAILINGS
	CLAY FILL
	ROCKFILL
	MIXED FILL
	NO SAMPLING
	EW/HW VOLCANICLASTIC
	SW/F VOLCANICLASTIC

ANNOTATED SECTION THROUGH SLUMP

CADIA NTSF FAILURE INDEPENDENT TECHNICAL REVIEW BOARD

DRAWING 5

DESIGNED	DRAWN	APPROVED
IG	PK	
DATE	DWG. No.	
13-02-2019	H356804-00000-22A-273-0100	



NOTES

1. ALL DIMENSIONS, ELEVATIONS AND COORDINATES ARE IN METERS, EXCEPT WHERE INDICATED OTHERWISE.
2. HORIZONTAL DATUM CORRESPONDS TO GDA 94 MGA ZONE 55.
3. VERTICAL DATUM CORRESPONDS TO AHD.
4. LIDAR SURVEY COMPLETED BY AAM ON THE 19TH OF MARCH 2018.
5. GEOLOGY BASED ON NEWCREST GEOLOGICAL MAP DATED 24/05/2000.

LEGEND

- PELLS SULLIVAN MEYNINK (DECEMBER, 1996) DRILLHOLE
- PELLS SULLIVAN MEYNINK (DECEMBER, 1996) TEST PIT
- WOODWARD-CLYDE (SEPTEMBER, 1995) DRILLHOLE
- WOODWARD-CLYDE (SEPTEMBER, 1995) TEST PIT
- NEWCREST DRILLHOLE
- NEWCREST TEST PIT
- ATCW (APRIL, 2017) DRILLHOLE
- ATCW (MARCH, 2018) TEST PIT
- ALLUVIUM (QUATERNARY)
- COLLUVIUM (QUATERNARY)
- GRAVELS (TERTIARY)
- BASALT (TERTIARY)
- CADIA COACH SHALE (SILURIAN)
- FOREST REEF VOLCANIC (ORDOVICIAN)
- WEEMALLA FORMATION (ORDOVICIAN)
- FAULT (MAPPED)
- FAULT (INFERRED)
- THRUST FAULT

NTSF GEOLOGY AND PREVIOUS INVESTIGATION LOCATIONS

CADIA NTSF FAILURE INDEPENDENT TECHNICAL REVIEW BOARD

DRAWING 6

DESIGNED	DRAWN	APPROVED
IG	PK	
DATE	DWG. No.	
13-02-2019	H356804-00000-22A-274-0002	



NOTES

1. ALL DIMENSIONS, ELEVATIONS AND COORDINATES ARE IN METERS, EXCEPT WHERE INDICATED OTHERWISE.
2. HORIZONTAL DATUM CORRESPONDS TO GDA 94 MGA ZONE 55.
3. VERTICAL DATUM CORRESPONDS TO AHD.
4. LIDAR SURVEY COMPLETED BY AAM ON THE 19TH OF MARCH 2018.

LEGEND

"2013 URS INVESTIGATION" CPT

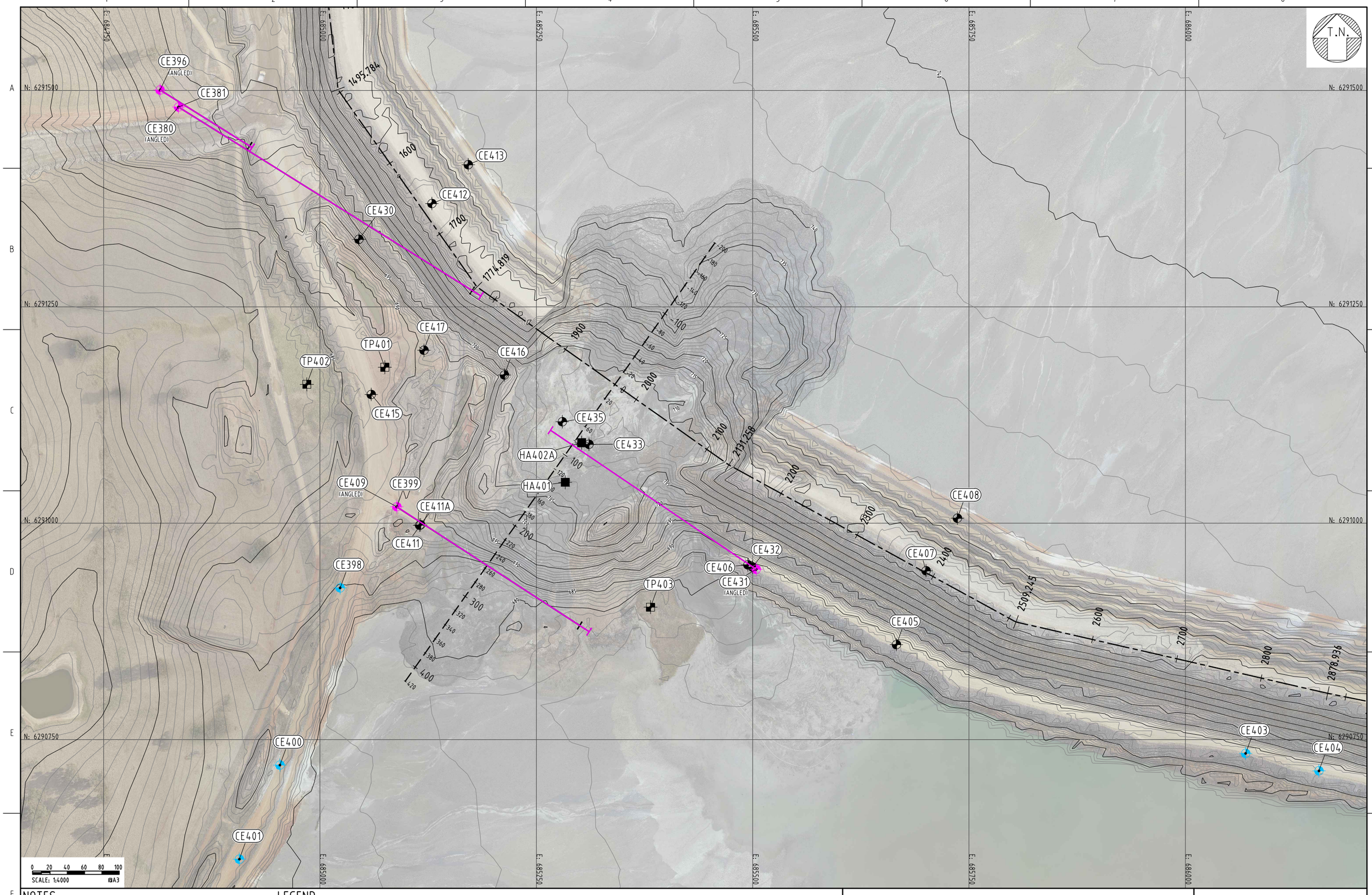
"2017 ATCW TAILINGS INVESTIGATION" CPT AND VWP

NTSF PLAN WITH CPT LOCATIONS

CADIA NTSF FAILURE INDEPENDENT TECHNICAL REVIEW BOARD

DRAWING 7

DESIGNED	DRAWN	APPROVED
IG	PK	
DATE	DWG. No.	
13-02-2019	H356804-00000-22A-270-0302	



NOTES

1. ALL DIMENSIONS, ELEVATIONS AND COORDINATES ARE IN METERS, EXCEPT WHERE INDICATED OTHERWISE.
2. HORIZONTAL DATUM CORRESPONDS TO GDA 94 MGA ZONE 55.
3. VERTICAL DATUM CORRESPONDS TO AHD.
4. LIDAR SURVEY COMPLETED BY AAM ON THE 19TH OF MARCH 2018.

LEGEND

- ITRB DRILLHOLE
- ITRB TEST PIT
- ITRB HAND AUGER
- GHD DRILLHOLE
- NEWCREST DRILLHOLE
- NTSF SETOUT LINE
- SLUMP CENTRELINE
- HORIZONTAL PROJECTION OF INCLINED DRILLHOLE

2018 INVESTIGATION LOCATIONS

CADIA NTSF FAILURE INDEPENDENT TECHNICAL REVIEW BOARD

DRAWING 8

DESIGNED	DRAWN	APPROVED
IG	PK	
DATE	DWG. No.	
13-02-2019	H356804-00000-22A-270-0101	